



---

# **Universidad de Valladolid**

SCHOOL OF MEDICINE

DEPARTMENT OF BIOCHEMISTRY AND MOLECULAR  
BIOLOGY AND PHYSIOLOGY

DOCTORAL THESIS:

## **Role of insulin-degrading enzyme (IDE) in diabetes mellitus and insulin resistance**

By Pablo Villa Pérez

Submitted to the academic thesis committee in  
fulfilment of the requirements for the Doctor of  
Philosophy Degree (PhD) from University of Valladolid

Tutored by:

Dra. Irene Cózar Castellano

Dr. Germán Perdomo Hernández

Dra. M<sup>a</sup>Carmen Domínguez Lobatón



This work was conducted within the Institute of Biology and Molecular Genetic (IBGM) in cooperation with University of Valladolid (UVa) and University of Burgos (UBu). It has been funded by:

- Grant I+D+I "Retos Investigación" - Call 2014 - (SAF2014-58702-C2-1-R & SAF2014-58702-C2-2-R)
- Grant I+D+I "Retos Investigación" - Call 2016 - (SAF2016-77871-C2-1-R & SAF2016-77871-C2-2-R)



**Index**



<b>1</b>	<b>Abbreviations .....</b>	<b>13</b>
<b>2</b>	<b>Introduction .....</b>	<b>23</b>
2.1	The pandemic of diabetes mellitus.....	23
2.2	Diagnosis and main types of diabetes mellitus.....	24
2.3	Obesity and T2DM .....	25
2.3.1	Obesity.....	25
2.3.2	Relationship between obesity and T2DM.....	27
2.4	Insulin resistance in obesity and T2DM .....	28
2.4.1	Insulin: the regulator of metabolism .....	28
2.4.2	Insulin signaling .....	29
2.4.3	Insulin resistance.....	31
2.4.4	Insulin resistance in liver, skeletal muscle and adipose tissue .....	33
2.5	Hepatic glucose metabolism .....	34
2.5.1	The liver in the fed state .....	35
2.5.2	The liver in the fasted state .....	37
2.6	Insulin-degrading enzyme (IDE).....	40
2.6.1	IDE substrates and its proteolytic activity.....	41
2.6.2	Animal models for the study of IDE .....	43
2.6.3	Pharmacological therapies against T2DM based on inhibition of IDE activity .....	44
<b>3</b>	<b>Hypotheses and Aims.....</b>	<b>49</b>
3.1	Hypotheses .....	49
3.2	Aims.....	49
<b>4</b>	<b>Material and Methods .....</b>	<b>53</b>
4.1	Animal procedures.....	53
4.1.1	Animal facilities.....	53
4.1.2	Breeding strategies of liver-IDE knockout mice (L-IDE-KO) .....	53
4.2	Experimental animals.....	54
4.3	Mouse genotyping.....	55
4.4	Metabolic characterization .....	58
4.4.1	Body weight .....	58
4.4.2	Food intake.....	58
4.4.3	Blood sampling .....	58

4.4.4	Plasma collection .....	59
4.4.5	Blood glucose levels .....	59
4.4.6	Homeostatic Model Assessment (HOMA) index.....	59
4.4.7	Plasma insulin levels.....	59
4.4.8	Plasma glucagon levels .....	60
4.4.9	Plasma A $\beta$ 40 levels .....	61
4.4.10	Plasma amylin levels .....	62
4.4.11	Plasma triglycerides levels .....	63
4.4.12	Plasma cholesterol levels .....	64
4.4.13	Plasma Non-Esterified Free Fatty Acids (NEFFAs) levels .....	64
4.4.14	Glucose tolerance test (GTT) .....	65
4.4.15	Insulin tolerance test (ITT).....	66
4.4.16	Pyruvate tolerance test (PTT).....	66
4.4.17	<i>In vivo</i> insulin clearance.....	66
4.4.18	Liver glycogen content.....	67
<b>4.5</b>	<b>Tissue dissection .....</b>	<b>67</b>
<b>4.6</b>	<b>Western blot.....</b>	<b>68</b>
<b>4.7</b>	<b>RNA isolation and cDNA synthesis .....</b>	<b>70</b>
<b>4.8</b>	<b>RT-qPCR.....</b>	<b>72</b>
<b>4.9</b>	<b>Statistical analysis .....</b>	<b>73</b>
<b>5</b>	<b>Results .....</b>	<b>77</b>
<b>5.1</b>	<b>Generation and analysis of Liver-specific <i>Ide</i> knock-out mice.....</b>	<b>77</b>
<b>5.2</b>	<b>Metabolic characterization of L-IDE-KO mice.....</b>	<b>78</b>
5.2.1	L-IDE-KO mice exhibit hyperglycemia after prolonged fasting, independently of body weight .....	78
5.2.2	L-IDE-KO male mice exhibit hyperglycemia in non-fasting conditions independently of body weight or food intake.....	80
5.2.3	Hepatic <i>Ide</i> ablation impairs glucose tolerance in L-IDE-KO mice .....	83
5.2.4	Hepatic <i>Ide</i> ablation causes insulin resistance in L-IDE-KO mice.....	85
5.2.5	L-IDE-KO mice exhibit insulin resistance despite similar plasma insulin levels ..	87
5.2.6	HOMA index confirms that L-IDE-KO mice exhibit insulin resistance despite having similar plasma insulin levels .....	89
5.2.7	Hepatic <i>Ide</i> ablation does not alter plasma lipid profiles in L-IDE-KO mice .....	90
5.2.8	Hepatic <i>Ide</i> deletion causes hyperglucagonemia in L-IDE-KO mice at 1 month of age.....	92
5.2.9	Plasma levels of A $\beta$ 40 and amylin in L-IDE-KO mice.....	94
5.2.10	Hepatic <i>Ide</i> ablation does not impair hepatic insulin clearance <i>in vivo</i> . .....	96

5.2.11	Hepatic <i>Ide</i> ablation impairs hepatic insulin signaling. ....	99
5.2.12	Hepatic ablation of <i>Ide</i> augments gene expression of <i>Pck1</i> and <i>G6pc</i> in L-IDE-KO mice	105
5.2.13	Insulin regulates hepatic IDE protein levels .....	108
<b>6</b>	<b><i>Discussion</i></b> .....	<b>113</b>
<b>7</b>	<b><i>Conclusions</i></b> .....	<b>127</b>
<b>8</b>	<b><i>References</i></b> .....	<b>131</b>



## **Abbreviations**



## **1 ABBREVIATIONS**

%	Percentage
a.m.	After Meridian
AD	Alzheimer Disease
ADP	Adenosine Diphosphate
AKT	Protein Kinase B
Alb-Cre	Albumin-Cre
ANOVA	Analysis of Variance
AS160	AKT substrate of 160 kDa
ATP	Adenosine Triphosphate
AUC	Area Under the Curve
A $\beta$	Amyloid $\beta$ -Protein
BMI	Body Mass Index
cAMP	Cyclic Adenosine Monophosphate
cDNA	Complementary Deoxyribonucleic Acid
CEACAM1	Carcinoembryonic Antigen-Related Cell Adhesion Molecule1
ChREBP	Carbohydrate-Responsive Element-Binding Protein
CoA	Co-enzyme A
CREB	cAMP Response Element-Binding

DAG	Diacylglycerol
DHAP	Dihydroxyacetone Phosphate
DNA	Deoxyribonucleic Acid
DPP-4	Dipeptidyl Peptidase-4
DPP-4	Dipeptidyl Peptidase-4
EDTA	Ethylenediaminetetraacetic Acid
EIA	Enzyme Immunoassay
ELISA	Enzyme-Linked Immunosorbent Assay
F1,6BP	Fructose-1,6-Biphosphate
F6P	Fructose-6-Phosphate
Fab site	Fragment Antigen-Binding Site
FBPase	Fructose Biphosphatase
Fc region	Fragment Crystallizable Region
FFA	Free Fatty Acid
FoxO	Forkhead Box
FoxO1	Forkhead Box O1
<i>g</i>	Gravitational Forces
G1P	Glucose-1-Phospahte
G6P	Glucose-6-Phosphate
G6Pase	Glucose-6-Phosphatase

G6pc	Glucose-6-phosphatase
GAPDH	Glyceraldehyde-3-Phosphate Dehydrogenase
GCGR	G-Protein-Coupled Glucagon Receptor
GCK	Glucokinase
GK	Glycerol Kinase
GK	Goto-Kakizaki Diabetic Rats
GLP-1	Glucagon-Like Peptide-1
GLUT2	Glucose Transporter 2
GS	Glycogen Synthase
GSK3	Glycogen Synthase Kinase 3
GTT	Glucose Tolerance Test
HDL	High-Density Lipoprotein
HIF-1	Hypoxia-Inducible Factor-1
HNF-4	Hepatocyte Nuclear Factor-4
HOMA	Homeostatic Model Assessment
HT	Heterozygous
IDE	Insulin-Degrading Enzyme
IGF-1	Insulin-like Growth Factor II
IKK $\beta$ /NF- $\kappa$ B	Inhibitor of Nuclear Factor Kappa-B / Nuclear Factor Kappa-Light-Chain-Enhancer of Activated B Cells Pathway

IL-1 $\beta$	Interleukin-1 Beta
IL-6	Interleukin-6
IPGTT	Intraperitoneal Glucose Tolerance Test
IPITT	Intraperitoneal Insulin Tolerance Test
IPPTT	Intraperitoneal Pyruvate Tolerance Test
IR	Insulin Receptor
IRS	Insulin Receptor Substrate
IR $\beta$	Insulin Receptor $\beta$ -Subunit
ITT	Insulin Tolerance Test
KLF-6	Kruppel-Lie Factor-6
LDH	Lactate Dehydrogenase
LDL	Low-Density Lipoprotein
L-IDE-KO	Liver-IDE Knock-out
LSB	Laemmli Sample Buffer
LXR	Liver X Receptor
MAPK	Mitogen Activated Protein Kinase
MCP-1	Monocyte Chemoattractant Protein-1
MHO	Metabolically Healthy Obese
MONW	Metabolically Obese Normal Weight
mRNA	Messenger Ribonucleic Acid

mTORC1	Mammalian Target of Rapamycin Complex-1
mTORC2	Mammalian Target of Rapamycin Complex-2
NEFFAs	Non-Esterified Free Fatty Acids
°C	Centigrade
p.m.	Post Meridian
PC	Pyruvate Carboxylase
<i>Pck1</i>	Phosphoenolpyruvate Carboxykinase 1
PCR	Polymerase Chain Reaction
PDH	Pyruvate Dehydrogenase
PDK1	3-Phosphoinositide-Dependent Kinase-1
PEP	Phosphoenolpyruvate
PEPCK	Phosphoenolpyruvate Carboxykinase
PH	Pleckstrin Homology Domain
PI3K	Phosphatidylinositol 3-Kinase
PIP <sub>2</sub>	Phosphatidylinositol-4,5-Biphosphate
PIP <sub>3</sub>	Phosphatidylinositol-3,4,5-Triphosphate
PKA	Protein Kinase A
PKC	Protein Kinase C
PKC $\theta$	Protein Kinase C-Theta
PPAR $\gamma$	Peroxisome Proliferator Activated Receptor Gamma

PPi	Pyrophosphoric Acid
PTT	Pyruvate Tolerance Test
PVDF	Polyvinylidene Difluoride
RNA	Ribonucleic Acid
RT-qPCR	Real-Time Reverse Transcription-Quantitative Polymerase Chain Reaction
SA-HRP	Streptavidin-Horseradish Peroxidase
SDS	Sodium Dodecyl Sulfate
SEM	Standard Error of the Mean
Ser	Serine
SFUs	Sulfonylureas
SH2	Src Homology 2
Src	Proto-Oncogene Tyrosine-Protein Kinase
SREBP-1c	Sterol Regulatory Element Binding Protein-1c
T1DM	Type 1 Diabetes Mellitus
T2DM	Type 2 Diabetes Mellitus
TBE	Tris-Borate-EDTA
TCFE3	Transcription Factor E3
TGF- $\alpha$	Transforming Growth Factor Alpha
Thr	Threonine

TMB	3, 3', 5, 5'- Tetramethylbenzidine
TNF- $\alpha$	Tumor Necrosis Factor-Alpha
UDP	Uridine Diphosphate
UTP	Uridine Triphosphate
UV	Ultra-Violet
UVa	University of Valladolid
VLDL	Very-Low-Density Lipoprotein
WAT	White Adipose Tissue
WHO	World Health Organization
WT	Wild Type



## **Introduction**



## 2 INTRODUCTION

### 2.1 The pandemic of diabetes mellitus

During the last twenty years the prevalence of diabetes has increased dramatically in the world, and the disease is now one of the largest global health emergencies of the 21<sup>st</sup> Century<sup>1</sup>.

Previous studies estimated that the number of diabetic patients worldwide would reach 366 million in 2030<sup>2</sup>; however, that number is already exceeded. At the end of 2015 there were 415 million people with diabetes in the world, and there will be 642 million people with diabetes in 2040<sup>3</sup> (**Figure 1**). In addition to the 415 million adults with diabetes, there are 318 million adults with impaired glucose tolerance, which puts them at high risk of developing the disease in the future<sup>3</sup>.

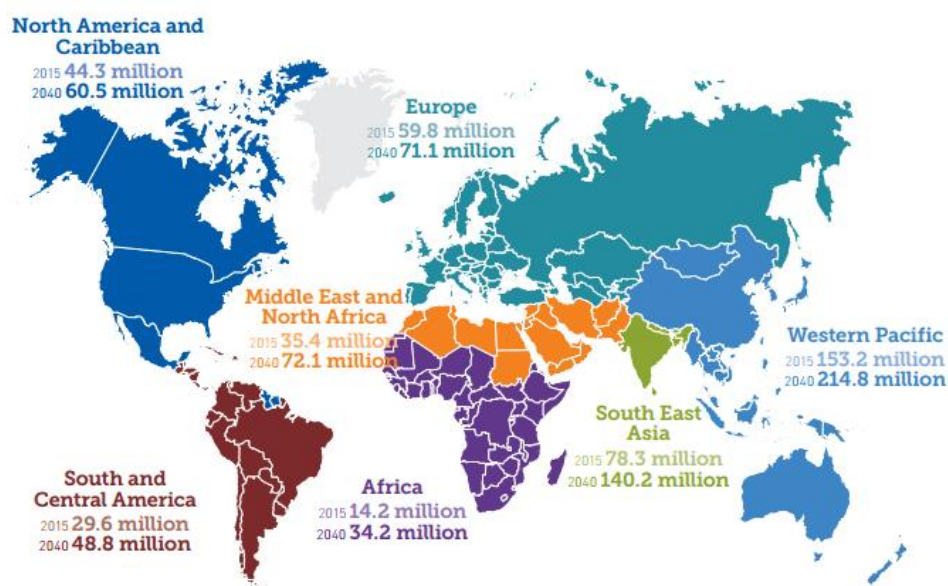


**Figure 1:** Prevalence of diabetes in 2015 and future estimation in 2040 worldwide<sup>1</sup>.

The last study of diabetes mellitus in Spain shows that the prevalence of this disease in adults was 13.8% in 2011; in addition, almost half of them did not know they had the disease (6.0%)<sup>4</sup>.

In 2012 around 1.5 million deaths were directly caused by diabetes and another 2.2 million deaths were attributable to high blood glucose<sup>5,6</sup>. Furthermore, direct medical cost of diabetic patients was 8% of total public health expenditures in Spain<sup>7</sup> and 12% of global health expenditure in the world<sup>3</sup>. The increasing social cost and the increasing prevalence of diabetes mellitus, combined with the high mortality and morbidity related to it, suggest the importance of developing effective ways to treat and manage diabetes.

## 2.2 Diagnosis and main types of diabetes mellitus

Diabetes mellitus is a group of metabolic diseases characterized by chronic hyperglycemia due to insufficient insulin production or due to impaired responsiveness to insulin produced by the pancreas<sup>8</sup>. Currently, according to the World Health Organization (WHO), the following criteria are utilized for the diagnosis of diabetes mellitus<sup>9,10</sup> (**Table 1**):

Status	Fasting Glucose Levels (mg/dL)	2 hour Glucose Levels (mg/dL)
Normal	<110	<140
Impaired fasting glucose	≥110 and <125	<140
Impaired glucose tolerance	<126	≥140 and <200
Diabetes	≥126	≥200

**Table 1:** WHO diabetes diagnosis criteria<sup>8</sup>.

There are two main types of diabetes. The first is type 1 diabetes mellitus (T1DM), which is characterized by insufficient insulin production as a result of pancreatic  $\beta$ -cells destruction via an autoimmune reaction. T1DM develops according to certain hereditary factors plus environmental or inducement factors<sup>11,12</sup>. T1DM is classified as fulminant, acute or slowly progressive depending on the manner of onset<sup>13</sup>.

Type 2 diabetes mellitus (T2DM), which is the most common form of diabetes, is characterized by the development of insulin resistance in the peripheral tissues

and by the failure of pancreatic  $\beta$ -cells to produce sufficient insulin due to the long-term need to increase insulin secretion to compensate for insulin resistance<sup>14</sup>. T2DM is associated with multiple genetic factors<sup>15,16</sup> and unhealthy lifestyle habits, such as daily high fat diet and lack of exercise, which finally ends in overweight and obesity. Onset of T2DM commonly occurs in middle age or later, despite the fact that T2DM has currently been shown to be increasing in young people and children. This type of diabetes accounts for over 90% of all diabetes cases around the world<sup>17</sup>.

## 2.3 Obesity and T2DM

### 2.3.1 Obesity

Obesity is defined as a body mass index (BMI) of  $\geq 30 \text{ kg/m}^2$  (**Table 2**).

BMI (kg/m <sup>2</sup> )	Classification
< 18.5	Underweight
18.5 – 24.9	Normal weight
25.0 – 29.9	Overweight
$\geq 30.0$	Obese

**Table 2:** WHO classification of adult obesity according to BMI<sup>18</sup>.

The prevalence of has risen since 1960 and has increased to 54.9% of adults in the last decade<sup>19</sup>. In 2014, 38% of adult men and 40% of adult women aged 18 years and older were overweight<sup>20</sup> (**Figure 2 and 3**).

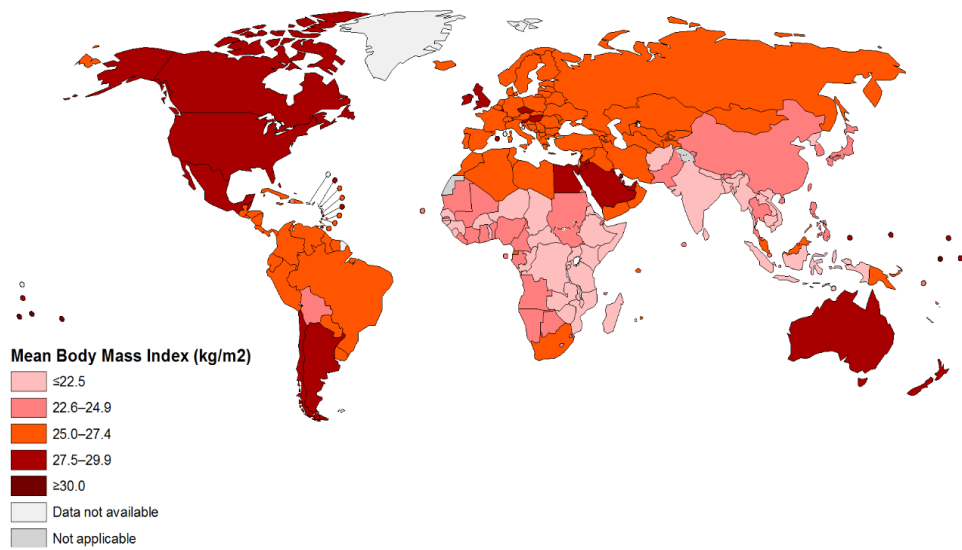


**Figure 2:** Age-standardized prevalence of obesity in men aged 18 years old and over (BMI  $\geq 30$  kg/m<sup>2</sup>), 2014<sup>21</sup>.

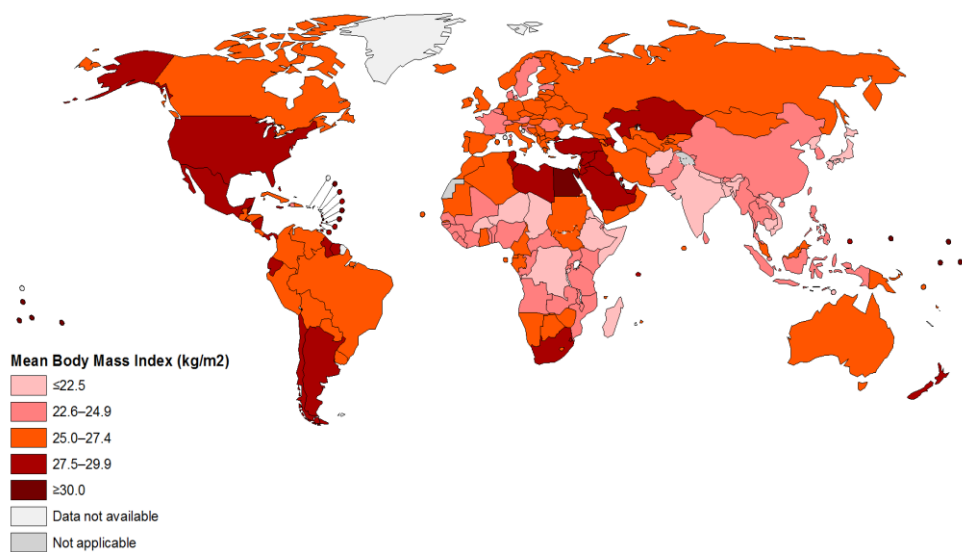


**Figure 3:** Age-standardized prevalence of obesity in women aged 18 years old and over (BMI  $\geq 30$  kg/m<sup>2</sup>), 2014<sup>21</sup>.

Obesity has become a serious global health problem, overall, in developing and industrialized countries. Moreover, obesity is responsible for enormous health care costs due to health risks associated with this disease, e.g.: cardiovascular disease, cancer and diabetes mellitus. For these reasons there is

a need to understand the mechanisms and pathogenesis of obesity-related diseases for developing new treatments and prevention strategies<sup>22</sup>.

### 2.3.2 Relationship between obesity and T2DM

The prevalence of T2DM is rising in parallel with obesity; in fact, more than 90% of individuals with T2DM are obese<sup>23</sup>. Primarily, the relationship between obesity and T2DM is based on impaired lipid and carbohydrate metabolism regulated by insulin<sup>24</sup>, which causes insulin resistance. Frequently, this insulin resistance is associated with obesity.

In contrast, certain populations with a high prevalence of obesity show a low prevalence of T2DM. In this way, we can indicate that being obese is not an indispensable condition for developing T2DM; indeed, lean individuals can develop this devastating disease<sup>25,26</sup>.

On the one hand, some studies indicate that the majority of obese people do not develop T2DM, and it only appears in people who are genetically predisposed to developing it<sup>27</sup>. On the other hand, many epidemiological studies suggest that obesity plays a direct role in the development of T2DM, scoring it as the major risk factor for this metabolic disease<sup>28,29</sup> (**Table 3**).

Disease	Relative risk-women	Relative risk-men
<b>T2DM</b>	<b>12.4</b>	<b>5.2</b>
Hypertension	4.2	2.6
Myocardial infarction	3.2	1.5
Cancer of the colon	2.7	3.0
Angina	1.8	1.8
Gall bladder disease	1.8	1.8
Ovarian cancer	1.7	-
Osteoarthritis	1.4	1.9
Stroke	1.3	1.3

**Table 3:** Estimated increased risk of suffering disease for obese versus lean population<sup>30,31</sup>.

## 2.4 Insulin resistance in obesity and T2DM

### 2.4.1 Insulin: the regulator of metabolism

Insulin is a peptide hormone produced and secreted by  $\beta$ -cells in the Islets of Langerhans in the pancreas, in response to high blood glucose levels<sup>32</sup>. In pancreatic  $\beta$ -cells, insulin is synthesized and processed by removing C-peptide, the center of the molecule, from the precursor molecule proinsulin through proteolytic enzymes<sup>33</sup>.

The three main target tissues for insulin action are liver, muscle and adipose tissue<sup>34</sup>. Insulin maintains blood glucose levels from 4 to 7nM regardless of nutritional status, but under conditions of high blood glucose levels, insulin promotes glycogen and lipid storage and inhibits the breakdown of glycogen (glycogenolysis) and the *de novo* synthesis of glucose (gluconeogenesis) in the liver<sup>35</sup>. In addition, in muscle insulin stimulates glucose uptake for storage in the form of glycogen<sup>34</sup> and inhibits protein degradation while increasing the release of amino acids<sup>36</sup>. Likewise, in adipose tissue, insulin inhibits lipolysis, reducing the release of free fatty acids and glycerol into bloodstream, while also triggering glucose uptake and lipid storage<sup>34,37</sup>.

Insulin produces other effects besides nutrient metabolism on non-target tissues. For example, in the brain, insulin is responsible for appetite suppression<sup>38-40</sup>, which has been shown to be reduced in insulin resistant and obese people<sup>41</sup>. Insulin also has an effect on vascular cells, where it stimulates vasodilatation and capillary recruitment enhancing glucose delivery and glucose uptake by the muscle<sup>38,42</sup>.

The main effects of insulin action on different tissues are summarized in **Table 4**.

Main effects of insulin on metabolism		
Organ/Tissue	Effect	
	Direct	Indirect
Skeletal muscle	↑ Glucose uptake ↑ Glucose oxidation ↑ Glycogen synthesis	↓ NEFA availability and oxidation
Liver	↓ Glycogenolysis ↓ Gluconeogenesis ↑ Glycogen synthesis ↑ Glycolysis ↑ Lipogenesis	↓ NEFA availability and oxidation
Adipose tissue	↑ Glucose uptake ↑ Lipogenesis	Regulation of adipokines synthesis and/or secretion ↓ Lipolysis
Pancreatic $\beta$ -cells	?	Permissive effect on glucose-stimulated insulin secretion
Brain	?	↓ Food intake
Vascular tissue	?	↑ Blood flow ↑ Capillary recruitment

**Table 4:** Direct and indirect effects of insulin on metabolic processes. Modified from Newsholme and Dimitriadis<sup>43</sup>.

### 2.4.2 Insulin signaling

Insulin signaling regulates glucose, lipid and energy homeostasis, predominantly via its action on liver, skeletal muscle and adipose tissue<sup>44</sup>.

Once secreted by  $\beta$ -cells, insulin binds to the insulin receptor (IR). The IR is formed by two extracellular  $\alpha$  subunits and two transmembrane  $\beta$  subunits which are linked by disulfide bonds<sup>45</sup>. On the  $\beta$  subunits there is a tyrosine kinase domain, which is activated by autophosphorylation when insulin binds to the IR<sup>46</sup>.

Downstream, the IR activation induces the recruitment of insulin receptor substrates (IRSs), via phosphorylation of certain tyrosine residues by the kinase activity of activated IR. Several intracellular IRSs have been identified<sup>47</sup>; however, IRS-1 and IRS-2 are the most important. IRS-1 is the main IRS responsible for controlling insulin action in muscle, while IRS-2 is essential for insulin signaling in the liver<sup>48</sup>. Phosphorylated IRS proteins are responsible for mediating activation of the two major insulin-signaling pathways: the mitogen activated

protein kinase (MAPK) pathway, which is important for cellular growth and development; and the phosphatidylinositol 3-kinase (PI3K)-protein kinase B (AKT) pathway, which is crucial for metabolic functions, mainly glucose and fat metabolism<sup>47,49</sup>.

PI3K is formed by a regulatory p85 subunit<sup>50</sup>, which has two proto-oncogene tyrosine-protein kinase (Src) homology 2 (SH2) domains that interact with phosphotyrosine residues on IRSs, and a catalytic p110 subunit<sup>51</sup>, which is able to phosphorylate phosphatidylinositol-4,5-bisphosphate (PIP<sub>2</sub>), a plasma-membrane glycolipid, to phosphatidylinositol-3,4,5-trisphosphate (PIP<sub>3</sub>)<sup>52</sup>. PIP<sub>3</sub> recruits AKT, one of the main metabolic steps of insulin signaling, and 3-phosphoinositide-dependent kinase-1 (PDK1) to the plasma membrane via its pleckstrin homology (PH) domain<sup>53</sup>.

Once localized to the plasma membrane, AKT is phosphorylated at threonine 308 (Thr<sup>308</sup>) by PDK1<sup>54</sup> and at serine 473 (Ser<sup>473</sup>) by the mammalian target of rapamycin complex-2 (mTORC2)<sup>55,56</sup>. Fully activated AKT is separated from plasma membrane to cytoplasm.

There are two isoforms of AKT (AKT1 and AKT2). AKT1 is required for normal growth, is involved in cellular survival, protein synthesis and inhibition of apoptosis, but dispensable for the maintenance of glucose homeostasis<sup>57</sup>. In contrast, AKT2 is essential for the maintenance of normal glucose homeostasis<sup>58</sup>.

AKT is capable of mediating changes in other kinases, such as glycogen synthase kinase 3 (GSK3), which is down-regulated by AKT phosphorylation<sup>59</sup>. This results in dephosphorylation and activation of glycogen synthase (GS) leads glycogen production<sup>47</sup>. In addition, AKT has other targets, such as AKT substrate of 160 kDa (AS160), involved in glucose transporter translocation; and the mammalian target of rapamycin complex-1 (mTORC1), a signaling hub involved in many cellular processes; sterol regulatory element binding protein-1c (SREBP-1c), which mediates many of insulin's effects on lipogenesis and cholesterol homeostasis<sup>60,61</sup>; and the forkhead box (FoxO) transcription factor, involved in gluconeogenesis processes<sup>62,63</sup> (**Figure 4**).

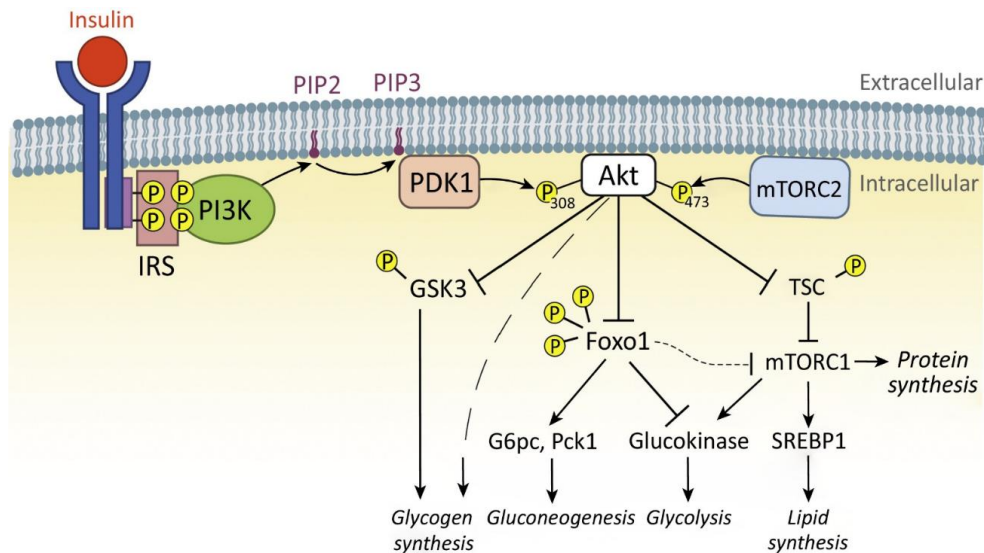


**Figure 4:** Liver-specific insulin signaling for the regulation of hepatic lipid and glucose metabolism<sup>63</sup>.

### 2.4.3 Insulin resistance

Obesity is one of the most important risk factors for developing insulin resistance<sup>64</sup>. The term insulin resistance was described and defined in 1988 by Reaven as “a state (of a cell, tissue, system or body) in which greater than normal amounts of insulin are required to elicit a quantitatively normal response”<sup>65</sup>.

In mechanistic terms, insulin resistance can occur at three different levels:

- Before the binding of insulin with the IR, such as increased insulin degradation or insulin competing to bind other proteins besides IR.
- At level of the IR, due to alterations in binding affinity or receptor levels.
- Downstream of the IR interaction, due to any of a number of changes from the hormone-receptor complex to the final effects<sup>66</sup>.

Patients with insulin resistance present with impaired glucose tolerance due to reduced ability of peripheral tissues to uptake and metabolize glucose<sup>67</sup>.

However, the precise cause(s) of T2DM and the mechanisms which underlie this metabolic disease in target cells are still being elucidated.

Formerly, adipose tissue was thought to be inactive in terms of metabolic functions; however, recently its role in metabolism has been described<sup>68</sup> and it has been defined as “*a highly active closely-regulated metabolic tissue*”<sup>69</sup>.

There are two principal theories seeking to explain the origin of insulin resistance. The fat overload theory<sup>70,71</sup> proposes that insulin resistance is triggered by elevated levels of free fatty acids (FFAs) in blood<sup>72</sup>, which can vary considerably with dietary intake. When there is high fat intake, adipose tissue begins to store large quantities of triglycerides, in order to prevent high blood triglyceride levels. However, when fat intake remains higher than fatty acid oxidation ratio, triglycerides begin to accumulate in liver, skeletal muscle and pancreatic  $\beta$ -cells, resulting in insulin resistance and impaired insulin secretion<sup>73–76</sup>. In addition, intermediates from incomplete  $\beta$ -oxidation as diacylglycerol (DAG) and ceramide accumulated in these cells, which inhibits the insulin-signaling pathway<sup>77</sup>.

An alternative theory to explain the development of insulin resistance is inflammation theory. It is known that obesity itself induces an inflammatory state in which macrophages are believed to infiltrate adipocytes, thus producing an augmented inflammatory response<sup>78,79</sup>. Consequently, different pro-inflammatory cytokines, such as tumor necrosis factor- $\alpha$  (TNF- $\alpha$ )<sup>80–82</sup>, interleukin-6 (IL-6)<sup>83</sup>, interleukin-1 $\beta$  (IL-1 $\beta$ ) and monocyte chemoattractant protein-1 (MCP-1)<sup>84</sup>, are secreted from adipocytes. Increased secretion of these cytokines impairs insulin signaling and glucose transport in peripheral tissues<sup>85</sup> (**Figure 5**).

In addition, both theories can be combined in one due to fat overload, through production of metabolites such as DAGs and ceramides, causes the activation of inflammatory pathways inducing an insulin resistance state.

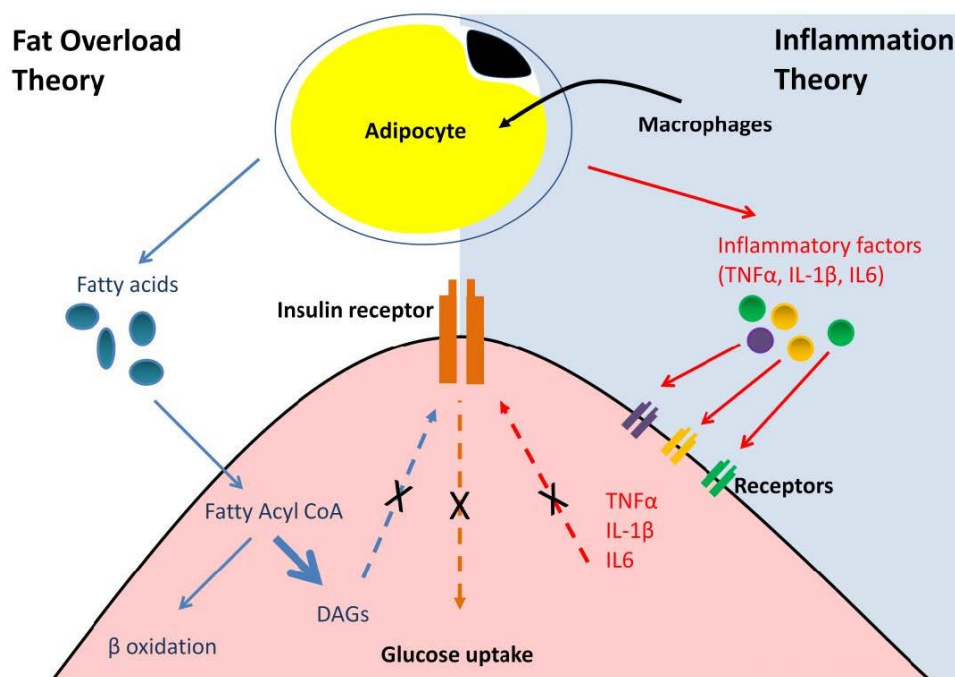


**Figure 5:** The two general theories to explain insulin resistance; fat overload theory (white background on the left) and inflammation theory (grey background on the right)<sup>86</sup>.

#### 2.4.4 Insulin resistance in liver, skeletal muscle and adipose tissue

The liver is one of the three principal target tissues for insulin action. The liver regulates systemic insulin levels through hepatic insulin clearance and maintains normoglycemia during fasting conditions<sup>87</sup>.

Under insulin-resistant conditions, hepatic gluconeogenesis and glycogenolysis are inadequately suppressed, resulting in hyperglycemia under both fasting and non-fasting conditions<sup>88</sup>. Also, a common response to insulin resistance is increased secretion of insulin by the pancreas; the resulting hyperinsulinemia induces an overstimulation of lipogenesis. Dyslipidemia is another common consequence of insulin resistance, being characterized by hypertriglyceridemia together with low high-density lipoprotein (HDL) cholesterol and elevated low-density lipoprotein (LDL) cholesterol in circulation. This profile is often present in individuals with T2DM<sup>89</sup>.

In addition, insulin resistance developed by skeletal muscle and adipose tissue affects glucose disposal and lipolysis due to the inability to take up glucose in response to insulin. Furthermore, insulin resistance established in adipose tissue

leads to unregulated lipolysis, which causes high blood free fatty acids levels and contributes to increased hepatic glucose output<sup>68,90</sup> (**Figure 6**).

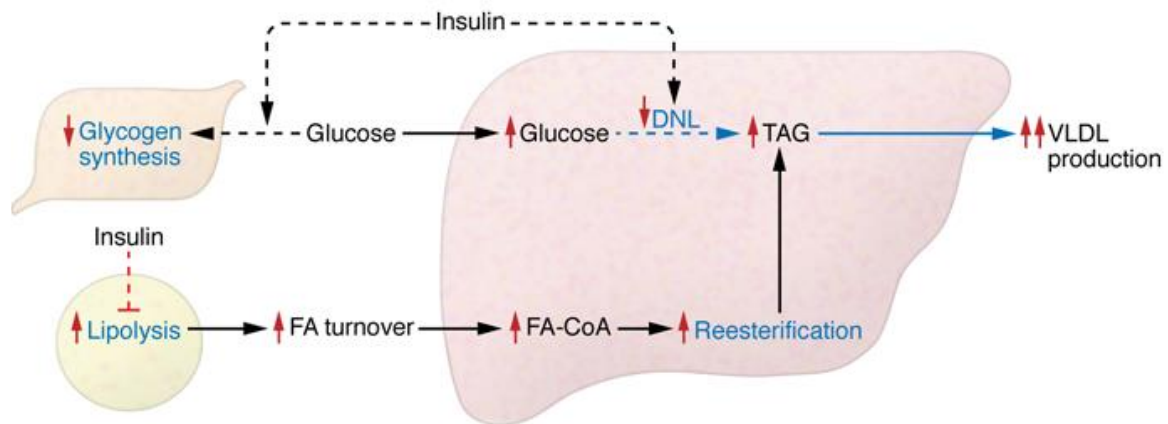


**Figure 6:** Liver, skeletal muscle and adipose tissue insulin resistance<sup>68</sup>.

## 2.5 Hepatic glucose metabolism

Many organs and cells use glucose as their major energy source, because numerous basic maintenance functions depend on glucose supply. In fact, the liver is the organ responsible for regulating glucose homeostasis by controlling the balance between glucose output during fasting periods, or glucose uptake during feeding periods<sup>91,92</sup>.

During feeding periods, insulin mediates hepatic glucose uptake which can be stored as glycogen (glycogenesis) or can be oxidized to supply necessary energy (glycolysis)<sup>93</sup>.

However, during fasting periods, other hormones such as glucagon stimulate glucose production by glycogen degradation (glycogenolysis) or activates *de novo* synthesis of glucose using glycerol, lactate and certain amino acids (gluconeogenesis)<sup>94</sup>.

### **2.5.1 The liver in the fed state**

In the fed state, glucose is transported in circulation from the gut and it is metabolized by a process regulated mostly by insulin. Insulin stimulates the liver and muscle to store excess glucose as glycogen via the process of glycogenesis<sup>59,95</sup>.

Circulating insulin, secreted by the pancreas in response to feeding, is cleared primarily by the liver, and to a lesser extent by the kidney<sup>96</sup>. Once insulin binds to IR in the liver, IR autophosphorylation occurs, inducing a signaling cascade via PI3K with the subsequent phosphorylation and activation of AKT<sup>91,97</sup>. The insulin-IR complex is then endocytosed and insulin is dissociated from the IR. Most evidence suggests that insulin is degraded at this point<sup>96,98</sup>.

Phosphorylated and activated AKT leads to fatty acid synthesis, activation of protein synthesis pathways and changes in other kinases, as GSK3, which is down-regulated by AKT phosphorylation<sup>59</sup>. This results in dephosphorylation and activation of GS leading to glycogen production<sup>47</sup> from glucose, which enters to the hepatocyte through glucose transporter 2 (GLUT2) located at the cell surface. In addition, forkhead box O1 (FoxO1) transcription factor is phosphorylated by full activated AKT, precluding its translocation from the cytoplasm to the nucleus<sup>95,97,99,100</sup> (**Figure 4**).

During glycogenesis, glucose enters in the liver through GLUT2<sup>101,102</sup>, which mediates the equilibrium of glucose concentrations in blood and hepatocytes<sup>101,103,104</sup> but is not directly regulated by insulin<sup>103</sup>. GLUT2 is the major glucose transporter in hepatocytes, but is also expressed in pancreatic islets, brain, intestine and kidney<sup>105,106</sup>.

Glycogenesis involves three different phases. In the first phase, glucose is metabolized to glucose-6-phosphate (G6P) by the action of glucokinase (GCK)<sup>107,108</sup>; this enzyme is expressed by hepatocytes and pancreatic  $\beta$ -cells and is involved in both glycogenesis and glycolysis. In the second phase, G6P is converted to glucose-1-phosphate (G1P); and, in the third phase, G1P reacts

with uridine triphosphate (UTP) forming uridine diphosphate-glucose (UDP-glucose) from which glycogen is finally obtained by the action of GS.

In addition, insulin secreted by the pancreas in response to feeding activates another metabolic pathway named glycolysis. Glycolysis occurs in the liver and is characterized by the conversion of glucose into pyruvate. As occurs in glycogenesis, glucose first enters in the hepatocyte through GLUT2<sup>101,102</sup> and is phosphorylated to G6P by the action of GCK. After that, however, G6P is processed through a different pathway that yields pyruvate as a final product<sup>109</sup>. Pyruvate can be converted into lactate or acetyl CoA which directly enters the Krebs cycle to generate energy in form of adenosine triphosphate (ATP)<sup>100,110</sup> (**Figure 7**).

GCK, which is involved at the beginning of both glycogenesis and glycolysis, is regulated mainly by insulin; however, its transcription in the liver is controlled by several transcription factors as FoxO1<sup>111,112</sup>, SREBP-1c<sup>113</sup>, hepatocyte nuclear factor-4 (HNF-4)<sup>111,112</sup>, peroxisome proliferator activated receptor gamma (PPAR $\gamma$ )<sup>113</sup>, hypoxia-inducible factor-1 (HIF-1)<sup>114,115</sup>, liver X receptor (LXR)<sup>113</sup>, transcription factor E3 (TCFE3)<sup>116</sup> and Kruppel-like factor-6 (KLF-6)<sup>117</sup>.

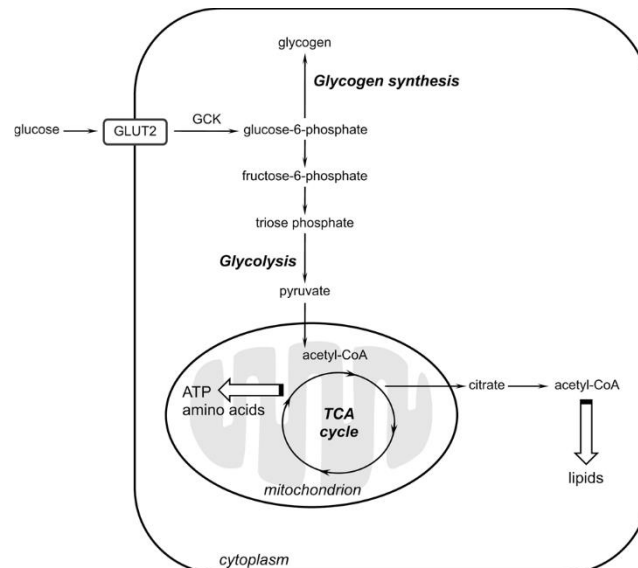


**Figure 7:** Simplified scheme of the major biochemical pathways activated during postprandial hepatic glucose uptake and storage<sup>118</sup>.

### **2.5.2 The liver in the fasted state**

In the fasted state, in response to decreasing blood glucose concentrations, circulating insulin levels and hepatic insulin signaling decrease; as a consequence, dephosphorylated and active GSK3 phosphorylates and inactivates GS, inhibiting glycogen synthesis by the liver<sup>119</sup>. In addition, the pancreas initiates glucagon secretion, a peptide hormone which has receptors in the brain, adipose tissue, heart, liver and kidney<sup>120</sup>.

In this metabolic condition, the energy of the entire body depends on glucose produced by the liver and, to a lesser extent, by the kidney, the two organs capable of carrying out glucose production and secretion<sup>121</sup>. In fact, glucose from glycogen storage in the muscle is only used to maintain its contraction abilities<sup>122–124</sup>.

Glucose release by the liver is essential to maintain energy supply to the muscle during physical exercise<sup>122,123</sup>, but overall it is indispensable to maintain energy supply to essential organs for life as the brain, which depends on a continuous flow of glucose by the blood to maintain its basic functions<sup>124,125</sup>.

Glycogenolysis begins when glucagon binds to its receptor named G-protein-coupled glucagon receptor (GCGR)<sup>126</sup>, which is present at the cell surface of hepatocytes. When glucagon interacts with GCGR, a downstream signaling cascade is initiated: intracellular cyclic adenosine monophosphate (cAMP) levels increase via adenylate cyclase, leading to the activation of protein kinase A (PKA), which activates glycogen phosphorylase<sup>119</sup>. Glycogen phosphorylase, the main enzyme involved in glycogenolysis process, is active when it is phosphorylated at serine 14 and is capable of removing a glucose residue from the non-reducing end of a glycogen chain, generating G1P<sup>127</sup>. Subsequently, G1P is converted to G6P by the action of a debranching enzyme and, finally, G6P is converted into glucose by glucose-6-phosphatase (G6Pase)<sup>128,129</sup>. Glucose is then released from the hepatocytes into the bloodstream.

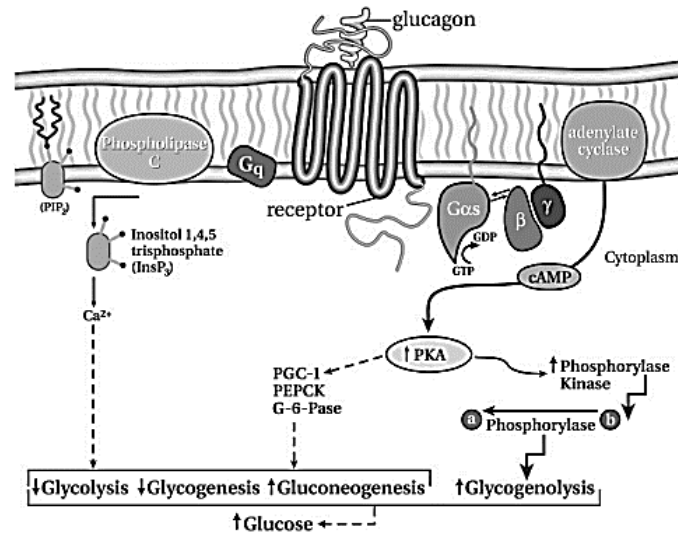


**Figure 8:** Glucagon hepatic signaling pathway<sup>128</sup>.

Glucagon signaling also induces hepatic glucose production from other substrates, such as glycerol, lactate, alanine and pyruvate, in a process named gluconeogenesis (**Figure 8**).

Gluconeogenesis is the reverse process of glycolysis—the generation of glucose from pyruvate—and it occurs when fasting exceeds ~8 hours in humans; at this time, gluconeogenesis replaces the breakdown of glycogen<sup>130</sup>. Molecularly, glucagon signaling inhibits pyruvate dehydrogenase (PDH), impeding glycolysis and also blocking the conversion of pyruvate to acetyl CoA. This mechanism allows pyruvate to be used as a substrate in gluconeogenesis<sup>120</sup>.

Other gluconeogenesis precursors are amino acids such as alanine and glutamine, which are converted into intermediates of the tricarboxylic acid cycle; lactate, which is converted into pyruvate by lactate dehydrogenase (LDH); and glycerol, which derives from increased lipolysis within white adipose tissue (WAT) under fasting conditions, where it is transformed into dihydroxyacetone phosphate (DHAP), a gluconeogenic intermediate, by glycerol kinase (GK) action<sup>119</sup>. Each of these precursors enters the gluconeogenic pathway through pyruvate, excepting glycerol which enters in this pathway as DHAP. All of them will be transformed into G6P<sup>131,132</sup>.

Gluconeogenesis happens primarily by three different steps<sup>133</sup>. The first step is characterized by the action of pyruvate carboxylase (PC), activated by mitochondrial acetyl-CoA (produced from increased fatty acid oxidation under fasting conditions), which transforms the pyruvate into oxalacetate<sup>119</sup>. Oxalacetate is converted into phosphoenolpyruvate (PEP) by phosphoenolpyruvate carboxykinase (PEPCK)<sup>134,135</sup>. Classically, PEPCK is considered the principal enzyme mediating gluconeogenesis<sup>99</sup>. In the second step, PEP is transformed into fructose-1,6-biphosphate (F1,6BP) by six sequential reactions, which are the reverse of glycolysis reactions. At this point, F1,6BP is transformed first, to fructose-6-phosphate (F6P) by the action of fructose biphosphatase (FBPase), and secondly, to G6P by a reverse reaction<sup>131,136</sup>. Finally, in the third step, the dephosphorylation of G6P to glucose occurs by G6Pase action<sup>137,138</sup> (**Figure 9**). G6Pase is expressed exclusively in liver and kidney, the only two organs capable of executing glucose production<sup>121,139–141</sup>. Glucose is then released from the hepatocytes into the bloodstream.

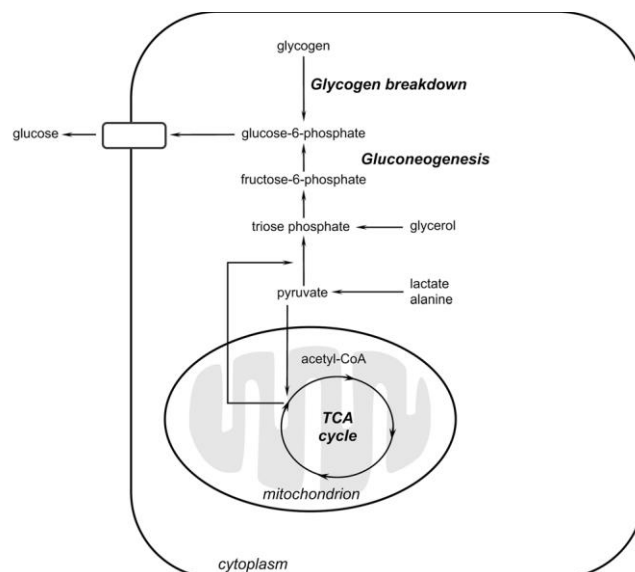


**Figure 9:** Simplified scheme of the major biochemical pathways activated during post-absorptive hepatic glucose production<sup>118</sup>.

In addition, cAMP response element-binding protein (CREB) and FoxO1, which is the best characterized and the most abundant FoxO family member in hepatocytes, represent the main transcriptional factors involved in hepatic

glucose production regulated by insulin/glucagon action<sup>142–145</sup>. Molecularly, in the fasted state, as consequence of active glucagon signaling<sup>146</sup>, nuclear CREB is activated via serine 133 phosphorylation by PKA, due to increased cAMP concentrations in the liver<sup>147</sup>; whereas FoxO1 remains in an un-phosphorylated state in the nucleus. Both activated CREB and un-phosphorylated FoxO1, increase the transcription rates of *Pepck*<sup>95,100,143–145</sup> and *G6p*<sup>145,148</sup> promoting hepatic glucose production. However, in the fed state and via insulin signaling, serine 133 of nuclear CREB is not phosphorylated; whereas AKT activation induces FoxO1 phosphorylation. As consequence, FoxO1 is excluded from the nucleus, ubiquitinated and degraded<sup>142,149,150</sup>. As a consequence, hepatic glucose production decreases, whereas glycogenesis and glycolysis increase<sup>99</sup>.

## 2.6 Insulin-degrading enzyme (IDE)

IDE is a 110-kDa metalloprotease, which requires a zinc atom to exert its catalytic activity (**Figure 10**), first identified and named based on its ability to bind to and degrade insulin<sup>96</sup>. IDE also degrades a number of other intermediate-sized (<80 amino acids) bioactive peptides, including glucagon, amylin and the amyloid  $\beta$ -protein (A $\beta$ )<sup>151</sup>.

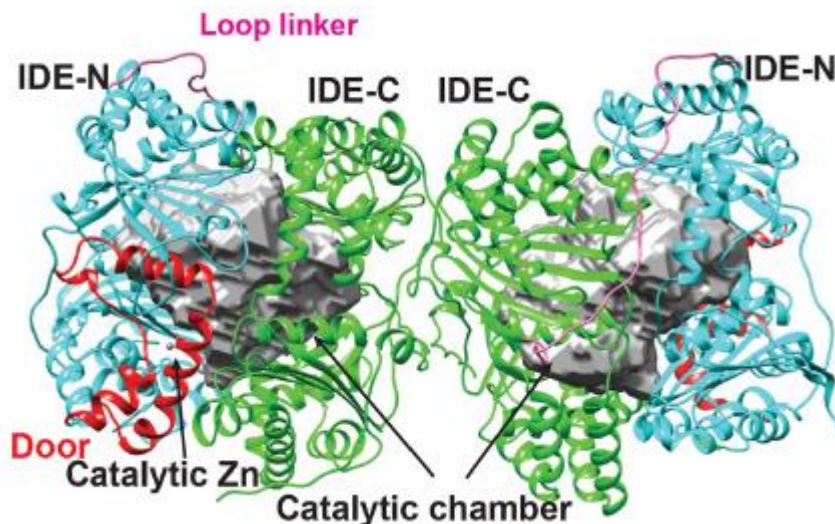


**Figure 10:** Crystal structure of a homodimer of IDE. IDE-N, IDE-C, catalytic zinc ion, and door subdomain are colored in cyan, green, grey and red, respectively; while the surface of catalytic chamber of IDE is in grey<sup>152</sup>.

IDE is ubiquitously expressed at varying levels in both insulin-responsive and nonresponsive cell types. Subcellularly, the protease is localized primarily within the cytosol, but it has been reported to exist within a number of intracellular vesicles, organelles, and associated with membranes, and it is also secreted into the extracellular space<sup>96,153,154</sup>. This distribution suggests a multifunctional role for this protein.

### **2.6.1 IDE substrates and its proteolytic activity**

The first IDE substrate described was insulin. Insulin has a short half-life in the bloodstream, due to the high efficiency of insulin clearance mechanisms, which occur primarily in liver and kidney, but also take place to a limited extent, in many other tissues<sup>96,155</sup>. Insulin clearance occurs by receptor-mediated internalization following the binding of insulin to the IR. Acidification of the endosomes after internalization leads to dissociation of insulin from its receptor. A subset of endosomes are returned to the cell surface, thus recycling the IR, while other endosomes travel to the lysosome, where insulin is believed to be degraded<sup>156–158</sup>. By this way, almost 50% of internalized insulin is degraded.

IDE also degrades and inactivates a number of other hormones, including glucagon, amylin<sup>159</sup> and beta-amyloid peptide (A $\beta$ )<sup>160</sup>. In addition, IDE degrades hormones, grow factors and neurotransmitters including endorphins, somatostatin, insulin-like growth factor II (IGF-II) and transforming growth factor alpha (TGF- $\alpha$ )<sup>96,151</sup>.

The substrate recognition mechanism of IDE is atypical, and follows from its unusual structure, which consists of two bowl-shaped halves (dubbed IDE-N and IDE-C) connected by a flexible linker that, together, form a large (~30,000 Å<sup>3</sup>), completely enclosed internal chamber (**Figure 10**). Substrates and products can enter and leave, respectively, only when IDE adopts an “open” conformation; conversely, IDE is only proteolytically active when in the “closed” conformation<sup>161–163</sup>. Due to the size of the catalytic chamber, IDE can cleave only peptides of up to 70 amino acids. In addition, substrates make numerous contacts throughout the internal chamber, thereby influencing which peptide bonds are

accessible to the active site; thus IDE does not show strong cleavage site specificity<sup>151</sup>.

Interestingly, some researchers think that IDE is involved in the regulation of proteasomal degradation. According to these researchers, association of IDE with the proteasome causes an increase in proteasome activity, which is closely involved in protein metabolism and is controlled by hormones, as insulin action<sup>164,165</sup>. In their proposed scenario, insulin activates protein synthesis and inhibits protein degradation by the dissociation of the IDE-proteasome complex due to IDE binding to and degrading insulin internalized into the cytosol (a controversial idea). As a consequence, insulin degradation by IDE is predicted to induce the dissociation of the IDE-proteasome complex which leads to the inhibition of proteasome activity<sup>166</sup>. Once insulin degradation is produced, cytosolic IDE is reassociated with the proteasome (**Figure 11**).

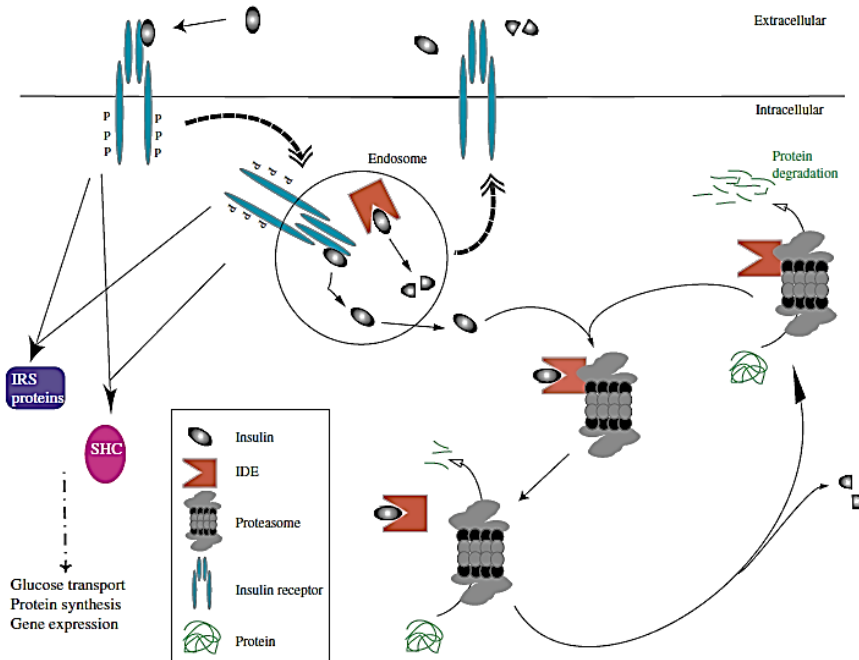


**Figure 11:** Schematic diagram of how insulin degradation acts to inhibit the proteasome<sup>167</sup>.

## 2.6.2 Animal models for the study of IDE

In order to clarify the physiological role of *Ide* and its links with T2DM, both invertebrate (e.g., *Drosophila*) and vertebrate (e.g., rodent) models have been developed and characterized. Genetic ablation of the *Ide* gene in *Drosophila* induced an increase of body weight and reduced blood glucose levels. In parallel, IDE overexpression resulted in body weight loss combined with an increase in blood glucose values<sup>168</sup>.

A well-known diabetic rat model developed by selective breeding for hyperglycemia and glucose intolerance, known as the Goto-Kakizaki (GK) rat, was discovered to harbor two missense mutations in the IDE gene, one of which results in partial loss of proteolytic function, thus strengthening the association of the *Ide* locus with susceptibility to T2DM<sup>169</sup>.

Mice with genetic deletion of *Ide* were first investigated by Farris *et al.*<sup>157</sup> Life-long, pancellular deletion (total knockout) of *Ide* in a combined genetic background (50% of C57BL/6 and 50% of 129SvEvBrd) at 4-8-months of age showed normal blood glucose levels, but exhibited pronounced glucose intolerance and hyperinsulinemia<sup>157</sup>.

The IDE knockout mice studied by Farris *et al.*, were characterized further by Abdul-Hay *et al.*<sup>170</sup>, this time in a complete C57BL/6 genetic background. Notably, these researchers conducted a longitudinal analysis, characterizing the same set of mice at 2, 4 and 6-months of age. As reported by Farris *et al.*, IDE knockout mice showed hyperinsulinemia at each time point. However, the glucose and insulin tolerance testing revealed a more complex, age-related phenotype. At 2-months of age, IDE knock-out mice exhibited a trend to establish modestly improved glucose tolerance and insulin sensitivity relative to controls. However, this trend was lost at 6-months of age, by which time IDE total knock-out mice exhibited marked glucose intolerance and insulin resistance. These researchers also found that IR levels were reduced in several peripheral tissues (liver, skeletal muscle and adipose tissue)<sup>170</sup>.

Finally, the same animal model was once again analyzed by Steneberg *et al.*<sup>171</sup>, who conducted an extensive investigation of the mechanistic basis underlying the insulin intolerance observed in IDE total knock-out mice. The metabolic characterization of 2-month-old mice disclosed a strong glucose intolerance without insulin resistance or hyperinsulinemia<sup>171</sup>. Steneberg *et al.*<sup>171</sup> emphasized the importance of IDE in insulin secretion regulation, since their IDE total knock-out mice showed decreased insulin secretion by pancreatic  $\beta$ -cells<sup>171</sup>.

### **2.6.3 Pharmacological therapies against T2DM based on inhibition of IDE activity**

Since the discovery of IDE in 1949 by I. Arthur Mirsky, it has been proposed that pharmacological inhibition of IDE might be a viable antidiabetic therapy. Assuming IDE is involved in the clearance of insulin, then in principle blocking the breakdown of insulin could boost insulin signaling. However, it would take more than 50 years before the first IDE inhibitors were developed, and inhibitors with sufficient properties to test this fundamental idea emerged only in the past few years<sup>172–175</sup>.

Despite the intuitive appeal of this idea, we need to take into account that different studies suggested that a strong decrease of IDE activity will not have a beneficial impact in whole metabolism of T2DM patients. In theory, if IDE is involved in insulin clearance, than chronic inhibition of IDE might result in persistent hyperglycemia, which could in turn further increase insulin resistance<sup>176</sup>. Chronic hyperinsulinemia can also lead to up-regulation of cell proliferation<sup>177</sup>. Moreover, numerous side effects are expected after IDE inhibition, due to IDE degradation activity on other metabolic substrates as glucagon, A $\beta$  and amylin. In the case of A $\beta$ , which accumulates abnormally in the brains of Alzheimer's patients, it has been shown that inhibitors of IDE that do not cross the blood-brain barrier do not effect A $\beta$ <sup>173</sup>. However, with regard to amylin, which accumulates in the pancreas, there is controversy about possible exacerbation of amylin deposition due to IDE inhibition. On the one hand, using a weak inhibitor of IDE, bacitracin, which is also not very selective Bennett *et al.*<sup>178</sup> reported that prolonged IDE inhibition leads to amyloid deposition<sup>178</sup> in

cultured islets. In contrast, using a much more potent and selective IDE inhibitor, Hogan *et al.*<sup>179</sup> reported that IDE inhibition does not increase islet amyloid deposition<sup>179</sup>. Apart from amylin, however, IDE inhibition could impede glucagon degradation, intensifying glucose intolerance as a consequence of an increase in postprandial gluconeogenesis values<sup>180</sup>. Moreover, assuming the veracity of studies implicating IDE in proteasomal degradation, inhibition of intracellular IDE might deregulate proteasomal degradation and autophagic flux<sup>171,181</sup> (**Figure 12**).

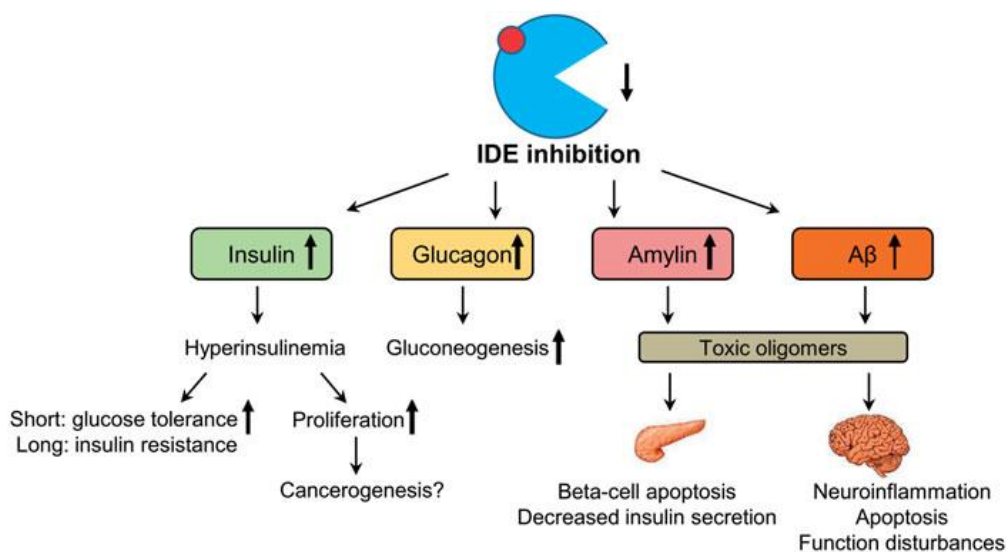


**Figure 12:** Possible side effects of pharmacological IDE inhibition<sup>182</sup>.

One of the most promising inhibitors of IDE is a highly potent and selective cyclic peptide known as 6bK, discovered and optimized by Maianti *et al.*<sup>173</sup> Acute administration of 6bK decreased blood glucose levels in lean and obese mice after glucose challenge. However, insulin, glucagon and amylin circulating levels were increased during intraperitoneal glucose tolerance test (IPGTT) after 6bK dose administration. Despite these abnormal hormonal concentrations found during IPGTT; insulin, glucagon and amylin levels remained unaltered in basal conditions<sup>173</sup>.

Durham *et al.*<sup>175</sup> developed another IDE inhibitor, known as NTE-1. Rats treated with NTE-1 showed improved glucose tolerance despite presenting with elevated plasma amylin concentrations. Interestingly, however, NTE-1 treatment

did not produce significant differences on insulin and glucagon degradation *in vivo*<sup>179</sup>.

Despite numerous studies linking IDE with T2DM, and despite IDE total-knock out mice having been generated and characterized, the role of IDE in the function of specific tissues remains unclear. To advance our understanding of the tissue-specific functions of IDE, the work within this thesis is focused on physiological and pathophysiological roles of IDE specifically in liver. In particular, we have extensively characterized the consequences of genetic ablation of *Id*e exclusively in liver, in order to elucidate the role of IDE in hepatic function, hepatic glucose metabolism and hepatic insulin action.

## **Hypotheses and Aims**



### **3 HYPOTHESES AND AIMS**

#### **3.1 Hypotheses**

- Hepatic depletion of IDE impairs plasma insulin clearance in the liver of mice.
- Genetic ablation of hepatic *Ide* causes insulin resistance and glucose intolerance in mice.
- IDE regulates intracellular insulin signaling through a molecular mechanism that impairs insulin signal transduction at the post-receptor level in mouse hepatocytes.

#### **3.2 Aims**

- To generate liver-specific *Ide* knockout (L-IDE-KO) mice by crossing the transgenic Albumin-Cre mouse and the IDE<sup>lox/lox</sup> mouse.
- To assess plasma insulin clearance in L-IDE-KO and wild type (WT) mice.
- To investigate glucose homeostasis in L-IDE-KO and WT mice (intraperitoneal glucose tolerance and insulin sensitivity).
- To quantify gene expression of the gluconeogenic genes *Pck1* and *G6pc* in the liver of L-IDE-KO and WT mice.
- To reveal the impact of hepatic *Ide* ablation on lipid metabolism.
- To analyze the impact of hepatic *Ide* ablation on intracellular insulin-signaling pathway in L-IDE-KO and WT mice liver.



## **Material and Methods**



## 4 MATERIAL AND METHODS

### 4.1 Animal procedures

#### 4.1.1 Animal facilities

Mice were housed in ventilated cages on a 14-h light, 10-h dark schedule at the animal facility of the University of Valladolid (UVa, Spain). Cage enrichment included cotton bedding. Water and food were available *ad libitum*, consisting of normal mouse chow. Experimental procedures were approved by the Animal Care and Use Committee of the UVa in accordance with the European and Spanish Guidelines for the Care and Use of Mammals in Research (European Commission Directive 86/609/CEE and Spanish Royal Decree 1201/2005) – Protocol number JCyL #5003931.

#### 4.1.2 Breeding strategies of liver-IDE knockout mice (L-IDE-KO)

Power analysis to determine animal cohort numbers was based on preliminary results and previous literature. The B6.Cg-Tg(Alb-cre)21Mgn/J (Alb-Cre) mouse was purchased from Jackson Laboratory, USA. The IDE<sup>Flox/Flox</sup> mouse was kindly provided by Dr. Malcolm A. Leissring from the University of California, Irvine, USA. This mouse has *loxP* sites flanking *exon 3* of the *Ide* gene. Cre recombinase-mediated deletion of *exon 3* causes a frameshift with two stop codons in *exon 4* and early termination of translation (**Figure 13**).

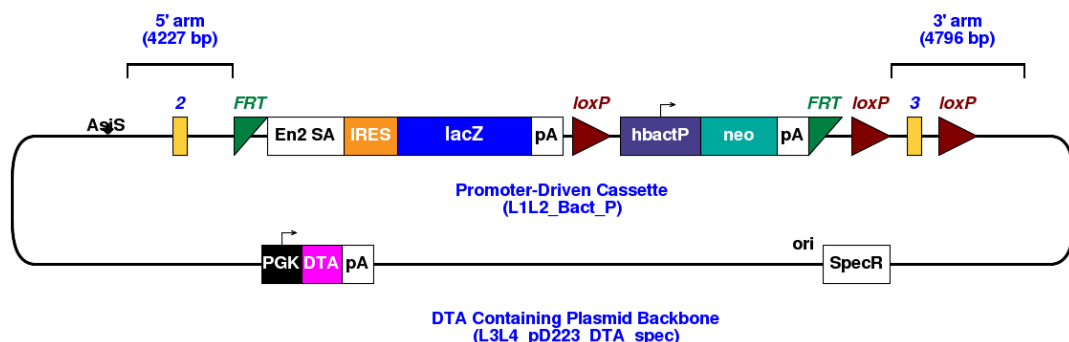


**Figure 13:** Details of *Ide* gene deletion in L-IDE-KO mice.

To generate hepatocyte-specific IDE-KO, Alb-Cre mice were crossed to IDE<sup>Flox/Flox</sup> to generate IDE<sup>Flox/Flox;Alb-Cre/+</sup>, or their littermate controls IDE<sup>Flox/Flox;+/+</sup> (Figure 14).

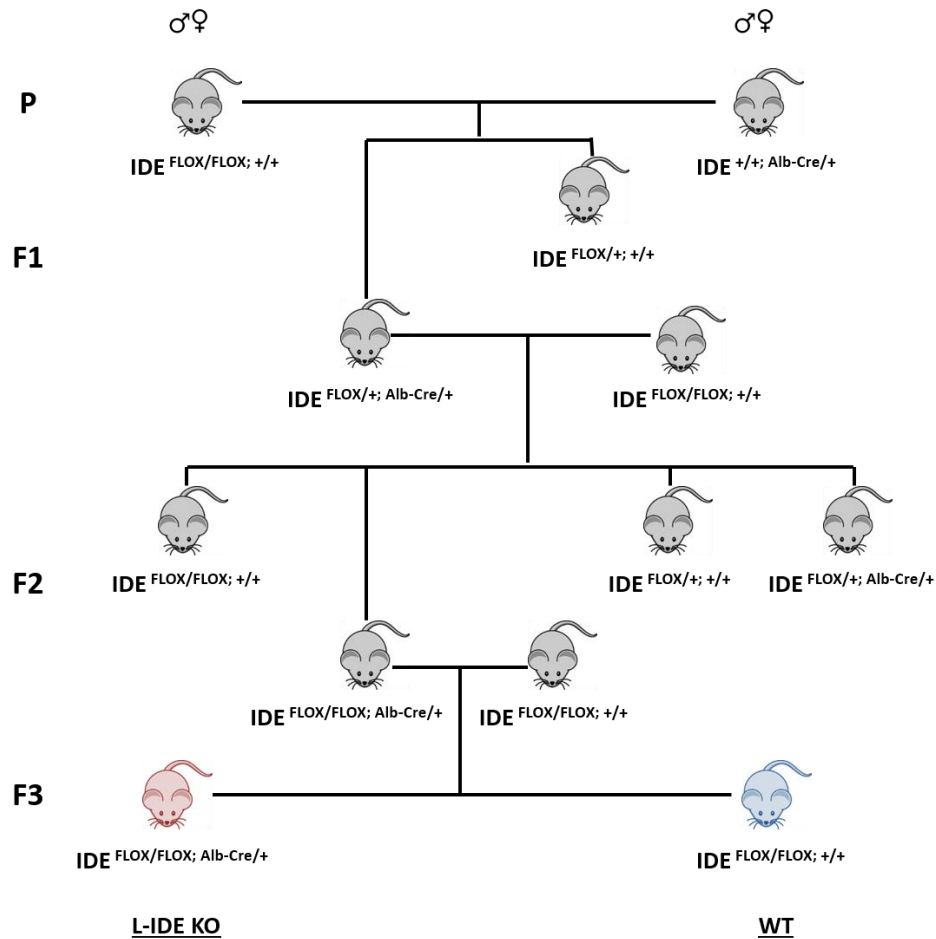


Figure 14: Breeding strategy for developing and maintaining the L-IDE-KO mouse colony.

## 4.2 Experimental animals

The experimental cohorts used in this study were males and females of the F3 generation. The F1 generation was composed of heterozygous IDE<sup>Flox/+;Alb-Cre/+</sup> and WT IDE<sup>Flox/Flox;+/+</sup>, from crosses of IDE<sup>Flox/Flox;+/+</sup> and IDE<sup>+/+;Alb-Cre/+</sup> in the parental generation.

F2 generation was composed of WT IDE<sup>Flox/Flox;+/+</sup>, IDE<sup>Flox/+;+/+</sup>, heterozygous IDE<sup>Flox/+;Alb-Cre/+</sup> and L-IDE-KO IDE<sup>Flox/Flox;Alb-Cre/+</sup> from crosses of heterozygous IDE<sup>Flox/+;Alb-Cre/+</sup> and IDE<sup>Flox/Flox;+/+</sup>.

In order to obtain only WT (IDE<sup>Flox/Flox;+/+</sup>) and L-IDE-KO (IDE<sup>Flox/Flox;Alb-Cre/+</sup>), F3 generation was generated from crosses between L-IDE-KO F2 generation (IDE<sup>Flox/Flox;Alb-Cre/+</sup>) and WT (IDE<sup>Flox/Flox;+/+</sup>) (**Figure 14**).

Twenty independent cohorts were used for the metabolic studies and collection of tissues in this work. Males and females were characterized at 1 and 3 months of age.

### 4.3 Mouse genotyping

DNA for genotyping was extracted from tails. Briefly, a tail snip of ~0.3-0.5 cm was incubated in 50 µL of Quick Extract (Epicentre, USA) at 65 °C for 8 min, followed by mixing by vortex for 10 to 15 s. Afterwards, samples were incubated 2 min at 98 °C, followed by 10-15 s mixing by vortex, and frozen at -20 °C until its use.

The PCR reaction preparation is listed in **Table 5**. The PCR reaction master mix was scaled up according the samples number.

Component	Stock Concentration	Volume per Reaction (µL)
Buffer Reaction Mix (Bioline, UK)	5x	8
Primer Forward (Metabion, Germany)	100 µM	0,20
Primer Reverse (Metabion, Germany)	100 µM	0,20
My Taq DNA Polymerase (Bioline, UK)	5 u/µL	0,25
Nuclease-free Water	-	30,35
DNA Sample	-	1
Final Volume		40

**Table 5:** PCR master mix reagents for the setup of one reaction.

Three different genes were routinely distinguished by PCR analysis. *GAPDH* was used as a control for the quality of DNA extraction, *Ide* and *Alb-Cre* were detected by using the primers showed in **Table 6**. In **Table 7**, **8** and **9** are described the PCR conditions for *GAPDH*, *Ide* and *Alb-Cre* genes respectively.

Gen	Sequence	pb
<b><i>GAPDH</i></b>	5' – CGT GGA GTC TAC TGG TGT CTT – 3' 5' – GAT GGC ATG GAC TGT GGT CAT – 3'	250
<b><i>Ide</i></b>	5' – AAC TGC CAC CTG TCC AAT CC – 3' 5' – CTC AGG GAT ACA ATG CGT GC – 3'	WT 418 only HT 650, 418 Homo 650 only
<b><i>Alb-Cre</i></b>	5' – TGC AAA CAT CAC ATG CAC AC – 3' 5' – TTG GCC CCT TAC CAT AAC TG – 3' 5' – GAA GCA GAA GCT TAG GAA GAT GG – 3'	WT 351 only HT 390. 351 Mutant 390 only

**Table 6:** Primer sequences used for mouse genotyping and the sizes of resulting amplicons.

<b><i>GAPDH</i> PCR Amplification Program</b>		
Step	Temperature	Time
Initial denaturation	94°C	5'
Denaturation Annealing Elongation	94°C 56°C 72°C	30" 30" 30" } 35 cycles
Elongation	72°C	7'
Hold	4°C	∞

**Table 7:** PCR conditions for amplification of *GAPDH*.

<b>Ide PCR Amplification Program</b>		
<b>Step</b>	<b>Temperature</b>	<b>Time</b>
Initial denaturation	94°C	5'
Denaturation Annealing Elongation	94°C 58°C 72°C	30" 30" 45" } 35 cycles
Elongation	72°C	7'
Hold	4°C	∞

**Table 8:** PCR conditions for amplification of IDE.

<b>Alb-Cre PCR Amplification Program</b>		
<b>Step</b>	<b>Temperature</b>	<b>Time</b>
Initial denaturation	94°C	2'
Denaturation Annealing Elongation	94°C 65°C (-0.5°C per cycle) 68°C	20" 15" 10" } 10 cycles
Denaturation Annealing Elongation	94°C 60°C 72°C	15" 15" 10" } 28 cycles
Elongation	72°C	2'
Hold	4°C	∞

**Table 9:** PCR conditions for amplification of Alb-Cre.

To visualize PCR products, samples were mixed with DNA-loading buffer (Bioline, UK) and loaded into 1% agarose gels (for GAPDH and IDE) or on 2% agarose gels (for Alb-Cre). Afterwards, samples were run at 120V for approximately half an hour in 1X TBE buffer (89 mM Tris-HCl, pH 7.6, 89 mM boric acid and 2 mM EDTA). Finally, agarose gels were stained with 2.5 µL red safe (iNtRON Biotechnology, South Korea) and visualized on a shortwave UV radiation transilluminator (**Figure 15**).

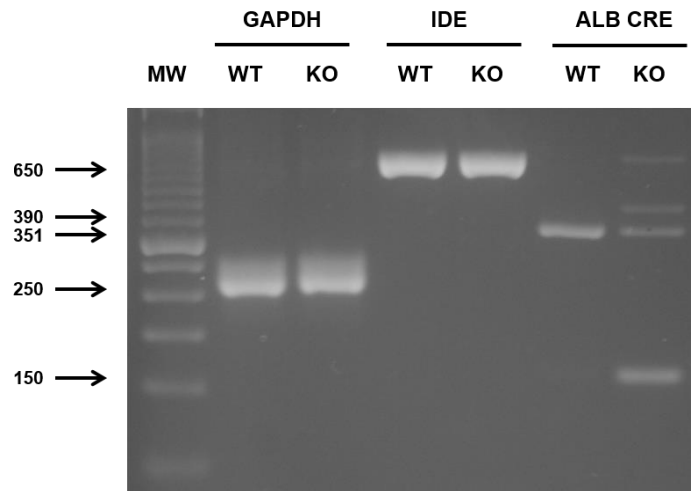


**Figure 15:** Representative image of mouse genotyping. On the left are depicted the molecular sizes of the amplicons (base pairs).

## 4.4 Metabolic characterization

### 4.4.1 Body weight

Body weight was monitored periodically using a digital weight scale (Adam Equipment, USA).

### 4.4.2 Food intake

For food intake determination, L-IDE-KO and WT mice were separated in individual cages (n = 7-11 mice per genotype). After 15 h fasting, food pellets (40 g) were added to each cage; and the food intake of each mouse was estimated from the difference in remaining food weight 24 h later. These weights were averaged to provide an estimate of the mean food intake of each genotype in 24 h.

### 4.4.3 Blood sampling

For obtaining blood, 1-2 mm of tissue was cut from the tail tip with a scalpel (Romed, Holland). Then, blood was obtained by direct flow or by gently massaging (“milking”) the tail and collecting the blood in a capillary tube coated with potassium-EDTA (Microvette, Stardest, Germany).

#### 4.4.4 Plasma collection

To acquire plasma, blood samples (50-100  $\mu$ L) obtained as described above, were centrifuged at 2600 X g for 10 min at room temperature. Afterwards, plasma was transferred into a clean polypropylene tube using a micropipette. The samples were kept on ice and then stored at -20 °C.

#### 4.4.5 Blood glucose levels

Blood glucose levels were determined using a Breeze 2 glucometer (Bayer, Germany). Blood glucose measurements were performed in mice under fasting or non-fasting conditions. Fasting conditions are considered as a period of 14-16 h without food and non-fasting conditions are considered just after the dark schedule, at 8:00 a.m.

#### 4.4.6 Homeostatic Model Assessment (HOMA) index

The HOMA index is a method used to quantify insulin resistance. This index is overnight fasting blood glucose levels x fasting plasma insulin levels/22.5. The normal HOMA value of healthy humans ranges from 1.5-2.0; however, values above 2.0 indicates significant insulin resistance<sup>183</sup>. In mice, there is not a HOMA cut off value; in practice, insulin resistance is determined by comparing HOMA values obtained from experimental mice to their control littermates. This index was first described under the name HOMA by Matthews *et al.* in 1985<sup>184</sup>.

In our study, data were analyzed by HOMA Calculator software (University of Oxford, United Kingdom).

#### 4.4.7 Plasma insulin levels

Insulin levels were assessed employing the Ultrasensitive Mouse and Human Insulin enzyme-linked immunosorbent assay (ELISA) kit (Mercodia, Sweden), using 10  $\mu$ L of mouse plasma. This ELISA is a solid-phase two-site enzyme immunoassay. It is based on the direct sandwich technique in which two monoclonal antibodies are directed against separate antigenic determinants on

the insulin molecule (**Figure 16**). Insulin in the plasma sample binds to anti-insulin antibodies attached to the microtitration well and the quantity is detected using another peroxidase-conjugated anti-insulin antibody. A simple washing step removes unbound enzyme-labeled antibody. The bound conjugate is detected by reaction with TMB (3,3',5,5'-tetramethylbenzidine). The reaction is stopped by adding acid to give a colorimetric endpoint that is read spectrophotometrically at a wavelength of 450 nm using a microplate reader (Heales, China). The intensity of this colored product is directly proportional to the concentration of insulin present in the original specimen. The concentration in plasma samples can be determined by conversion of the values of absorbance using a standard curve.

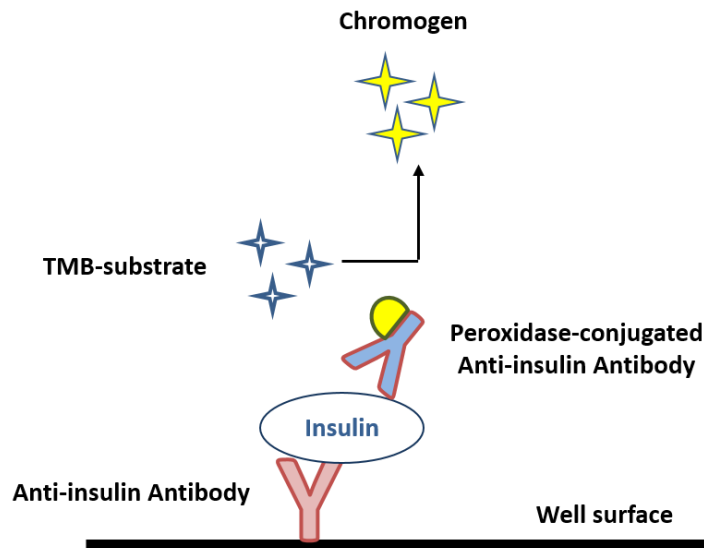


**Figure 16:** Illustration of insulin detection using the ELISA technique.

#### 4.4.8 Plasma glucagon levels

Glucagon levels were assessed employing the glucagon ELISA kit (Merckodia, Sweden), using 10  $\mu$ L of mouse plasma. This glucagon ELISA kit recognizes glucagon from mouse, rat and human origin. This ELISA is a solid-phase two-site enzyme immunoassay. It is based on the direct sandwich technique in which two monoclonal antibodies are directed against separated antigenic determinants on the glucagon molecule (**Figure 17**). Glucagon in the plasma sample binds to anti-glucagon antibodies (clone M5F9S) attached to microplate wells and are

detected by a different peroxidase-conjugated anti-glucagon antibody (clone E6A11K). A simple washing step removes unbound enzyme labelled antibody. The bound conjugate is detected by reaction with TMB. The reaction is stopped by adding acid to give a colorimetric endpoint that is read spectrophotometrically at a wavelength of 450 nm using a microplate reader (Heales, China). The intensity of this colored product is directly proportional to the concentration of glucagon present in the original specimen. A standard curve of known concentration can be established accordingly. The unknown concentration in samples can be determined by reference to this standard curve.

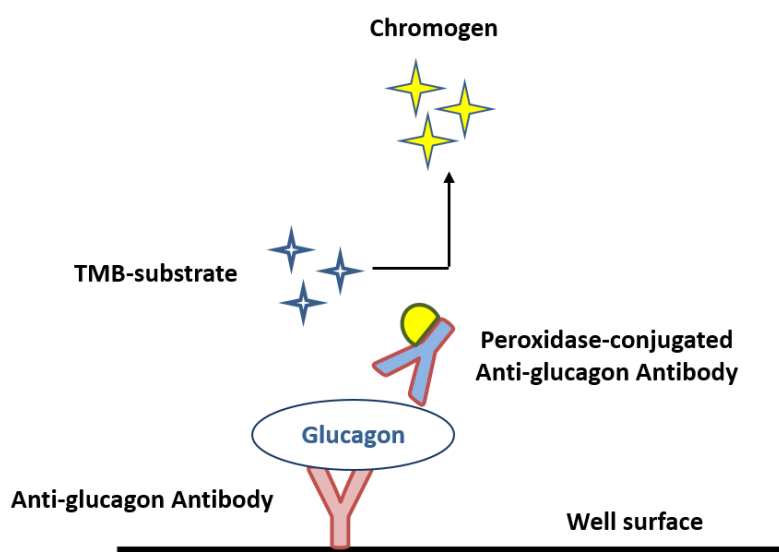
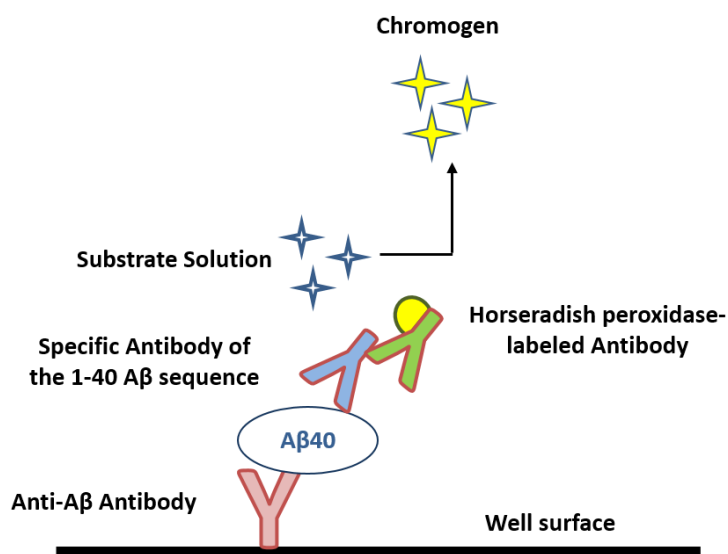


Figure 17: Illustration of glucagon detection using the ELISA technique.

#### 4.4.9 Plasma A $\beta$ 40 levels

A $\beta$ 40 levels were assessed employing the Mouse A $\beta$ 40 ELISA kit (Invitrogen, USA), using 100 $\mu$ L of mouse plasma. This ELISA is a solid-phase sandwich-based assay. A monoclonal antibody of mouse A $\beta$  has been coated onto the wells of the microtiter strips. Samples, including standards of known mouse A $\beta$ 40 content, are pipetted into these wells. The A $\beta$ 40 antigen binds to the immobilized antibody. After washing, a rabbit antibody specific for the 1-40 A $\beta$  sequence is added to the wells. Bound rabbit antibody is detected by the use of a horseradish peroxidase-labeled anti-rabbit antibody. After removal excess of anti-rabbit

antibody, a substrate solution is added and it reacts to the bound enzyme to produce color (**Figure 18**). The microplate is read spectrophotometrically at a wavelength of 450 nm using a microplate reader (Heales, China). The intensity of this colored product is directly proportional to the concentration of Mouse A $\beta$ 40 present in the original specimen. A standard curve of known concentration can be established accordingly. The unknown concentration in samples can be determined by extrapolation to this standard curve.



**Figure 18:** Illustration of A $\beta$ 40 detection using the ELISA technique.

#### 4.4.10 Plasma amylin levels

Amylin levels were assessed employing the mouse amylin enzyme immunoassay (EIA) kit (Phoenix Pharmaceuticals, USA), using 50  $\mu$ L of mouse plasma. The immunoplate in this kit is pre-coated with secondary antibody and the nonspecific binding sites are blocked. The secondary antibody can bind to the crystallizable fragment (Fc) region of the primary antibody whose antigen-binding fragment (Fab) site will be competitively bound by both biotinylated peptide and standard peptide or targeted peptide in samples. The biotinylated peptide interacts with streptavidin-horseradish peroxidase (SA-HRP) which catalyzes the substrate solution (**Figure 19**). The microplate is read spectrophotometrically at a wavelength of 450 nm using a microplate reader

(Heales, China). The intensity of the yellow is directly proportional to the amount of biotinylated peptide-SA-HRP complex but inversely proportional to the amount of the peptide in standard solutions or samples. This is due to the competitive binding of the biotinylated peptide with the standard peptide or samples to the peptide antibody (primary antibody). A standard curve of known concentration can be established accordingly. The unknown concentration in samples can be determined by reference to this standard curve.

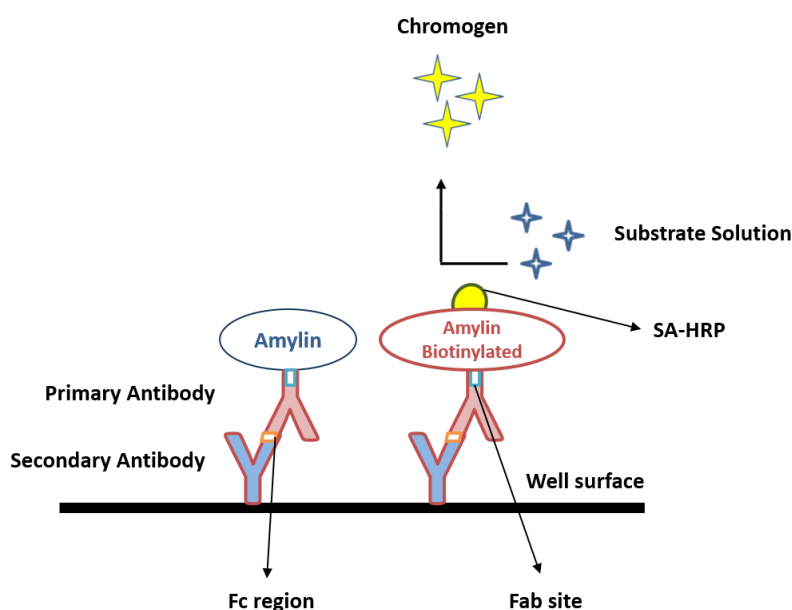
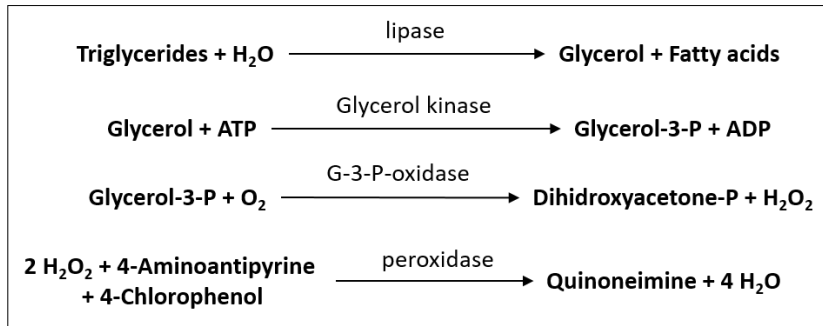


Figure 19: Illustration of amylin detection using the competitive ELISA technique.

#### 4.4.11 Plasma triglycerides levels

Triglycerides levels were assessed employing the triglycerides colorimetric kit (Biosystems, Spain), using 3  $\mu$ L of mouse plasma. Triglycerides in the samples result in, by means of coupled reactions (**Figure 20**), a colored complex that can be measured by spectrophotometry at a wavelength of 500 nm using a microplate reader (Heales, China). The intensity of this colored product is directly proportional to the concentration of triglycerides present in the original specimen. A standard curve of known concentration can be established accordingly. The unknown concentration in samples can be determined by reference to this standard curve.



**Figure 20:** Principle of the method to assess plasma triglycerides levels.

#### 4.4.12 Plasma cholesterol levels

Cholesterol levels were assessed employing the cholesterol colorimetric kit (Biosystems, Spain), using 3  $\mu\text{L}$  of mouse plasma. Free and esterified cholesterol in the samples results in, by means of the coupled reactions (**Figure 21**), a colored complex that can be measured by spectrophotometry at a wavelength of 500 nm using a microplate reader (Heales, China). The intensity of this colored product is directly proportional to the concentration of free and esterified cholesterol present in the original specimen. A standard curve of known concentration can be established accordingly. The unknown concentration in samples can be determined by reference to this standard curve.

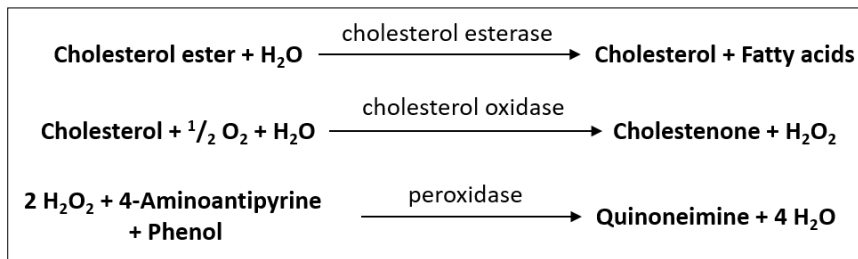


**Figure 21:** Principle of the method to assess plasma cholesterol levels.

#### 4.4.13 Plasma Non-Esterified Free Fatty Acids (NEFFAs) levels

NEFFAs were assessed employing the NEFFA-HR(2) kit (Wako, Germany), using 5  $\mu\text{L}$  of mouse plasma. The contents of one flask of “reagent A” were dissolved with 50 mL of “buffer A” to obtain “solution A”. “Solution B” was prepared by dissolving the contents of one flask of “reagent B” with 25 mL of “buffer B”. 5  $\mu\text{L}$  of mouse plasma were sampled and mixed with 200  $\mu\text{L}$  of

“solution A” and incubated at 37 °C for 5 min. Thereafter, 100 µL of “solution B” was added and incubated for 5 min at 37 °C. After the second incubation period, the microplate was read spectrophotometrically at a wavelength of 562 nm using a microplate reader (Heales, China). The intensity of this colored product is directly proportional to the concentration of NEFFAs present in the original specimen. A standard curve of known concentration can be established accordingly. The unknown concentration in samples can be determined by extrapolation to this standard curve.

The principle of the method and the chemical reactions occurring in this process are described in **Figure 22**.

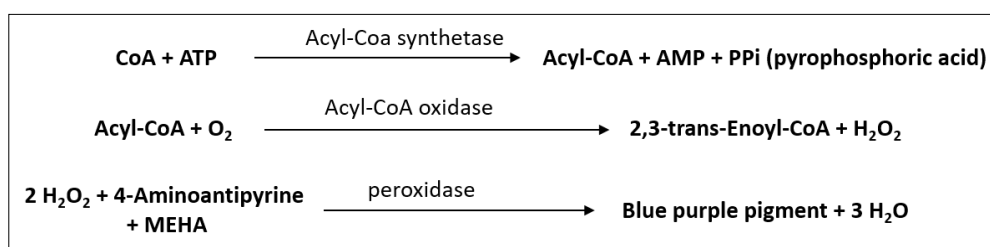


**Figure 22:** Principle of the method to assess plasma non-esterified free fatty acids levels.

#### 4.4.14 Glucose tolerance test (GTT)

To evaluate alterations in glucose homeostasis *in vivo*, we performed intraperitoneal glucose tolerance test (IPGTT) when mice were 1 and 3 months old. Mice were fasted overnight from 6 p.m. to 9 a.m. Glucose (Merck, USA) at 2 g/kg body weight was injected into the intraperitoneal cavity. Blood glucose levels were measured before glucose challenge (time 0) and 15, 30, 60 and 120 min after glucose injection using a Breeze 2 glucometer (Bayer, Germany).

The area under the curve (AUC) is the area between the graph and the X-axis, it is given by the definite integral below. A definite integral has start and end values: in this case, time 0 and time 120 minutes.

#### 4.4.15 Insulin tolerance test (ITT)

To evaluate insulin action *in vivo*, we performed intraperitoneal insulin tolerance test (IPITT) when mice were 1 and 3 months old. Mice were in non-fasted conditions. Human insulin (Humulin; Lilly, USA) at a dose of 0.75 U/kg body weight was injected intraperitoneally in mice. Blood glucose levels were monitored before insulin injection (time 0) and 15, 30, 60, 90, 120, 240 min after insulin injection using a Breeze 2 glucometer (Bayer, Germany).

The area under the curve (AUC) is the area between the graph and the X-axis, it is given by the definite integral below. A definite integral has start and end values: in this case, time 0 and time 240 minutes.

#### 4.4.16 Pyruvate tolerance test (PTT)

To evaluate alterations in hepatic glucose production *in vivo*, we performed intraperitoneal pyruvate tolerance test (IPPTT) when mice were 3 months old. Mice were fasted overnight from 6 p.m. to 9 a.m. Pyruvate (Sigma, USA) at 2 g/kg body weight was injected into the intraperitoneal cavity. Blood glucose levels were measured before pyruvate injection (time 0) and 15, 30, 60 and 120 min after pyruvate injection using a Breeze 2 glucometer (Bayer, Germany).

The area under the curve (AUC) is the area between the graph and the X-axis, it is given by the definite integral below. A definite integral has start and end values: in this case, time 0 and time 120 min.

#### 4.4.17 *In vivo* insulin clearance

3-month-old mice were fasted for 2 h (from 8 a.m. to 10 a.m.) and then anesthetized using a solution of medetomidine + ketamine at 0,125m-k/100 g body weight. Afterwards, human insulin (Humulin; Lilly, USA) was injected intra-orbitally at 1 nmol/kg. Immediately after injection, timing was started and blood samples were collected from the tail vein 0, 5, 10, 20, 30 and 60 min after insulin administration. These samples were prepared as described in section 4.4.4 and used for determination of human plasma insulin levels.

#### **4.4.18 Liver glycogen content**

Liver glycogen content was assessed employing the glycogen content assay kit (Sigma, USA), an enzymatic colorimetric assay.

Liver samples (10 mg) were homogenized in 100  $\mu$ L ultrapure water supplemented with protease and phosphatase cocktail inhibitors (Sigma, USA) on ice. Homogenates were boiled at 100  $^{\circ}$ C for 5 min to inactivate enzymes and centrifuged 5 min at 12300 X g at room temperature to remove insoluble materials.

Liver homogenates were collected and diluted 1:100 in duplicate in hydrolysis buffer up to a final volume of 50  $\mu$ L. To one of the duplicates 2  $\mu$ L of hydrolysis enzyme mix were added; while, to the other duplicates 2  $\mu$ L of ultrapure water were added. These last samples were used as controls of hepatic glucose content in each liver. After that, the microplate was incubated for 30 min at room temperature. Then, 50  $\mu$ L of master reaction mix, which contains the development buffer (46  $\mu$ L), the development enzyme mix (2  $\mu$ L) and the fluorescent peroxidase substrate (2  $\mu$ L), was added to each well and incubated for 30 min at room temperature. During the reaction incubation, the plate was protected from light. Finally, the microplate was read spectrophotometrically at a wavelength of 562 nm using a microplate reader (Heales, China). The intensity of this colored product is directly proportional to the concentration of glycogen present in the original specimen. A standard curve of known concentration can be established accordingly. The unknown concentration in samples can be determined by reference to this standard curve.

#### **4.5 Tissue dissection**

As a general procedure, mice were euthanized using cervical dislocation or by CO<sub>2</sub> inhalation. For those experiments that required insulin signaling activation, 3-month-old mice were fasted overnight from 6 p.m. to 9 a.m. Then, mice were injected intraperitoneally with human insulin (Humulin; Lilly, USA) at a dose of 0.75 U/kg body weight or with saline solution. After 10 min, mice were

anesthetized with isoflurane atmosphere, followed by exsanguination and tissues removal. Blood and plasma samples were prepared and stored as described in section 1.5.4.

Liver, white adipose tissue (WAT), brain, lungs, kidneys, heart, soleus and gastrocnemius muscles were removed and snap frozen in liquid nitrogen and stored at -80 °C until analysis.

## 4.6 Western blot

Protein lysates from animal tissues were prepared by homogenizing the tissues in lysis buffer (Cell signaling, USA) supplemented with protease and phosphatase cocktail inhibitors (Sigma, USA). Lysates were sonicated for 20 min on ice, and were centrifuged at 18500 X *g* for 10 min at 4 °C to separate and discard insoluble materials. Supernatants were kept and quantified for protein content using the Pierce BCA proteins assay kit (Thermo-Fisher, USA).

For the extraction of membrane proteins from liver tissues, we used the Plus Membrane Protein Extraction Kit (Thermo-Fisher, USA) following manufacturer's instructions. Briefly, to separate cytosolic and membrane fractions 30 mg of liver was cut and washed with the Cell Wash Solution, transferred to a glass tissue grinder where it was homogenized by 6-10 strokes and incubated 10 min at 4 °C with constant mixing. Lysates were centrifuged at 18500 X *g* for 15 min at 4 °C to separate cytosolic (supernatant) and membrane (pellet) fractions. Subsequently, supernatant was removed and pellet was resuspended in Solubilization Buffer by pipetting, incubated 40 min at 4 °C with constant mixing and centrifuged at 18500 X *g* for 15 min at 4 °C. The supernatant, which contains the membrane and membrane-associated proteins, was transferred to a new tube. Again, proteins were quantified by Pierce BCA proteins assay kit (Thermo-Fisher Scientific, USA). Afterwards, 40 µg of protein from the tissue lysate soluble fraction were boiled 5 min in Laemmli Sample Buffer (LSB) (62.5 mM Tris-HCl, 5% glycerol, 1% SDS, 2.5% β-mercaptoethanol and 0.02% w/v bromophenol blue). Protein samples were separated by their molecular weight using 10% SDS-PAGE

precast polyacrylamide gel (Criterion Tris-HCl protein gel, Bio Rad, USA) and electro-transferred onto polyvinylidene difluoride filters (PVDF; Millipore, USA) for immunoblotting by conventional means. Electro-transferred PVDF membranes were blocked for 1 h at room temperature using blocking buffer (1X PBS, 0.1% Tween-20 with 5% w/v non-fat dry milk). After being probed with specific antibodies, the membranes were stripped using stripping buffer (2% SDS, 62.5mM Tris-HCl, pH 6.8 and 100mM  $\beta$ -mercaptoethanol) for 30 min at 50 °C and then washed and reprobed with other antibodies. Signals were detected by chemiluminescence (Clarity Western ECL Substrate kit; Bio Rad, USA) and band densitometry was quantified with Image J software (National Institutes of Health, USA).

A list of the antibodies, dilutions and incubation times used in this work is provided in **Table 10** and **11**.

Antibody	Supplier	Catalog Number	Dilution in Blocking Buffer	Incubation Time & °C	Species	Size
p-IGF-IR $\beta$ (Tyr1135/1136)	Cell Signaling	#3024	1:1000	O/N 4°C	Rabbit	95 kDa
IR $\beta$	Cell Signaling	#3025	1:1000	O/N 4°C	Rabbit	95 kDa
p-Akt1 (Ser473)	Cell Signaling	#9271	1:1000	O/N 4°C	Rabbit	60 kDa
Akt1	Cell Signaling	#9272	1:1000	O/N 4°C	Rabbit	60 kDa
p-Akt2 (Ser474)	Cell Signaling	#8599	1:1000	O/N 4°C	Rabbit	60 kDa
Akt2	Cell Signaling	#3063	1:1000	O/N 4°C	Rabbit	60 kDa
p-GSK-3 $\alpha/\beta$ (Ser21/9)	Cell Signaling	#9327	1:1000	O/N 4°C	Rabbit	51, 46 kDa
GSK-3 $\alpha/\beta$	Cell Signaling	#5676	1:1000	O/N 4°C	Rabbit	51, 46 kDa
IDE	Millipore	AB9210	1:15000	O/N 4°C	Rabbit	110 kDa
Actin Ab-5	BD Bioscience	612656	1:8000	O/N 4°C	Mouse	42 kDa
$\alpha$ Na/K-ATPase	Abcam	ab7671	1:10000	O/N 4°C	Mouse	112 kDa

**Table 10:** List of primary antibodies.

Antibody	Supplier	Catalog Number	Dilution in Blocking Buffer	Incubation Time & °C
Anti-Rabbit IgG-HRP	Jackson Immuno	711-035-152	1:12000	30 min RT
Anti-Mouse IgG-HRP	GE Healthcare	NA9310	1:2000	30 min RT

**Table 11:** List of secondary antibodies.

## 4.7 RNA isolation and cDNA synthesis

Tissues obtained from L-IDE-KO and WT mice were lysed in 1 mL of Trizol (Invitrogen Life Technologies, USA) by micro tissue homogenizer. Following homogenization, samples were incubated for 5 min at room temperature, to complete the dissociation of nucleoprotein complexes, and centrifuged at 10500 X *g* for 10 min at 4 °C to remove insoluble material from the homogenate. The resulting pellet contained extracellular membranes and high molecular weight DNA, while the supernatant contained RNA. This supernatant was transferred to a new tube. Then, 200 µL of chloroform (PanReac AppliChem, Germany) was added, and samples were incubated 2-3 min at room temperature after a vigorous shaking by hand. Samples were centrifuged at 10500 X *g* for 15 min at 4 °C and consequently the mixture was separated in 3 different phases: a lower red phase rich in proteins, a deep red interphase rich in DNA, and a colorless or aqueous phase rich in RNA. The aqueous phase was transferred to a new tube.

Afterwards, 500 µL of isopropyl alcohol (PanReac AppliChem, Germany) was added to precipitate the RNA from the aqueous phase. Samples were mixed vigorously by hand, incubated 15 minutes at room temperature and centrifuged at 10500 X *g* for 10 min at 4 °C. The RNA precipitate forms a pellet on the side and bottom of the tube. The supernatant was removed. In order to wash the RNA obtained, 1 mL of 75% ethanol was added to each sample, mixed vigorously by hand and centrifuged at 4000 X *g* for 5 min at 4 °C. At the end of this procedure, supernatants were removed and the RNA pellet was air-dried for 20 min. Finally, RNA was dissolved in RNase-free water and incubated for 5 min at 60 °C. The amount of RNA from each sample was quantified by NanoDrop (Thermo-Fisher Scientific, USA) using 1 µL of sample (**Figure 23**).

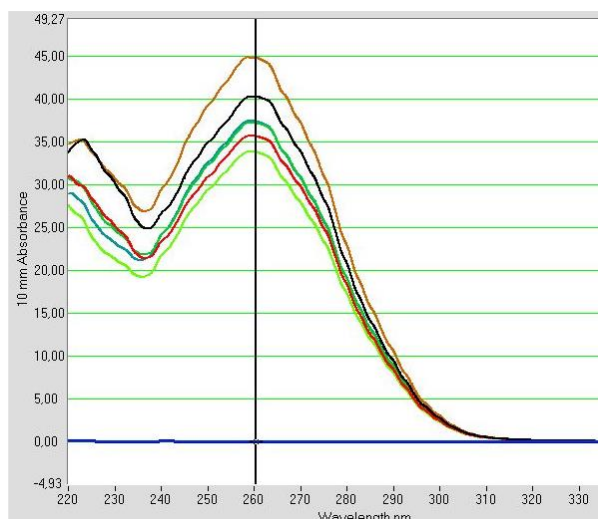


**Figure 23:** Representative illustration of RNA quantification by NanoDrop.

Once RNA isolation was completed, DNA residues were removed by RapidOut DNA removal kit (Thermo-Fisher Scientific, USA), which ensured complete digestion of DNA without RNA damaging. First, RNA sample was treated with recombinant DNase-I 30 min at 37 °C. Second, DNase-I was safely removed using DNase removal reagent, which binds DNase-I, allowing the complex to be pelleted by centrifugation. The purified RNA was collected in the supernatant fraction.

To perform cDNA synthesis from RNA, iScript cDNA synthesis kit (Bio Rad, USA) was used, which is a sensitive, fast, and convenient reagent for gene expression analysis using real-time reverse transcription quantitative PCR (RT-qPCR). To carry out the reverse transcription reaction, a mixture was made as indicated in the **Table 12**.

Component	Stock Concentration	Volume per Reaction ( $\mu\text{L}$ )
Buffer Reaction Mix (Bio Rad, USA)	5x	4
Reverse Transcriptase Enzyme (Bio Rad, USA)	-	1
Nuclease-free Water	-	5,5
RNA Template	100ng/ $\mu\text{L}$	9,5
<b>Final Volume</b>		20

**Table 12:** Reverse transcription reaction mix.

Once the reaction mixture was prepared, was incubated in the 2720 thermal cycler (Applied Biosystems, USA) using the following protocol (**Table 13**) to obtain the cDNA necessary to carry out the RT-qPCR.

Retro-transcriptase Reaction Program		
Step	Temperature	Time
Priming	25°C	5'
Reverse Transcription	46°C	30'
RT inactivation	85°C	5'
Final Step	4°C	$\infty$

**Table 13:** Thermocycler retro-transcription reaction protocol.

## 4.8 RT-qPCR

Prior to initiate the RT-qPCR, a PCR master mix solution was prepared as shown in **Table 14**.

Component	Stock Concentration	Volume per Reaction (μL)
qPCR Master Mix (Thermo-Fisher Scientific, USA)	2x	10
TaqMan® Probe (Applied Biosystems, USA)	-	1
Nuclease-free Water	-	8
cDNA Sample	-	1
Final Volume		20

**Table 14:** RT-qPCR master mix reagents for one reaction.

mRNA levels were determined by RT-qPCR with TaqMan® probes (Applied Biosystems, USA) using a Rotor-Gene 3000 thermocycler (Corbett Life Science, USA). Data were analyzed with the threshold cycle relative quantification method ( $\Delta\Delta C_t$ ) and normalized to an endogenous control (ribosomal protein L18). TaqMan assays were used for *Ide*, *Pck1* and *G6pc* (Applied Biosystems, USA) genes.

## 4.9 Statistical analysis

Statistical analysis of data was performed using the GraphPad Prism Software 6.0 (CA, USA). Distributions were checked with the Kolmogorov-Smirnov test. Data are presented as means  $\pm$  SEM. Homogeneity of variance was performed using the Levene test. Comparisons between two groups were done using the unpaired Students' T-test (if homogeneity of variance) or the Welch test (if heterogeneity of variance) when a variable was distributed normally; in the case of a non-parametric variable the Mann-Whitney U-test was used. Comparisons between more than two groups were done using the one-way ANOVA or the Kruskal-Wallis test when a variable was distributed normally or non-normally, respectively. For post-hoc analyses the Bonferroni test or Durnett test was used if homogeneity or heterogeneity of variance respectively. Differences were considered significant at  $p < 0.05$ .



## **Results**



## 5 RESULTS

### 5.1 Generation and analysis of Liver-specific *Ide* knock-out mice

To ablate *Ide* in hepatocytes, we bred mice homozygous for a floxed *Ide* allele (Dr. Malcolm Leissring, University of California, Irvine) with albumin-Cre mice (Jackson Laboratory, USA). Hereafter, these mice will be named L-IDE-KO. Hepatic *Ide* mRNA levels (**Figure 24**) and protein (**Figure 25**) levels were decreased by ~90-95% in L-IDE-KO mice, compared to controls.

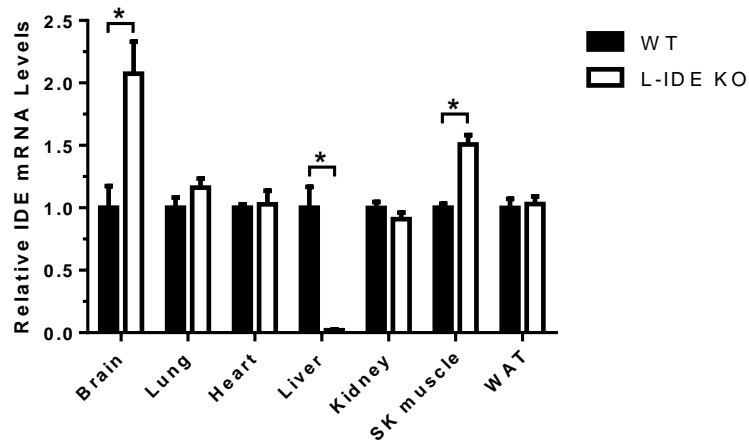


**Figure 24: Expression levels of *Ide* in L-IDE-KO and WT mice.** Expression of *Ide* in 3-month-old L-IDE-KO and their littermate WT male mice. Tissues from L-IDE-KO and WT mice were collected and mRNA isolated. RT-qPCR was performed as described in Material and Methods section. All samples were normalized by the L18 mRNA. mRNA expression levels are represented as mean  $\pm$  SEM. n=4 per genotype. \*  $p$  value < 0.05 vs. WT by Students' T-test.

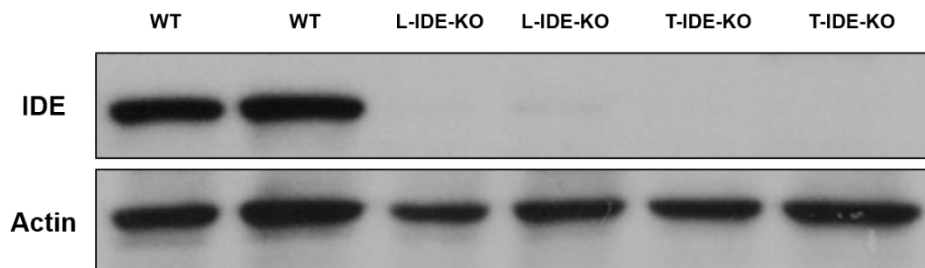


**Figure 25: IDE levels in the liver of L-IDE-KO, Total-IDE-KO and WT mice.** Representative western blots of liver lysates (40  $\mu$ g protein/sample) isolated from 3-month-old L-IDE-KO, Total-IDE-KO and WT mice using anti-IDE and anti-actin antibodies. n= 2 per genotype.

Surprisingly, RT-qPCR analysis showed higher mRNA expression levels in skeletal muscle of L-IDE-KO in comparison to WT mice (**Figure 24**). However, this increase did not affect IDE protein expression levels, as it is shown by western blot analysis (**Figure 26**).

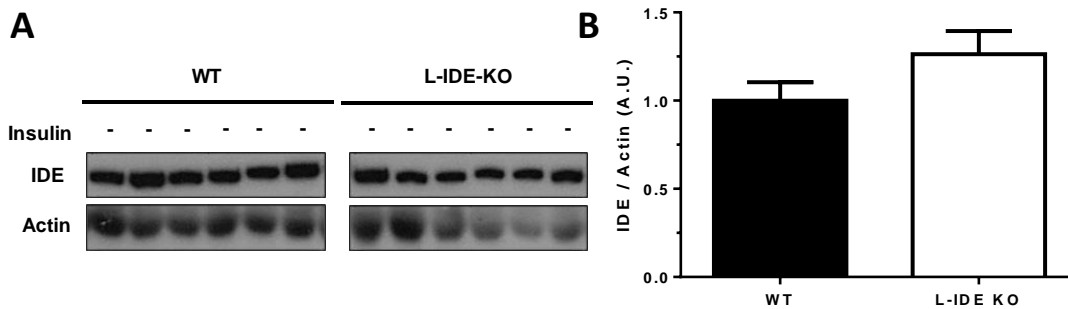


**Figure 26: IDE levels in the skeletal muscle of L-IDE-KO and WT male mice.** (A) Representative western blots of skeletal muscle lysates (40  $\mu$ g protein/sample) isolated from 3-month-old L-IDE-KO and WT male mice using anti-IDE and anti-Actin antibodies. (B) Relative amounts of IDE, after normalizing to actin. n= 6 per genotype. Data are mean  $\pm$  SEM.

## 5.2 Metabolic characterization of L-IDE-KO mice

In order to clarify the role of hepatic IDE on the hepatic glucose metabolism, and the relationship between hepatic IDE function and the development of T2DM, we performed a metabolic characterization of L-IDE-KO mice.

### 5.2.1 L-IDE-KO mice exhibit hyperglycemia after prolonged fasting, independently of body weight

Metabolic characterization of the L-IDE-KO and WT mice began with the analysis of blood glucose levels after prolonged (15 h) fasting. These measurements were done at 1 and 3 months of age in both sexes. Fasting blood glucose levels were similar in 1-month-old female L-IDE-KO and WT mice. However, at 3 months of age, L-IDE-KO female mice exhibited higher blood glucose levels (**Figure 27**)

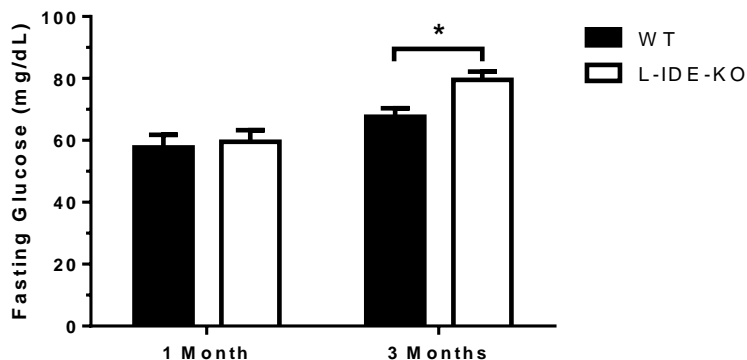


**Figure 27: Fasting blood glucose levels of L-IDE-KO and WT female mice.** Blood glucose measurements were obtained after an overnight fasting at 1 and 3 months of age. n= 11-21 per genotype. Data are mean  $\pm$  SEM. \*  $p < 0.05$  vs. WT by Students' T-test.

In contrast, 1-month-old male L-IDE-KO mice displayed lower fasting glucose levels than littermate controls (**Figure 28**). Surprisingly, at 3 months of age, L-IDE-KO male mice exhibited higher glucose levels than WT mice (**Figure 28**). Taken together, these results indicate that 3-month-old male and female L-IDE-KO mice have higher blood glucose levels than WT mice.

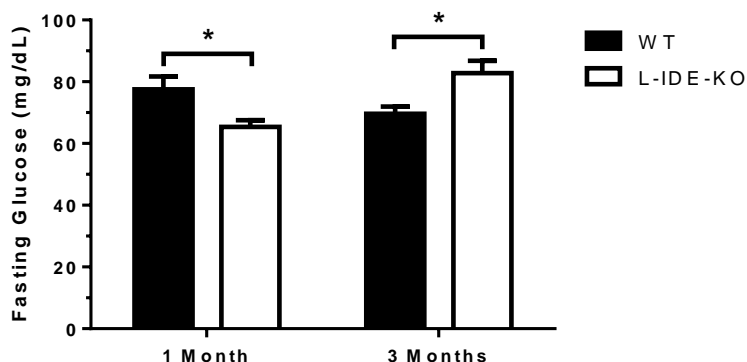


**Figure 28: Fasting blood glucose levels of L-IDE-KO and WT male mice.** Blood glucose measurements were obtained after an overnight fasting at 1 and 3 months of age. n= 8-15 per genotype. Data are mean  $\pm$  SEM. \*  $p < 0.05$  vs. WT by Students' T-test.

An increase in body weight can result in higher blood glucose levels. To reveal whether or not body weight is related to the observed alterations in blood glucose levels, 1- and 3-month-old male and female mice were weighed. As shown in **Figure 29** and **30**, body weight remained unchanged between L-IDE-KO and their littermates WT mice.

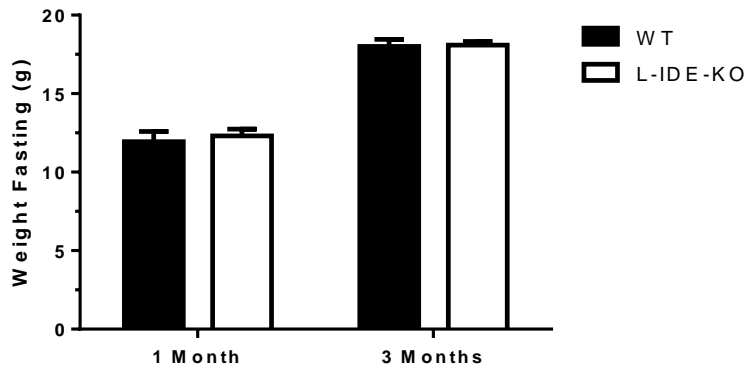


**Figure 29: Fasting body weight of L-IDE-KO and WT female mice.** Body weight measurements were monitored after an overnight fasting at 1 and 3 months of age.  $n= 11-21$  per genotype. Data are mean  $\pm$  SEM.

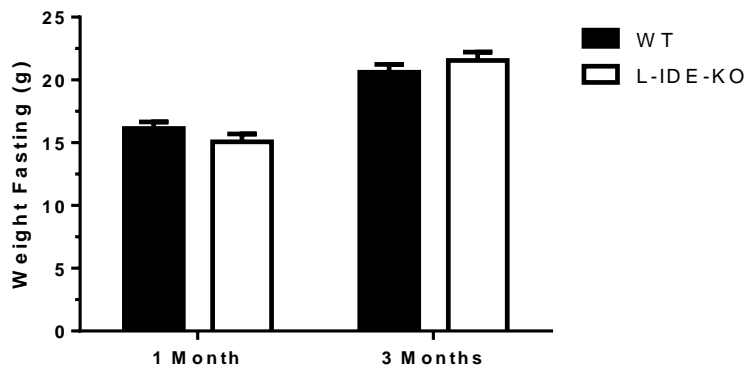


**Figure 30: Fasting body weight of L-IDE-KO and WT male mice.** Body weight measurements were monitored after an overnight fasting at 1 and 3 months of age.  $n= 8-15$  per genotype. Data are mean  $\pm$  SEM.

### 5.2.2 L-IDE-KO male mice exhibit hyperglycemia in non-fasting conditions independently of body weight or food intake

In non-fasting conditions, 1- and 3-month-old L-IDE-KO female mice showed similar blood glucose levels compared to WT mice (**Figure 31**). Likewise, body weight remained unchanged between L-IDE-KO and their littermate WT mice (**Figure 32**).

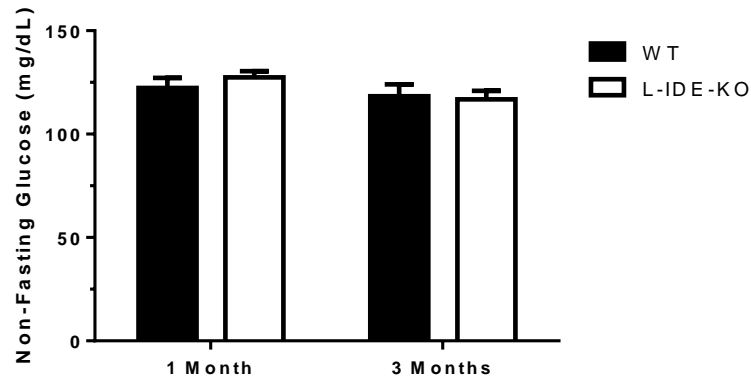


**Figure 31: Non-fasting blood glucose levels of L-IDE-KO and WT female mice.** Blood glucose measurements were obtained in non-fasting conditions at 1 and 3 months of age. n= 11-21 per genotype. Data are mean  $\pm$  SEM.

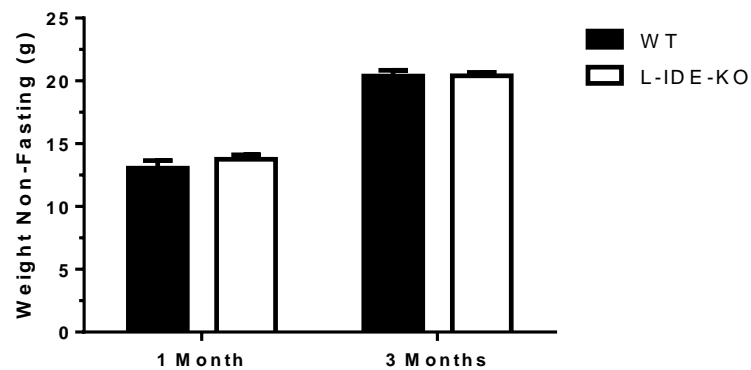


**Figure 32: Non-fasting body weight of L-IDE-KO and WT female mice.** Body weight measurements were monitored in non-fasting conditions at 1 and 3 months of age. n= 11-21 per genotype. Data are mean  $\pm$  SEM.

On the other hand, 1- and 3-month-old L-IDE-KO male mice showed a significant increase in non-fasting glucose levels compared to WT mice (**Figure 33**). This phenotype in glucose homeostasis was independent of body weight (**Figure 34**) or food intake (**Figure 35**).

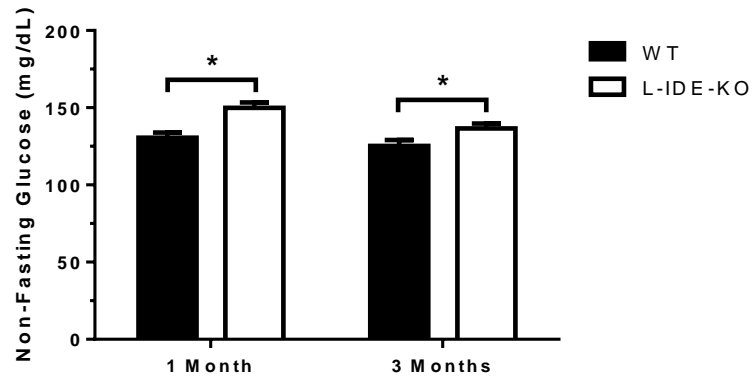


**Figure 33: Non-fasting blood glucose levels of L-IDE-KO and WT male mice.** Blood glucose measurements were obtained in non-fasting conditions at 1 and 3 months of age. n= 8-15 per genotype. Data are mean  $\pm$  SEM. \*  $p < 0.05$  vs. WT by Students' T-test.

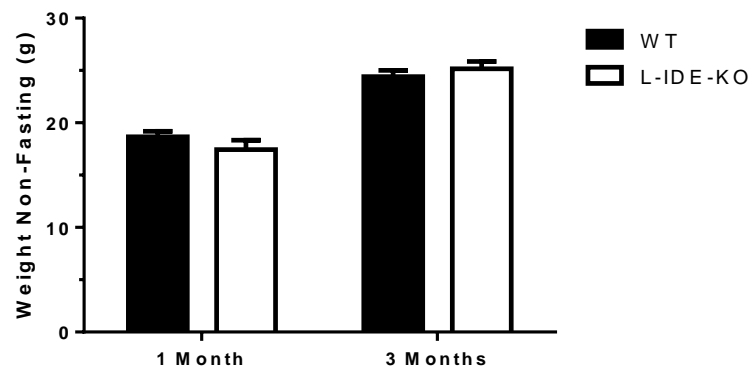


**Figure 34: Non-fasting body weight of L-IDE-KO and WT male mice.** Body weight measurements were monitored in non-fasting conditions at 1 and 3 months of age. n= 8-15 per genotype. Data are mean  $\pm$  SEM.

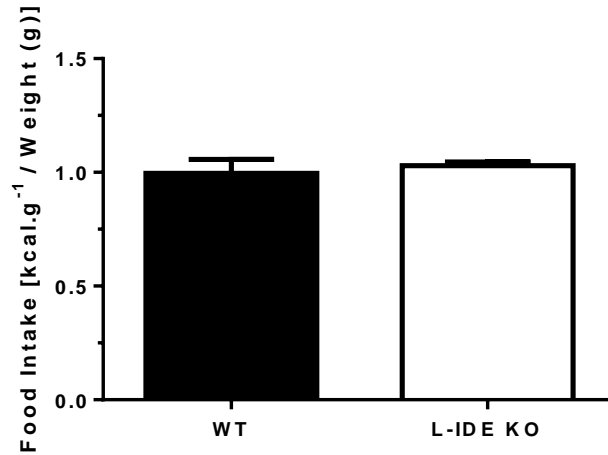


**Figure 35: Caloric intake in L-IDE-KO and WT male mice.** Food intake measurements in 3-month-old male mice were obtained as described in the Materials and Methods after an overnight fasting. n= 6 per genotype. Data are mean  $\pm$  SEM.

### 5.2.3 Hepatic *Ide* ablation impairs glucose tolerance in L-IDE-KO mice

Glucose homeostasis was analyzed in L-IDE-KO and WT mice by an IPGTT at 1 and 3 months of age.

L-IDE-KO female mice exhibited glucose intolerance at 1 month of age (**Figure 36**) compared to WT mice. Of note, the phenotype persisted at 3 months of age. (**Figure 37**).

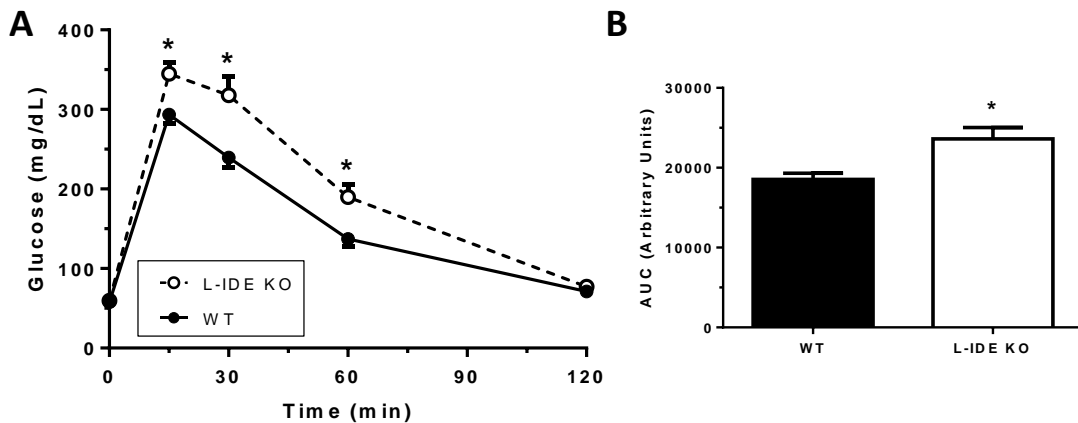


**Figure 36: IPGTT of 1-month-old L-IDE-KO and WT female mice.** (A) 1-month-old L-IDE-KO and WT female mice were intraperitoneally injected with a bolus of glucose at a dose of 2 g/kg of body weight after an overnight fasting. Glucose measurements were done at the indicated times. (B) AUC of IPGTT. n= 11-13 per genotype. Data are mean  $\pm$  SEM. \*  $p < 0.05$  vs. WT by Students' T-test.

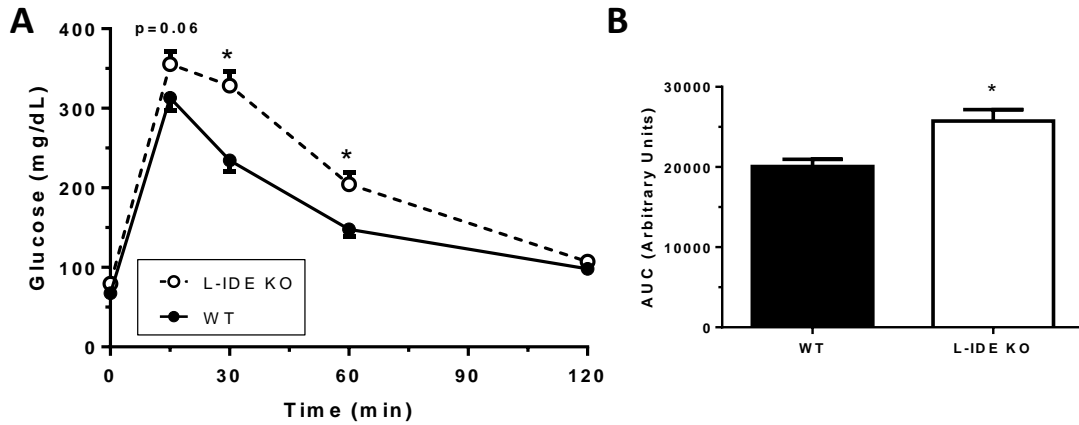


**Figure 37: IPGTT of 3-month-old L-IDE-KO and WT female mice.** (A) 3-month-old L-IDE-KO and WT female mice were intraperitoneally injected with a bolus of glucose at a dose of 2 g/kg of body weight after an overnight fasting. Glucose measurements were done at the indicated times. (B) AUC of IPGTT.  $n = 12-21$  per genotype. Data are mean  $\pm$  SEM. \*  $p < 0.05$  vs. WT by Students' T-test.

On the other hand, 1-month-old L-IDE-KO male mice exhibited similar glucose tolerance compared to WT mice (**Figure 38**).

However, at 3 months of age, L-IDE-KO male mice exhibited a robust phenotype of glucose intolerance compared to WT mice (**Figure 39**).

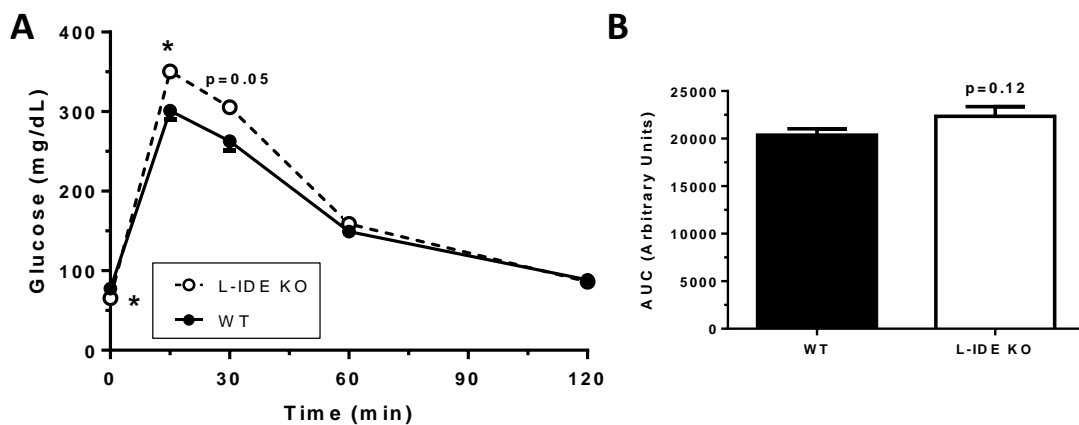


**Figure 38: IPGTT of 1-month-old L-IDE-KO and WT male mice.** (A) 1-month-old L-IDE-KO and WT male mice were intraperitoneally injected with a bolus of glucose at a dose of 2g/kg of body weight after an overnight fasting. Glucose measurements were done at the indicated times. (B) AUC of IPGTT.  $n = 8-15$  per genotype. Data are mean  $\pm$  SEM. \*  $p < 0.05$  vs. WT by Students' T-test.

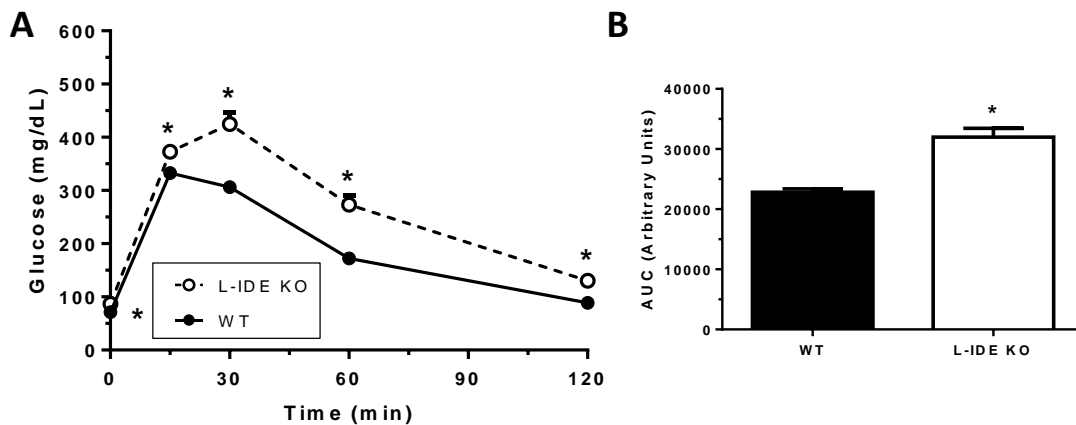


**Figure 39: IPGTT of 3-month-old L-IDE-KO and WT male mice.** (A) 3-month-old L-IDE-KO and WT male mice were intraperitoneally injected with a bolus of glucose at a dose of 2 g/kg of body weight after an overnight fasting. Glucose measurements were done at the indicated times. (B) AUC of IPGTT. n= 8-10. Data are mean  $\pm$  SEM. \*  $p < 0.05$  vs. WT by Students' T-test.

Taken together, these data indicate that hepatic deletion of *Ide* in male and female mice results in impaired glucose tolerance and higher blood glucose levels at 3 months of age.

#### 5.2.4 Hepatic *Ide* ablation causes insulin resistance in L-IDE-KO mice

To further explore the phenotype of altered glucose homeostasis observed in L-IDE-KO mice, we investigated insulin sensitivity. To this end, 1- and 3-month-old male and female mice underwent an IPITT.

At 1 and 3 months of age, L-IDE-KO female mice exhibited marked insulin resistance in comparison to WT mice (**Figure 40** and **41**).

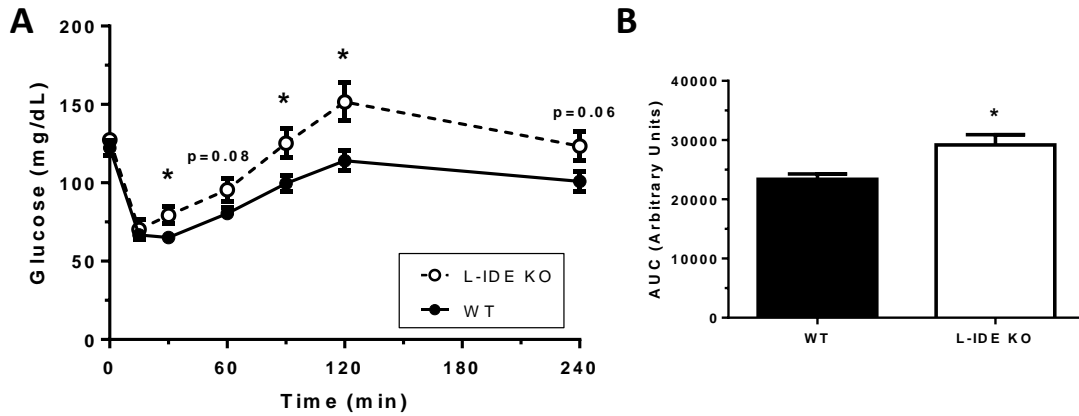


**Figure 40: IPITT in 1-month-old L-IDE-KO and WT female mice.** (A) 1-month-old L-IDE-KO and WT female mice were injected with a bolus of insulin (0.75U/kg of body weight). Glucose measurements were performed at the indicated times. (B) AUC of IPITT.  $n = 11-13$  per genotype. Data are mean  $\pm$  SEM. \*  $p < 0.05$  vs. WT by Students' T-test.

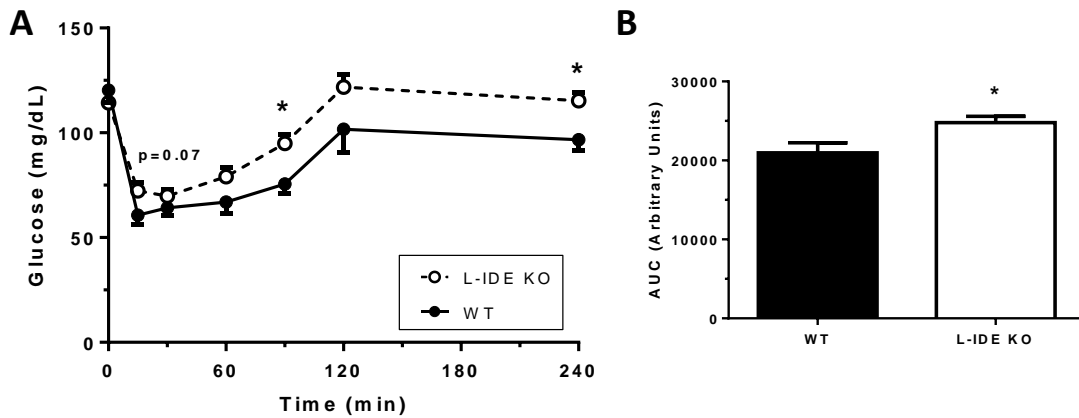


**Figure 41: IPITT in 3-month-old L-IDE-KO and WT female mice.** (A) 3-month-old L-IDE-KO and WT female mice were injected with a bolus of insulin (0.75U/kg of body weight). Glucose measurements were performed at the indicated times. (B) AUC of IPITT.  $n = 11-20$  per genotype. Data are mean  $\pm$  SEM. \*  $p < 0.05$  vs. WT by Students' T-test.

In contrast, 1-month-old L-IDE-KO male mice exhibited mild but statistically significant insulin resistance (**Figure 42**). However, at 3 months of age, L-IDE-KO male mice showed marked insulin resistance (**Figure 43**).

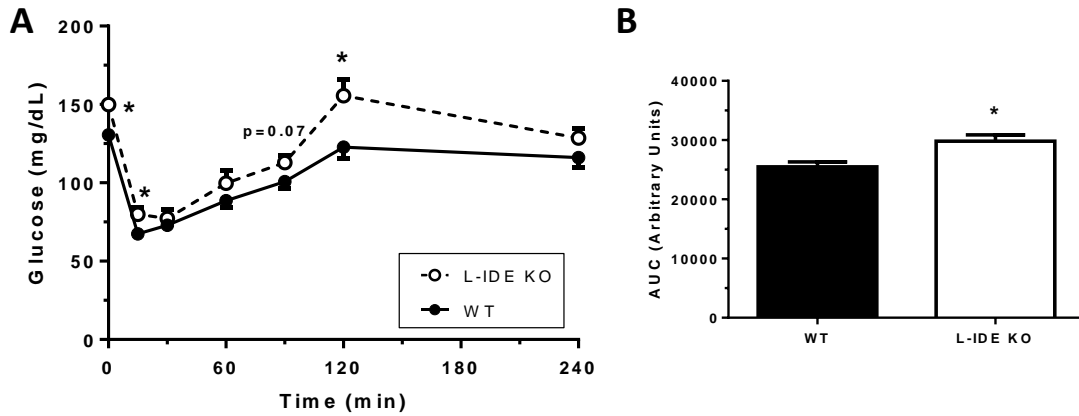


**Figure 42: IPITT in 1-month-old L-IDE-KO and WT male mice.** (A) 1-month-old L-IDE-KO and WT male mice were injected with a bolus of insulin (0.75 U/kg of body weight). Glucose measurements were performed at the indicated times. (B) AUC of IPITT. n= 8-15 per genotype. Data are mean  $\pm$  SEM. \*  $p < 0.05$  vs. WT by Students' T-test.

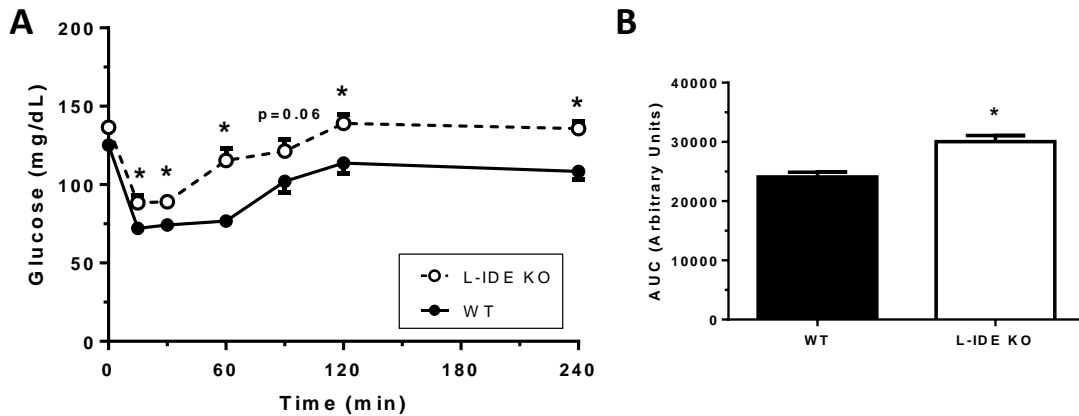


**Figure 43: IPITT in 3-month-old L-IDE-KO and WT male mice.** (A) 3-month-old L-IDE-KO and WT male mice were injected with a bolus of insulin (0.75 U/kg of body weight). Glucose measurements were performed at the indicated times. (B) AUC of IPITT. n= 12-13 per genotype. Data are mean  $\pm$  SEM. \*  $p < 0.05$  vs. WT by Students' T-test.

Taken together, these data indicate that hepatic deletion of *Ide* in L-IDE-KO male and female mice results in impaired insulin sensitivity at 1 and 3 months of age, which are in good agreement with a phenotype of glucose intolerance.

### 5.2.5 L-IDE-KO mice exhibit insulin resistance despite similar plasma insulin levels

To gain further insights into the metabolic phenotype of L-IDE-KO mice, we next investigated fasting and non-fasting plasma insulin levels. As shown in

**Figure 44**, plasma insulin levels in 1 and 3-month-old L-IDE-KO female mice remaining unchanged, compared to WT mice.

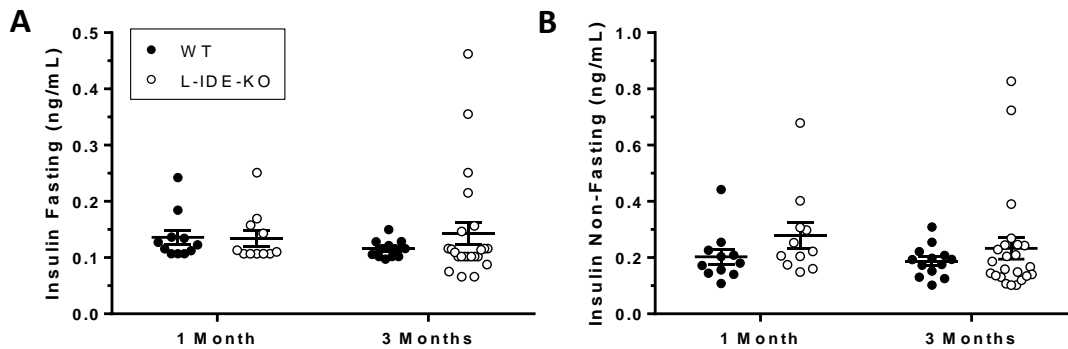


**Figure 44: Plasma insulin levels in L-IDE-KO and WT female mice.** (A) Fasting plasma insulin levels in 1- and 3-month-old L-IDE-KO and WT female mice were assessed as described in the Material and Methods section.  $n = 11-23$  per genotype. (B) Non-fasting plasma insulin levels in 1- and 3-month-old L-IDE-KO and WT female mice.  $n = 11-23$  per genotype. Data are mean  $\pm$  SEM.

Likewise, no differences in plasma insulin levels were observed in L-IDE-KO male mice under fasting (**Figure 45.A**) or non-fasting (**Figure 45.B**) conditions at 1 and 3 months of age.

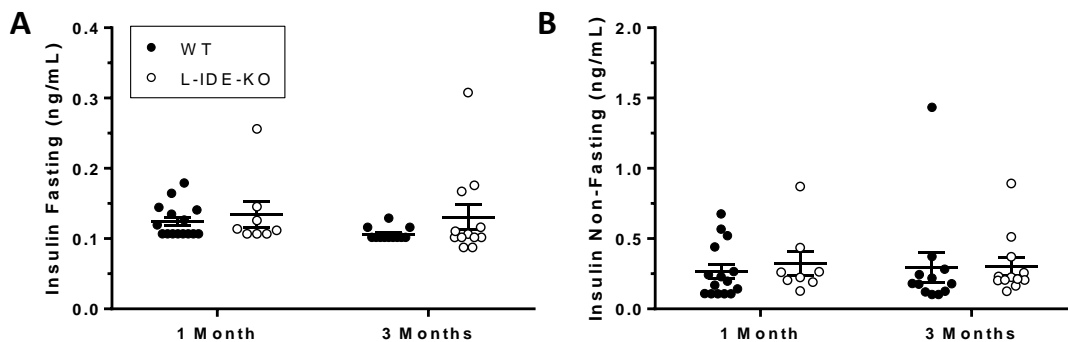


**Figure 45: Plasma insulin levels in L-IDE-KO and WT male mice.** (A) Fasting plasma insulin levels in 1- and 3-month-old L-IDE-KO and WT male mice were assessed as described in the Material and Methods section.  $n = 8-15$  per genotype. (B) Non-fasting plasma insulin levels in 1- and 3-month-old L-IDE-KO and WT male mice.  $n = 8-15$  per genotype. Data are mean  $\pm$  SEM.

These results were completely unexpected as they question previous theories published in the literature regarding the role of *Ide* in hepatic insulin clearance.

### 5.2.6 HOMA index confirms that L-IDE-KO mice exhibit insulin resistance despite having similar plasma insulin levels

Calculation of the HOMA index was used as a confirmatory test to demonstrate the presence of insulin resistance in the L-IDE-KO mice. As shown in **Figure 46**, 1- and 3-month-old L-IDE-KO female mice exhibited insulin resistance since their HOMA values are significantly higher than WT mice.

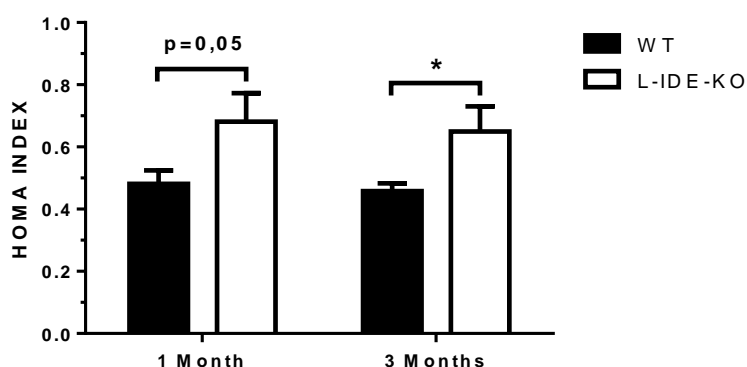


**Figure 46: HOMA index in L-IDE-KO and WT female mice.** HOMA index in 1- and 3-month-old L-IDE-KO and WT female mice was calculated as described in the Materials and Methods section. n= 11-23 per genotype. Results are represented as mean + SEM. \*  $p < 0.05$  vs. WT by Students' T-test.

Similarly, 3-month-old L-IDE-KO male mice exhibited insulin resistance (**Figure 47**). However, 1-month-old L-IDE-KO male mice, did not show insulin resistance (**Figure 47**). These data are in good agreement with those presented in **Figure 42** and **43**.

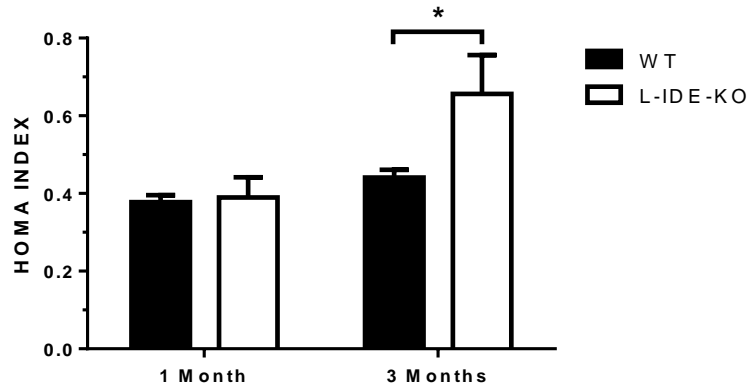


**Figure 47: HOMA index in L-IDE-KO and WT male mice.** HOMA index in 1- and 3-month-old L-IDE-KO and WT male mice was calculated as described in the Materials and Methods section.  $n = 8-15$  per genotype. Results are represented as mean + SEM. \*  $p < 0.05$  vs. WT by Students' T-test.

### 5.2.7 Hepatic *Ide* ablation does not alter plasma lipid profiles in L-IDE-KO mice

Insulin resistance is closely associated with dyslipemia. Therefore, we next investigated the impact of hepatic *Ide* ablation on plasma triglycerides and cholesterol levels. As shown in **Figure 48**, fasting and non-fasting plasma triglyceride levels of 1- and 3-month-old L-IDE-KO female mice remained unchanged compared to WT mice. Likewise, no significant differences were found in fasting and non-fasting plasma cholesterol levels (**Figure 49**).

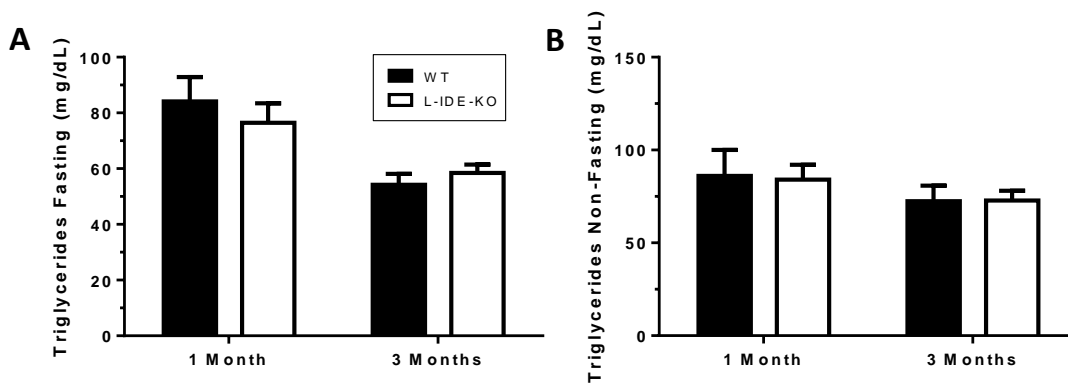


**Figure 48: Plasma triglycerides levels in L-IDE-KO and WT female mice.** Plasma triglycerides levels were assessed as described in the Materials and Methods section. (A) Fasting triglycerides levels in 1 and 3-month-old L-IDE-KO and WT female mice.  $n = 11-23$  per genotype. (B) Non-fasting triglycerides levels in 1 and 3-month-old L-IDE-KO and WT female mice.  $n = 11-23$  per genotype. Data are mean  $\pm$  SEM.

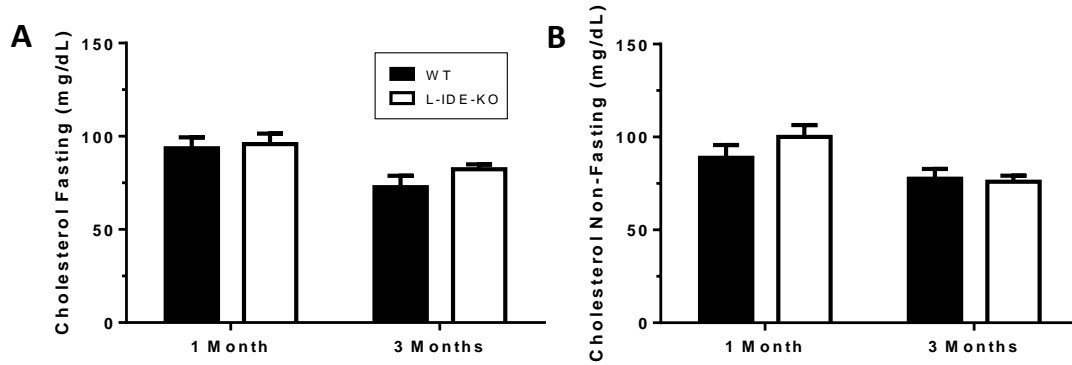


**Figure 49: Plasma cholesterol levels in L-IDE-KO and WT female mice.** Plasma cholesterol levels were assessed as described in the Materials and Methods section. (A) Fasting cholesterol levels in 1 and 3-month-old L-IDE-KO and WT female mice.  $n = 11-23$  per genotype. (B) Non-fasting cholesterol levels in 1 and 3-month-old L-IDE-KO and WT female mice.  $n = 11-23$  per genotype. Data are mean  $\pm$  SEM.

Similarly, fasting and non-fasting plasma triglycerides levels of 1- and 3-month-old L-IDE-KO male mice remained unchanged compared to WT mice (**Figure 50**). Likewise, no significant differences were found in fasting and non-fasting plasma cholesterol levels in 1-month-old L-IDE-KO male mice compared to WT mice (**Figure 51**). Surprisingly, fasting and non-fasting plasma cholesterol levels in 3-month-old L-IDE-KO male mice were lower than their littermate WT mice.

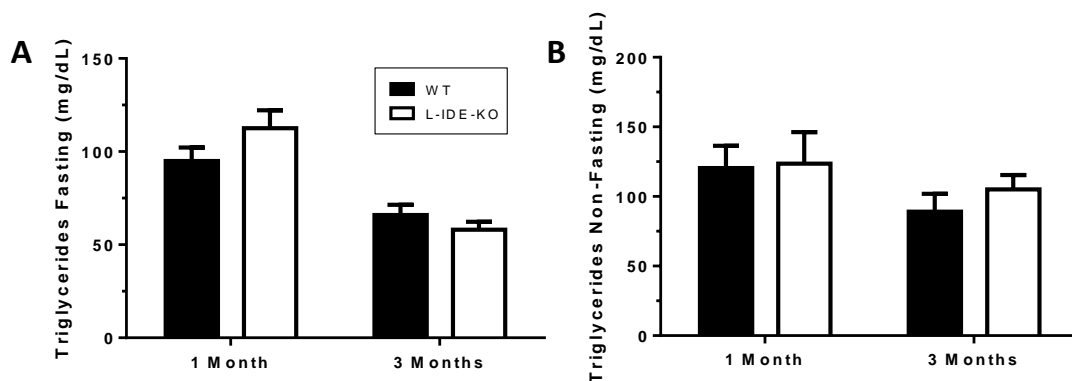


**Figure 50: Plasma triglycerides levels in L-IDE-KO and WT male mice.** Plasma triglycerides levels were assessed as described in the Materials and Methods section. (A) Fasting triglycerides levels in 1 and 3-month-old L-IDE-KO and WT male mice.  $n = 8-15$  per genotype. (B) Non-fasting triglycerides levels in 1 and 3-month-old L-IDE-KO and WT male mice.  $n = 8-15$  per genotype. Data are mean  $\pm$  SEM.

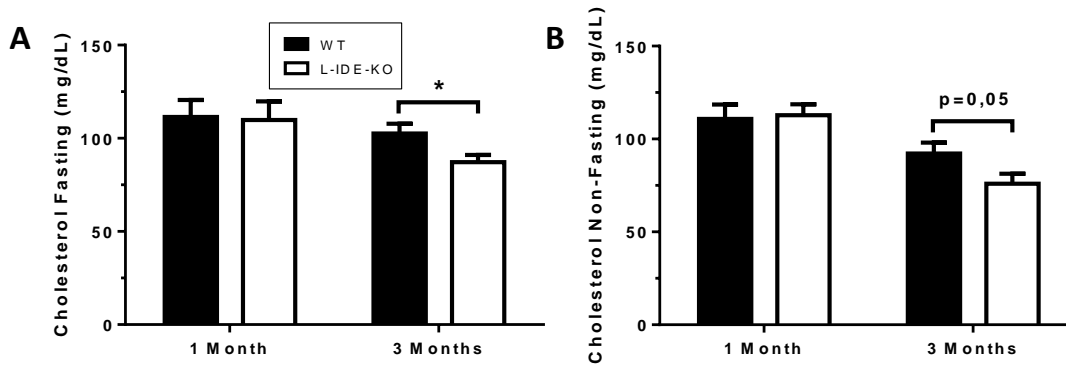


**Figure 51: Plasma cholesterol levels in L-IDE-KO and WT male mice.** Plasma cholesterol levels were assessed as described in the Materials and Methods section. (A) Fasting cholesterol levels in 1 and 3-month-old L-IDE-KO and WT male mice.  $n = 8-15$  per genotype. (B) Non-fasting cholesterol levels in 1 and 3-month-old L-IDE-KO and WT male mice.  $n = 8-15$  per genotype. Data are mean  $\pm$  SEM. \*  $p < 0.05$  vs. WT by Students' T-test.

In summary, despite the finding that L-IDE-KO mice exhibit marked insulin resistance, overall plasma lipid profiles remained unchanged. Notably, in a sex- and age-dependent manner, L-IDE-KO male mice showed diminished plasma cholesterol levels.

### 5.2.8 Hepatic *Ide* deletion causes hyperglucagonemia in L-IDE-KO mice at 1 month of age

In order to further elucidate the molecular mechanisms by which hepatic ablation of *Ide* is associated with glucose intolerance and insulin resistance, we measured plasma glucagon levels in L-IDE-KO and their littermate WT mice. This hormone regulates glucose homeostasis under fasting conditions, opposing the action of insulin. In addition, glucagon is a substrate of IDE protease activity.

As shown in **Figure 52**, fasting and non-fasting plasma glucagon levels of 1- and 3-month-old L-IDE-KO female mice remaining unchanged as compared to WT mice. It should be noted that non-fasting plasma glucagon levels in 1-month-old L-IDE-KO female mice exhibited a modest, but statistically non-significant elevation (**Figure 52.B**).

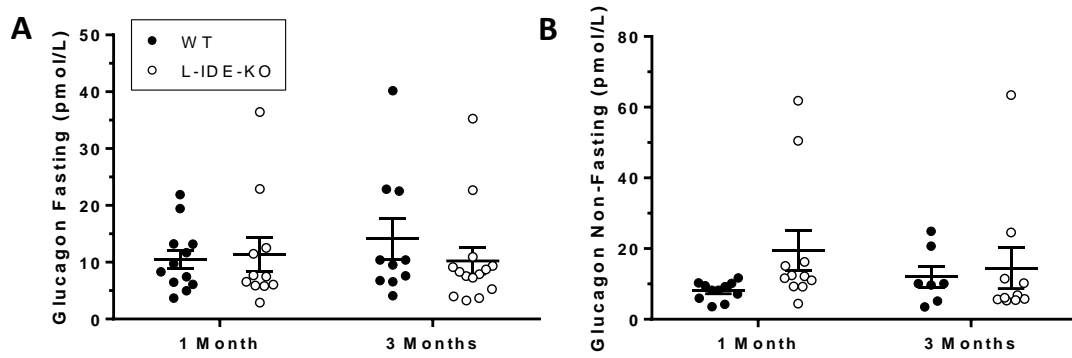


**Figure 52: Plasma glucagon levels in L-IDE-KO and WT female mice.** Plasma glucagon levels were assessed as described in the Materials and Methods section. (A) Fasting glucagon levels in 1- and 3-month-old L-IDE-KO and WT female mice.  $n = 7-11$  per genotype. (B) Non-fasting glucagon levels in 1- and 3-month-old L-IDE-KO and WT female mice.  $n = 7-11$  per genotype. Data are mean  $\pm$  SEM.

Similarly, fasting plasma glucagon levels of 1- and 3-month-old L-IDE-KO male mice remained unchanged compared to WT mice (**Figure 53**). Surprisingly, non-fasting plasma glucagon levels in 1-month-old L-IDE-KO male mice were higher than their littermate WT mice (**Figure 53.B**). At 3 months of age, some degree of elevation persisted, although this did not achieve statistical significance (**Figure 53.B**).

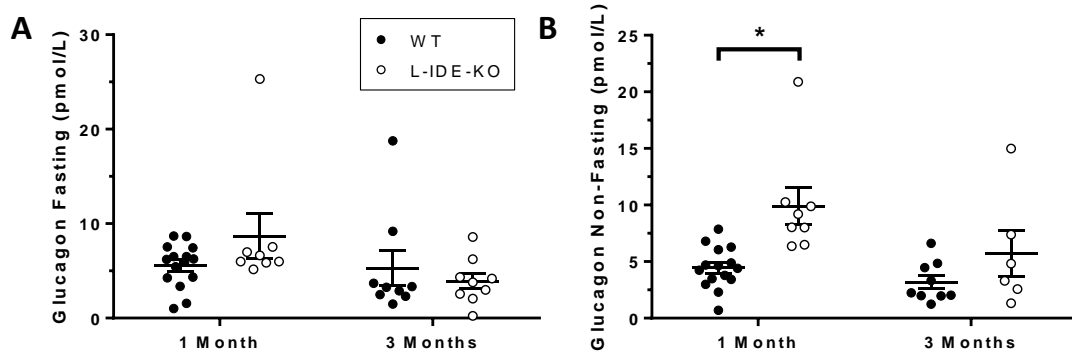


**Figure 53: Plasma glucagon levels in L-IDE-KO and WT male mice.** Plasma glucagon levels were assessed as described in the Materials and Methods section. (A) Fasting glucagon levels in 1- and 3-month-old L-IDE-KO and WT male mice.  $n = 8-15$  per genotype. (B) Non-fasting glucagon levels in 1- and 3-month-old L-IDE-KO and WT male mice.  $n = 6-15$  per genotype. Data are mean  $\pm$  SEM. \*  $p < 0.05$  vs. WT by Student's T-test.

In summary, L-IDE-KO mice exhibited augmented plasma glucagon levels, potentially due to a reduced capacity for glucagon plasma clearance. This

phenotype was more evident in 1-month-old L-IDE-KO male mice, but with aging shifted towards a more subtle phenotype.

### 5.2.9 Plasma levels of A $\beta$ 40 and amylin in L-IDE-KO mice

IDE is a metalloprotease that, in addition to insulin and glucagon, degrades amylin and A $\beta$ 40<sup>159,160</sup>. On the other hand, insulin resistance triggers increased secretion of oligomerized amylin from pancreatic islets in the blood<sup>185</sup>; whereas plasma A $\beta$ 40 levels are closely associated with insulin resistance<sup>186</sup>. To investigate the impact of hepatic *Ide* ablation on plasma levels of amylin and A $\beta$ 40, plasma samples from L-IDE-KO and WT mice were assayed as described in the Material and Methods section. As shown in **Figure 54**, A $\beta$ 40 levels were significantly reduced in 3-month-old L-IDE-KO female mice, compared to WT mice. However, amylin levels remained unchanged (**Figure 55**). Likewise, plasma A $\beta$ 40 and amylin levels in 3-month-old L-IDE-KO male mice remained unchanged, compared to WT mice (**Figure 56** and **57**).

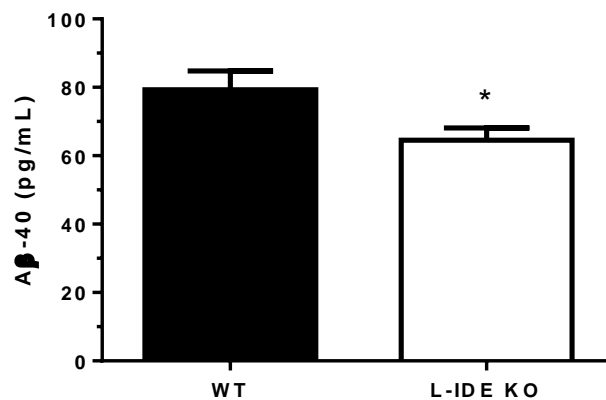


**Figure 54: Plasma A $\beta$ 40 levels in L-IDE-KO and WT female mice.** Fasting plasma A $\beta$ 40 levels were assessed in 3-month-old L-IDE-KO and WT female mice as described in the Materials and Methods section. n= 11-12 per genotype. Data are mean  $\pm$  SEM. \*  $p < 0.05$  vs. WT by Students' T-test.

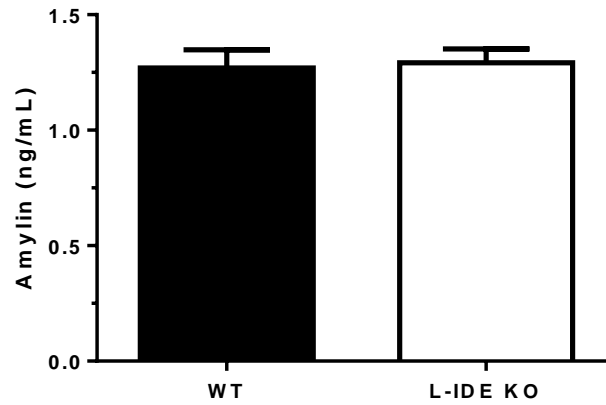


**Figure 55: Plasma amylin levels in L-IDE-KO and WT female mice.** Fasting plasma amylin levels were assessed in 3-month-old L-IDE-KO and WT female mice as described in the Materials and Methods section. n= 12-13 per genotype. Data are mean  $\pm$  SEM.

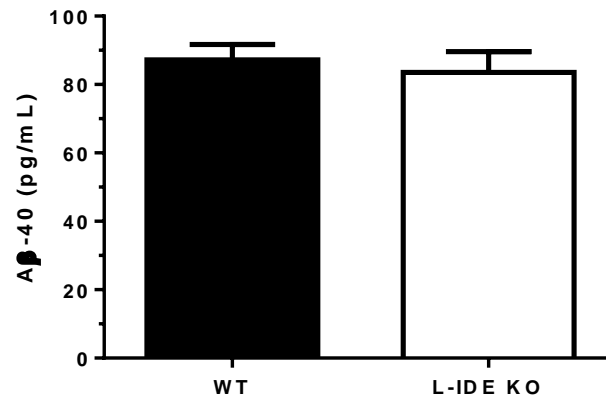


**Figure 56: Plasma A $\beta$ 40 levels in L-IDE-KO and WT male mice.** Fasting plasma A $\beta$ 40 levels were assessed in 3-month-old L-IDE-KO and WT male mice as described in the Materials and Methods section. n= 10-15 per genotype. Data are mean  $\pm$  SEM.

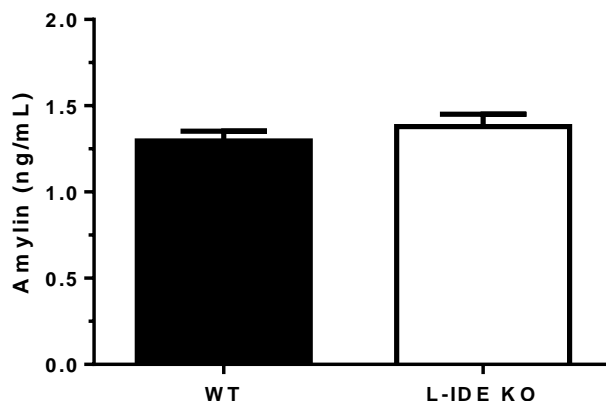


**Figure 57: Plasma amylin levels in L-IDE-KO and WT male mice.** Fasting plasma amylin levels were assessed in 3-month-old L-IDE-KO and WT male mice as described in the Materials and Methods section. n= 10-14 per genotype. Data are mean  $\pm$  SEM.

In summary, these results demonstrate that plasma A $\beta$ 40 and amylin are not associated with glucose intolerance and insulin resistance in L-IDE-KO mice. Because IDE is implicated in the degradation of these substrates, such that genetic deletion should increase, rather than decrease their levels, these results suggest that hepatic IDE does not participate in the *in vivo* plasma clearance of A $\beta$ 40 and amylin.

#### 5.2.10 Hepatic *Ide* ablation does not impair hepatic insulin clearance *in vivo*.

It has been proposed that IDE participates in hepatic insulin clearance<sup>157,170</sup>. However, we have shown in this work that plasma insulin levels remained unchanged in L-IDE-KO, compared to WT mice. To clarify the role of IDE in hepatic insulin clearance *in vivo*, we performed an insulin clearance test by an intra-orbital insulin injection as described in the Material and Methods section.

Contrary to expectations, insulin clearance in 3-month-old L-IDE-KO female and male mice were similar to their littermate WT mice (**Figure 58 and 59**).

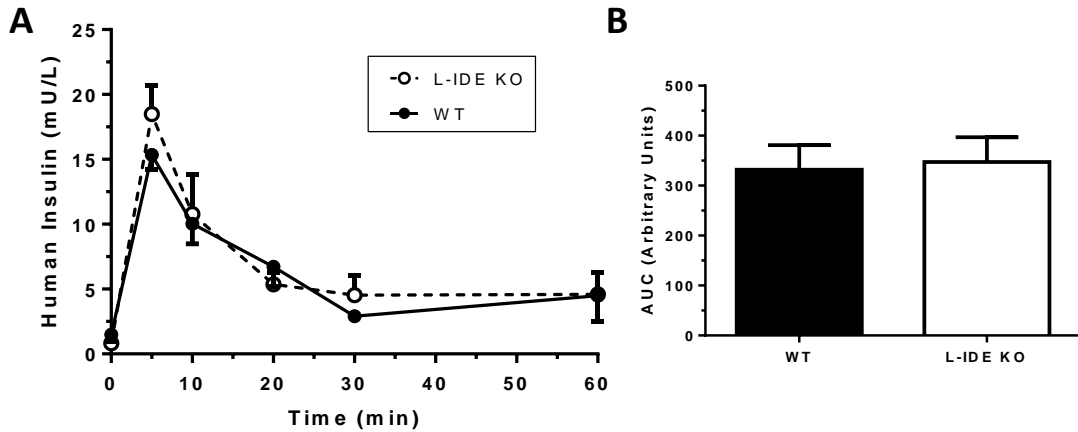


**Figure 58: Hepatic insulin clearance test of L-IDE-KO and WT female mice.** (A) 3-month-old L-IDE-KO and WT female mice were anesthetized and infected intra-orbitally with human insulin (1 nmol/kg body weight). Afterwards, blood was collected at the indicated time points. Plasma human insulin was assessed as described in the Materials and Methods section. (B) AUC of hepatic insulin clearance test. n= 8 per genotype. Data are mean ± SEM.

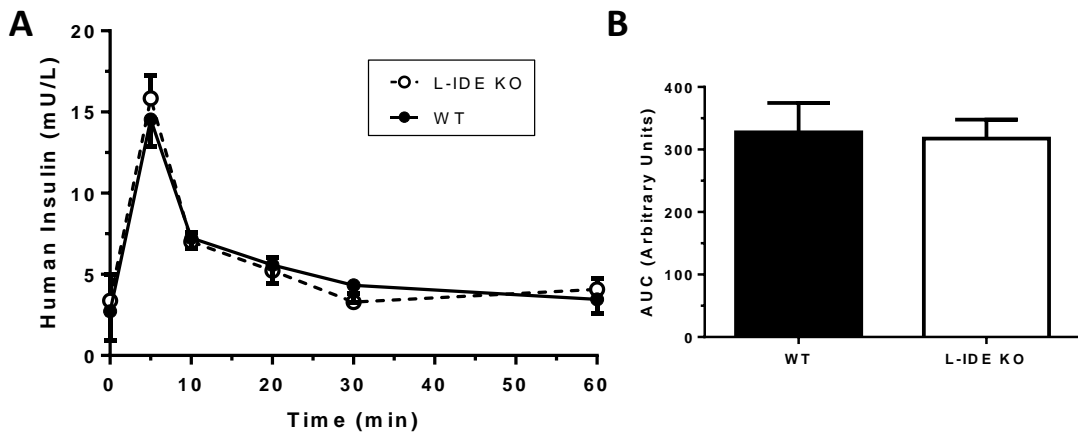


**Figure 59: Hepatic insulin clearance test of L-IDE-KO and WT male mice.** (A) 3-month-old L-IDE-KO and WT male mice were anesthetized and infected intra-orbitally with human insulin (1 nmol/kg body weight). Afterwards, blood was collected at the indicated time points. Plasma human insulin was assessed as described in the Materials and Methods section. (B) AUC of hepatic insulin clearance test. n= 6-9 per genotype. Data are mean ± SEM.

Extrahepatic tissues such as kidneys and skeletal muscle are also involved in plasma insulin clearance *in vivo*<sup>96</sup>. Therefore, we decided to analyze IDE levels in kidneys and skeletal muscle of L-IDE-KO mice, in order to test the hypothesis that elevations in IDE in those tissues could counteract the absence of IDE within liver to regulate plasma insulin clearance in L-IDE-KO mice.

On the one hand, western blot analyses indicated that IDE protein levels in the kidney of L-IDE-KO mice were decreased in comparison to WT mice (**Figure 60**).

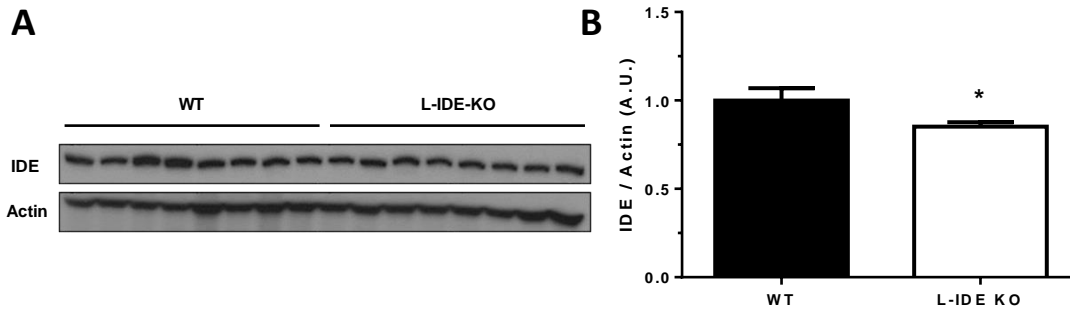


**Figure 60: IDE levels in kidneys of L-IDE-KO and WT male mice.** (A) Representative western blot of kidney lysates (40  $\mu$ g protein/sample) isolated from 3-month-old L-IDE-KO and WT male mice using anti-IDE and anti-Actin antibodies. (B) Relative amounts of IDE, after normalizing to actin. n= 8 per genotype. Data are mean  $\pm$  SEM. \*  $p < 0.05$  vs. WT by Students' T-test.

On the other hand, IDE levels in skeletal muscle analyzed by western blot remained unchanged in L-IDE-KO compared to WT mice (**Figure 61**).

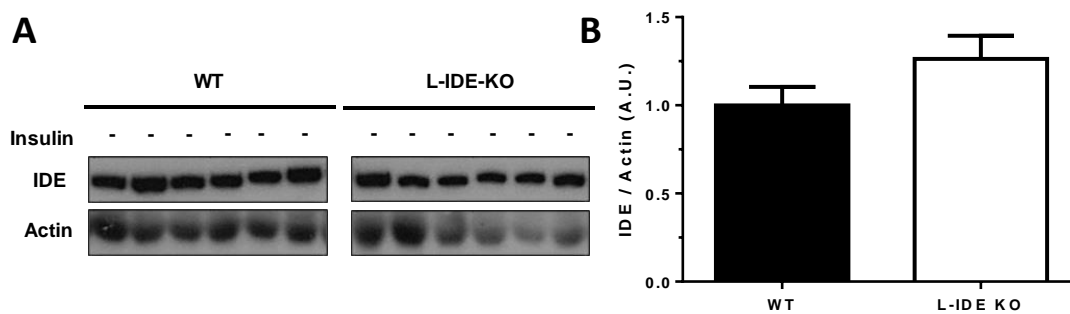


**Figure 61: IDE levels in the skeletal muscle of L-IDE-KO and WT male mice.** (A) Representative western blot of skeletal muscle lysates (40  $\mu$ g protein/sample) isolated from 3-month-old L-IDE-KO and WT male mice using anti-IDE and anti-Actin antibodies. (B) Relative amounts of IDE, after normalizing to actin. n= 6 per genotype. Data are mean  $\pm$  SEM.

In summary, hepatic deletion of *Ide* does not alter *in vivo* plasma insulin clearance. In addition, extrahepatic IDE levels in tissues such as skeletal muscle and kidneys do not compensate for the loss of hepatic IDE, since IDE levels in kidneys were slightly reduced and in skeletal muscle remained unchanged.

These findings suggest that IDE is not the principal or rate-limiting factor involved in hepatic insulin clearance, because insulin clearance is unaltered in the absence of hepatic *Ide* (L-IDE-KO).

### 5.2.11 Hepatic *Ide* ablation impairs hepatic insulin signaling.

To help elucidate the molecular basis underlying the insulin resistance observed in L-IDE-KO mice, we analyzed multiple components of the intracellular insulin-signaling pathway in liver and skeletal muscle, two key tissues involved in the regulation of whole-body glucose homeostasis.

To this end, 3-month-old L-IDE-KO and WT male mice were fasted overnight, followed by an intraperitoneal injection of a bolus of insulin (0.75 U/Kg) or saline solution. Ten minutes later, mice were euthanized and tissues were dissected.

Hepatic *Ide* deletion resulted in a significant 30% reduction of IR $\beta$  in the hepatocytes plasma membrane of L-IDE-KO mice (**Figure 62**), consistent with previous findings in total IDE knockout mice<sup>170</sup>. Furthermore, insulin-mediated activation of the IR $\beta$  was impaired by 55% in L-IDE-KO mice compared to WT mice (**Figure 63**).

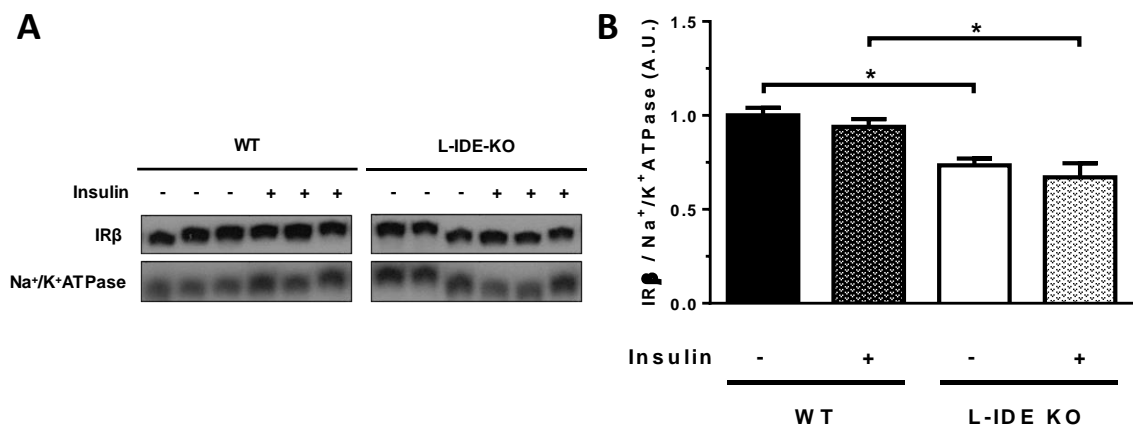


**Figure 62: Plasma membrane IR $\beta$  levels in the liver of L-IDE-KO and WT male mice.** (A) Representative western blot of liver lysates (40  $\mu$ g protein/sample) isolated from 3-month-old L-IDE-KO and WT male mice, using anti-IR $\beta$  and anti-Na<sup>+</sup>/K<sup>+</sup>ATPase antibodies. (B) Relative amounts of IR $\beta$ , after normalizing to Na<sup>+</sup>/K<sup>+</sup>ATPase. n = 6 per genotype. Data are mean  $\pm$  SEM. \*  $p < 0.05$  vs. WT by ANOVA.

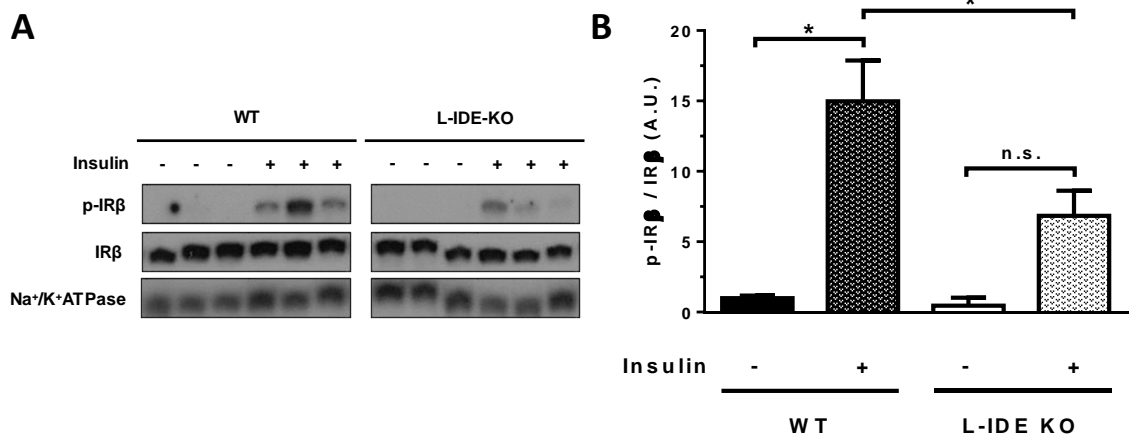


**Figure 63: Plasma membrane p-IR $\beta$  levels in the liver of L-IDE-KO and WT male mice.** (A) Representative western blots of liver lysates (40  $\mu$ g protein/sample) isolated from 3-month-old L-IDE-KO and WT male mice, using anti-p-IR $\beta$  and anti-IR $\beta$  antibodies. (B) Relative amounts of p-IR $\beta$ , after normalizing to IR $\beta$ .  $n = 6$  per genotype. Data are mean  $\pm$  SEM. \*  $p < 0.05$  vs. WT by ANOVA.

AKT1 phosphorylation (**Figure 64**), which is involved in cell survival, protein synthesis and inhibition of apoptosis, and AKT2 phosphorylation (**Figure 65**), which is involved in metabolism exclusively, were both impaired, exhibiting significant reductions of 45% and 40%, respectively. Given that AKT1/2 phosphorylation is downstream of insulin-induced IR autophosphorylation, these results are in excellent agreement with those in **Figure 63**.

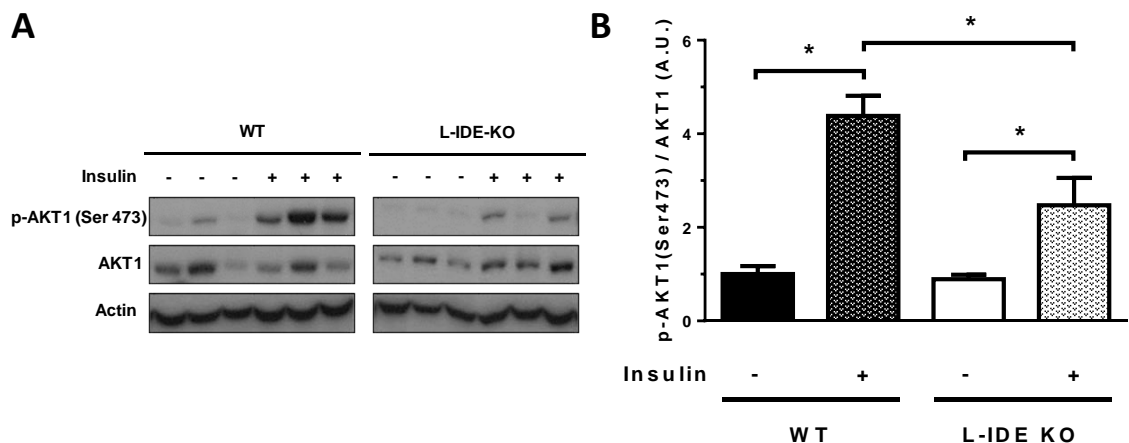


**Figure 64: p-AKT1(Ser473) levels in the liver of L-IDE-KO and WT male mice.** (A) Representative western blots of liver lysates (40  $\mu$ g protein/sample) isolated from 3-month-old L-IDE-KO and WT male mice, using anti-p-AKT1(Ser473) and anti-AKT1 antibodies. (B) Relative amounts of p-AKT1(Ser473), after normalizing to AKT1.  $n = 6$  per genotype. Data are mean  $\pm$  SEM. \*  $p < 0.05$  vs. WT by ANOVA.

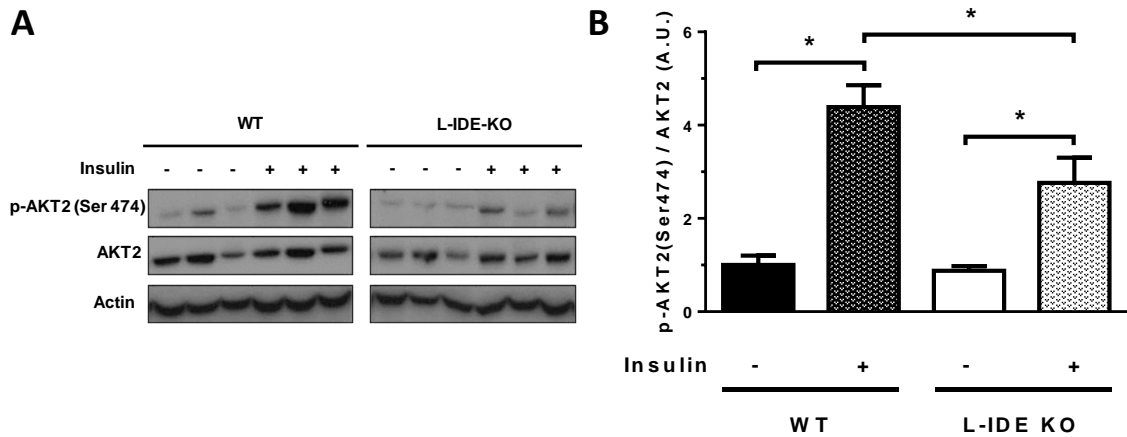


**Figure 65: p-AKT2(Ser474) levels in the liver of L-IDE-KO and WT male mice.** (A) Representative western blots of liver lysates (40  $\mu$ g protein/sample) isolated from 3-month-old L-IDE-KO and WT male mice, using anti-p-AKT2(Ser474) and anti-AKT2 antibodies. (B) Relative amounts of p-AKT2(Ser474), after normalizing to AKT2. n= 6 per genotype. Data are mean  $\pm$  SEM. \*  $p < 0.05$  vs. WT by ANOVA.

We also analyzed GSK3, an enzyme involved in hepatic glycogen synthesis, which is downstream of AKT in the insulin-signaling pathway. Upon insulin stimulation, AKT phosphorylates and inactivates GSK3, which in turn restores GS activity, leading to glycogen synthesis. Unexpectedly, hepatic deficiency of *Ide* was associated with 3.5-fold increase in GSK3 phosphorylation levels in the absence of insulin, and 1.5-fold in the presence of insulin compared to WT mice (Figure 66).

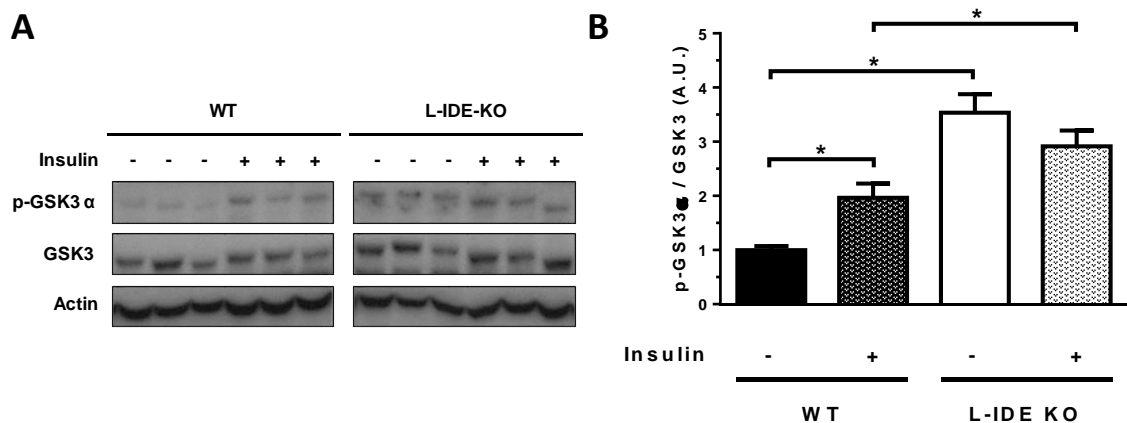


**Figure 66: p-GSK3 $\alpha$  levels in the liver of L-IDE-KO and WT male mice.** (A) Representative western blots of liver lysates (40  $\mu$ g protein/sample) isolated from 3-month-old L-IDE-KO and WT male mice, using anti-p-GSK3 $\alpha$  and anti-GSK3 antibodies. (B) Relative amounts of p-GSK3 $\alpha$ , after normalizing to GSK3. n= 6 per genotype. Data are mean  $\pm$  SEM. \*  $p < 0.05$  vs. WT by ANOVA.

We hypothesized that the increase of GSK3 phosphorylation levels was due to compensatory mechanisms to allow glycogen synthesis, since reduced AKT activation led to lower capacity for glycogen synthesis in response to insulin in L-IDE-KO mice.

For this reason, we decided to analyze the glycogen levels stored in the liver of L-IDE-KO and WT mice in non-fasting conditions. As shown in **Figure 67**, hepatic *Ide* ablation did not alter glycogen levels in L-IDE-KO mice as compared to WT mice. Taken together, these results suggest that *Ide* deficiency in liver does not alter the capacity for storing glycogen in the liver, at least not by a mechanism involving phosphorylation of GSK3 independently of AKT.

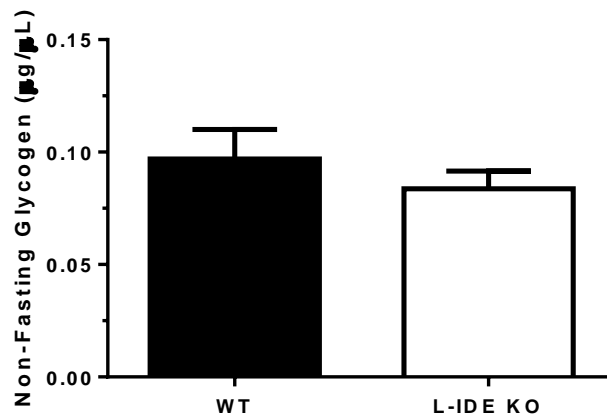


**Figure 67: Hepatic glycogen levels in L-IDE-KO and WT male mice.** Non-fasting livers of 3-month-old L-IDE-KO and WT male mice were used to quantify the amount of glycogen deposits as described in the Materials and Methods section. n= 4 per genotype. Data are mean  $\pm$  SEM.

On the other hand, analysis of insulin-signaling pathway in skeletal muscle by western blots indicated that hepatic *Ide* ablation did not alter insulin-mediated stimulation of the insulin-signaling pathway, as AKT phosphorylation levels revealed (**Figure 68**).

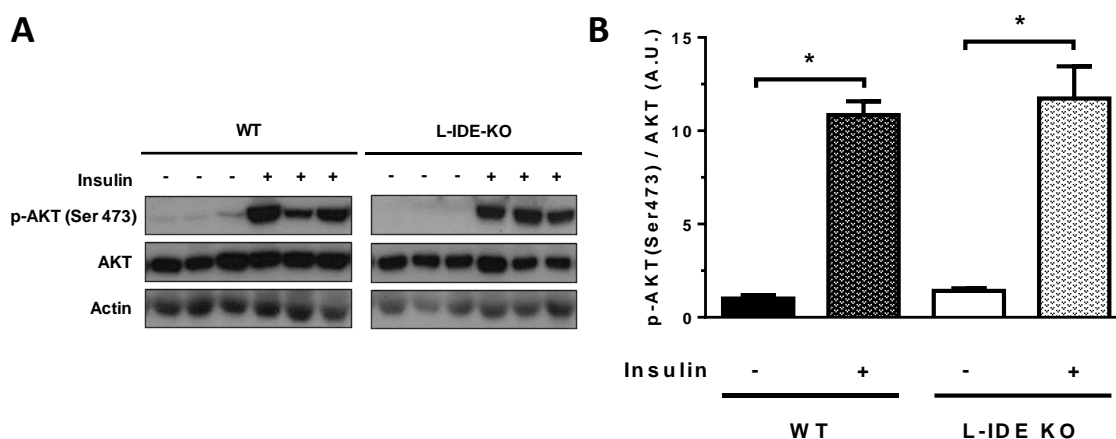


**Figure 68: p-AKT(Ser473) levels in the skeletal muscle of L-IDE-KO and WT male mice.** (A) Representative western blots of skeletal muscle lysates (40  $\mu$ g protein/sample) isolated from 3-month-old L-IDE-KO and WT male mice, using anti-p-AKT(Ser473) and anti-AKT antibodies. (B) Relative amounts of p-AKT(Ser473), after normalizing to AKT.  $n = 6$  per genotype. Data are mean  $\pm$  SEM. \*  $p < 0.05$  vs. WT by ANOVA.

Under physiological conditions, one of the actions of insulin on adipose tissue is to suppress lipolysis (i.e. the release of FFAs into bloodstream) in the fed state, because no extra energy supply is required by the whole organism.

Hence, we investigated the impact of *Ide* deficiency on the levels of circulating FFAs. To this end, fasted 3-month-old L-IDE-KO and WT male mice were intraperitoneally injected with a bolus of human insulin (0.75 U/Kg) or saline solution, and 10 min later, mice were euthanized, plasma was collected and FFAs levels were assessed as described in the Material and Methods section.

As expected, insulin reduced FFAs levels in control and L-IDE-KO mice compared to saline injections in female (**Figure 69**) and male (**Figure 70**) mice. Interestingly, insulin lowered by 40% plasma FFAs levels in L-IDE-KO female mice (**Figure 69**) and by 50% in male L-IDE-KO (**Figure 70**) compared to WT mice.

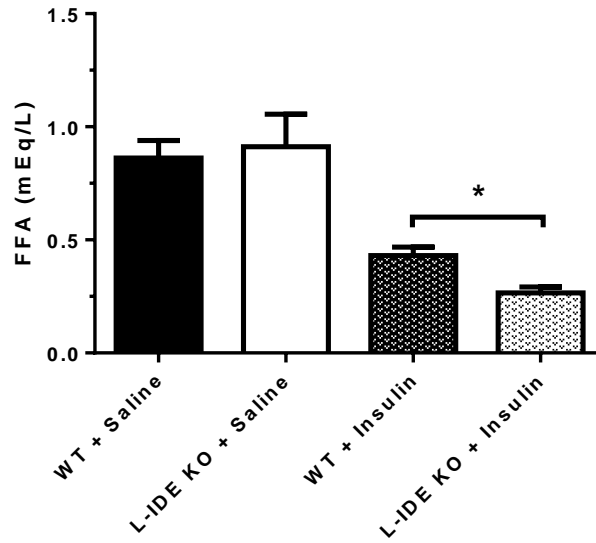


**Figure 69: Plasma FFAs concentrations in L-IDE-KO and WT female mice in response to insulin.** Fasted plasma FFAs, from 3-month-old L-IDE-KO and WT female mice, were assessed as described in the Materials and Methods section.  $n = 5-9$  per genotype. Data are mean  $\pm$  SEM. \*  $p < 0.05$  vs. WT by ANOVA.

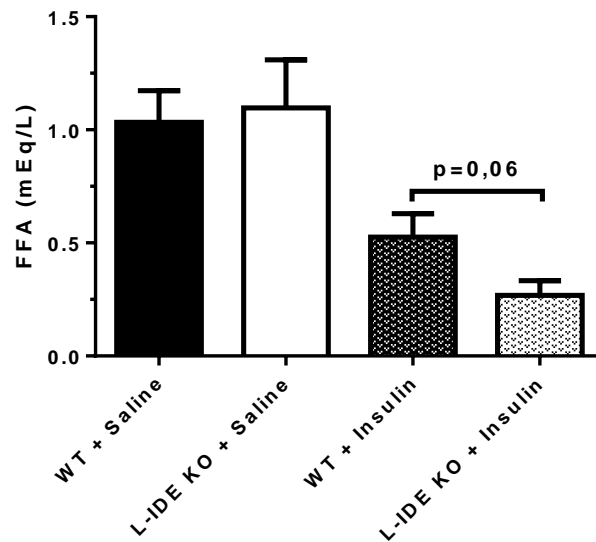


**Figure 70: Plasma FFAs concentrations in L-IDE-KO and WT male mice in response to insulin.** Fasted plasma FFAs, from 3-month-old L-IDE-KO and WT male mice, were assessed as described in the Materials and Methods section.  $n = 4-8$  per genotype. Data are mean  $\pm$  SEM by ANOVA.

Taken together, these results suggest that hepatic ablation of *Ide* improves insulin sensitivity in the adipose tissue of L-IDE-KO mice.

In summary, genetic deletion of *Ide* in liver significantly alters the intracellular insulin-signaling pathway by reducing both the levels and the insulin-responsiveness of plasma membrane IR $\beta$ . Consequently, insulin-mediated activation of AKT is impaired. However, despite this deficiency in intracellular insulin signaling, the downstream target of AKT, GSK3, is phosphorylated and inactivated by an unknown mechanism, leading to a correct regulation of glycogen synthesis, as indicated by unaltered stores of hepatic glycogen in L-IDE-KO mice. Regarding the impact of hepatic insulin resistance on peripheral insulin sensitivity, insulin signaling in skeletal muscle was not affected by hepatic *IDE* deficiency but the levels of circulating FFAs suggested improved insulin sensitivity in the adipose tissue of L-IDE-KO mice.

#### **5.2.12 Hepatic ablation of *Ide* augments gene expression of *Pck1* and *G6pc* in L-IDE-KO mice**

Under physiological conditions during the non-fasting state, insulin inhibits hepatic gluconeogenesis. However, under pathophysiological conditions, such as insulin resistance, the suppression of hepatic gluconeogenesis can be severely attenuated. In this way, hepatic glucose production is uncontrolled, leading to hyperglycemia.

To investigate the effects of hepatic *Ide* ablation on the regulation of gluconeogenesis, we analyzed liver mRNA levels of *Pck1* and *G6pc* using RT-qPCR as described in Material and Methods section. As shown in **Figure 71**, fasting and non-fasting mRNA levels of *Pck1* were elevated by 15% and 70%, respectively, in 3-month-old L-IDE-KO male mice as compared to WT mice.

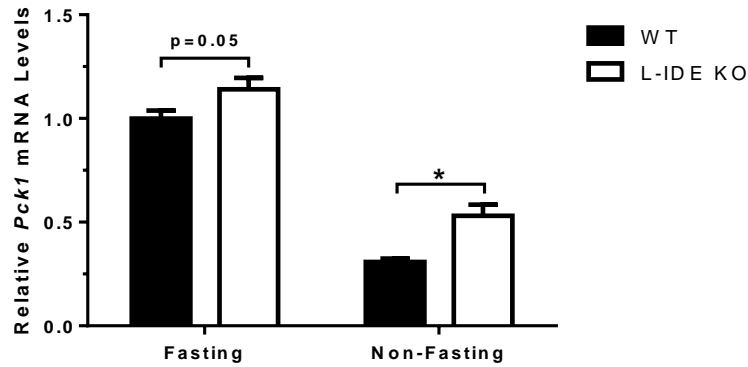


**Figure 71: Fasting and non-fasting relative mRNA levels of *Pck1* in L-IDE-KO and WT male mice.** Livers from 3-month-old L-IDE-KO and WT male mice were collected, RNA isolated, and quantified by RT-qPCR. All samples were normalized to L18.  $n = 4$  per genotype. Data are mean  $\pm$  SEM. \*  $p < 0.05$  vs. WT by Students' T-test.

Likewise, fasting and non-fasting mRNA levels of *G6pc* were elevated by 20% and 40%, respectively, in 3-month-old L-IDE-KO male mice as compared to WT mice (**Figure 72**).

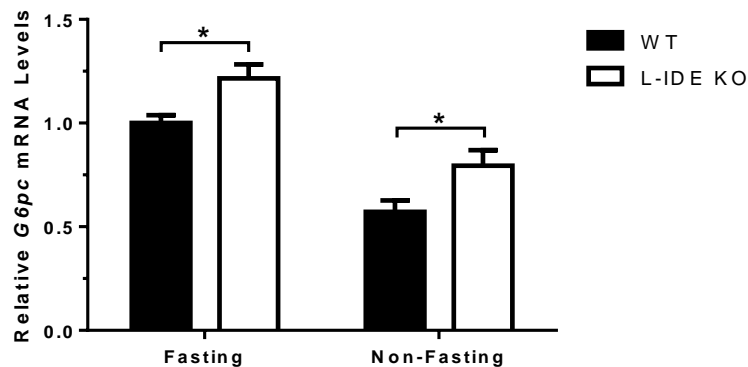


**Figure 72: Fasting and non-fasting relative mRNA levels of *G6pc* in L-IDE-KO and WT male mice.** Livers from 3-month-old L-IDE-KO and WT male mice were collected, RNA isolated, and quantified by RT-qPCR. All samples were normalized to L18.  $n = 4$  per genotype. Data are mean  $\pm$  SEM. \*  $p < 0.05$  vs. WT by Students' T-test.

In summary, these data demonstrate that impaired hepatic insulin signaling in L-IDE-KO mice leads to an upregulation of gluconeogenic genes in both, fasting and non-fasting conditions. In addition, these results begin to explain the molecular mechanisms by which *Ide* deficiency leads to glucose intolerance and augmented blood glucose levels in L-IDE-KO mice.

To confirm that hepatic insulin resistance developed by L-IDE-KO mice induced an increase of hepatic gluconeogenesis process, we performed an IPPTT.

Surprisingly, neither L-IDE-KO female mice (**Figure 73**) nor L-IDE-KO male mice (**Figure 74**) showed any difference in hepatic gluconeogenesis values regarding to WT mice, during the IPPTT.

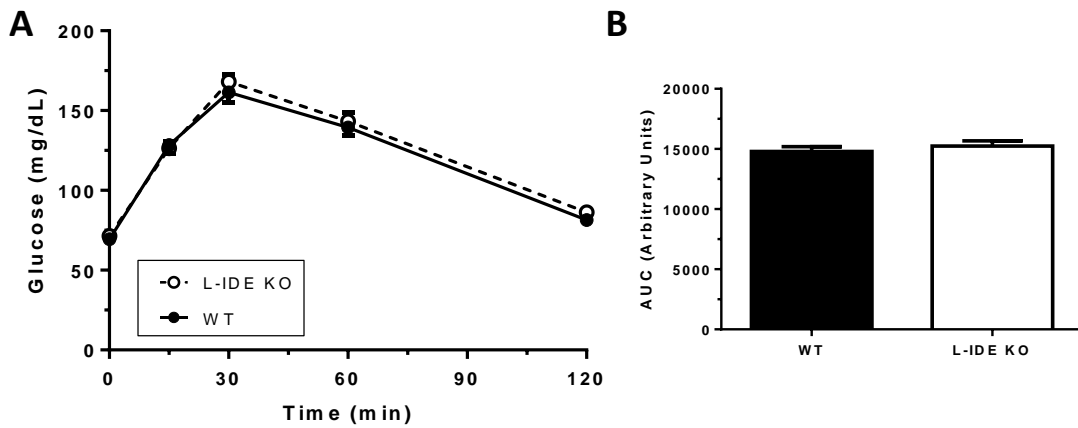


**Figure 73: IPPTT of 3-month-old L-IDE-KO and WT female mice.** (A) 3-month-old L-IDE-KO and WT female mice were intraperitoneally injected with a bolus of pyruvate at a dose of 2 g/kg of body weight after an overnight fasting. Glucose measurements were done at the indicated times. (B) AUC of IPPTT. n= 12-21 per genotype. Data are mean  $\pm$  SEM.

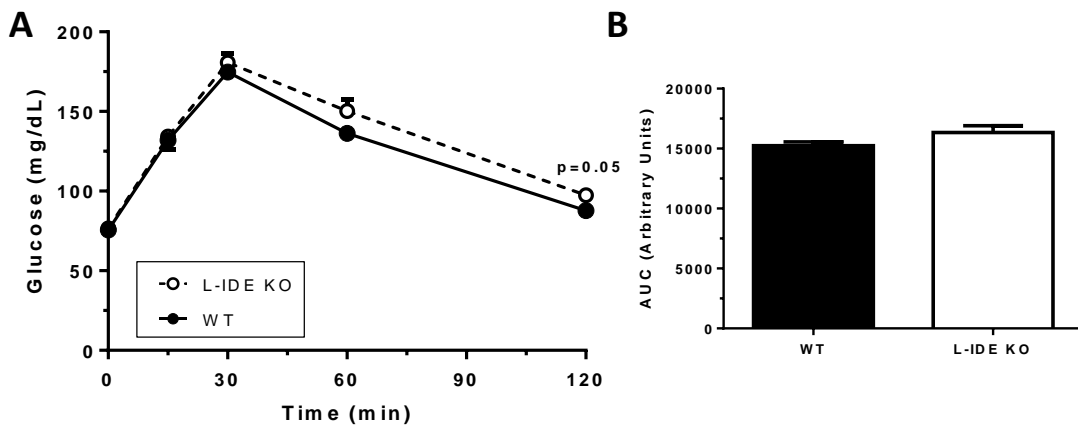


**Figure 74: IPPTT of 3-month-old L-IDE-KO and WT male mice.** (A) 3-month-old L-IDE-KO and WT male mice were intraperitoneally injected with a bolus of pyruvate at a dose of 2 g/kg of body weight after an overnight fasting. Glucose measurements were done at the indicated times. (B) AUC of IPPTT. n= 12-13 per genotype. Data are mean  $\pm$  SEM.

These results suggest that pyruvate is not a major gluconeogenic substrate for hepatic gluconeogenesis in our experimental conditions. However, it is plausible to propose that administration of other gluconeogenic substrates such as glycerol, amino-acids or lactate, may result in enhanced hepatic glucose production.

### 5.2.13 Insulin regulates hepatic IDE protein levels

With the purpose of investigating whether insulin action alters IDE protein levels, we analyzed the IDE content in liver and skeletal muscle by western blots in L-IDE-KO and WT mice.

Surprisingly, insulin treated WT mice showed lower hepatic IDE protein levels than mice injected with saline solution (**Figure 75**).

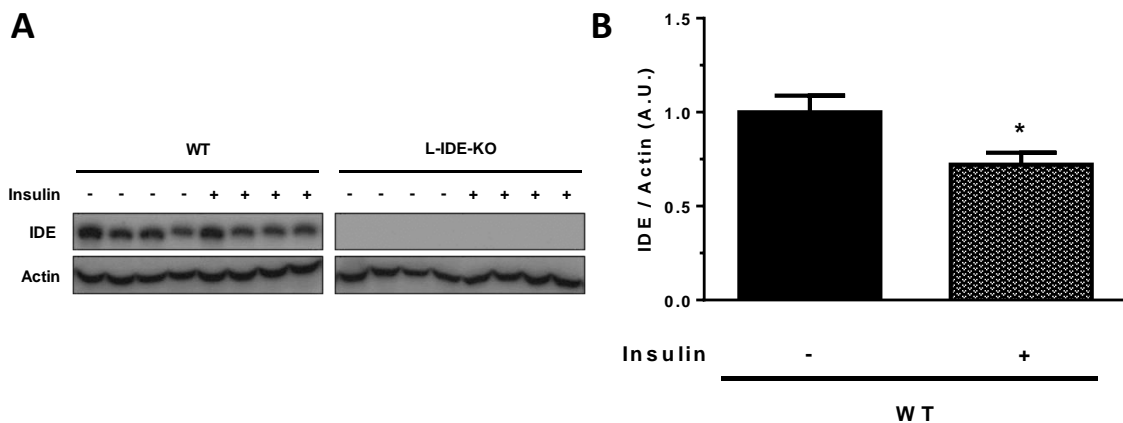


**Figure 75: IDE levels in the liver of L-IDE-KO and WT male mice.** (A) Representative western blots of liver lysates (40  $\mu$ g protein/sample) isolated from 3-month-old L-IDE-KO and WT male mice using anti-IDE and anti-actin antibodies. (B) Relative amounts of IDE, after normalizing to actin.  $n = 6$  per genotype. Data are mean  $\pm$  SEM. \* $p < 0.05$  vs. WT by Student's  $T$ -test.

In contrast, insulin did not alter the protein levels of IDE in skeletal muscle of L-IDE-KO and WT mice (**Figure 76**).

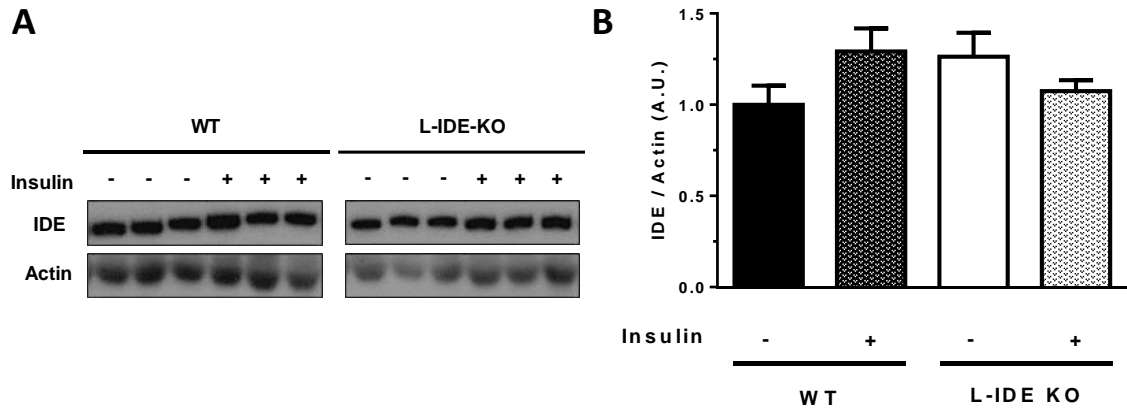


**Figure 76: IDE levels in the skeletal muscle of L-IDE-KO and WT male mice.** (A) Representative western blots of skeletal muscle lysates (40  $\mu$ g protein/sample) isolated from 3-month-old L-IDE-KO and WT male mice using anti-IDE and anti-Actin antibodies. (B) Relative amounts of IDE, after normalizing to Actin. n= 6 per genotype. Data are mean  $\pm$  SEM.

These results uncover an unidentified post-transcriptional regulatory mechanism of IDE in the liver.



## **Discussion**



## 6 **DISCUSSION**

A hallmark of obesity and T2DM is the presence of insulin resistance. Despite many efforts to elucidate the etiology of insulin resistance, the precise mechanism(s) responsible remain undetermined. Taking into account the epidemic of obesity<sup>20-22</sup>, and the fact that most obese patients are insulin resistant<sup>23,24</sup>, the principal hypotheses put forward to explain this condition have emerged from an adipocentric point of view. On the one hand, *fat overload theory* postulates that ectopic deposition of elevated circulating plasma FFAs in peripheral tissues led to accumulation of toxic lipid intermediaries, such as diacylglycerol, which causes inhibition of the intracellular insulin-signaling pathway by activation of protein kinase C (PKC) isoforms<sup>70,77</sup>. On the other hand, *inflammation theory* postulates that circulating pro-inflammatory cytokines, stemming from dysfunctional adipose tissue, are involved in the interruption of intracellular insulin-signaling pathway through a cross-talk with inflammatory signaling pathways, such as inhibitor of nuclear factor kappa-B / nuclear factor kappa-light-chain-enhancer of activated B cells (IKK $\beta$ /NF- $\kappa$ B) pathway<sup>187</sup>.

However, the traditional paradigm is confounded by the existence of metabolically obese normal weight (MONW) patients, around 10-27% of lean individuals (BMI < 25) exhibit insulin resistance<sup>188,189</sup>; and by the metabolically healthy obese (MHO) subjects, around 13-29% of obese patients do not present insulin resistance<sup>188-190</sup>. For both scenarios, current hypotheses fail to explain insulin resistance etiology.

Delineating the precise etiology (or etiologies) of insulin resistance will not be trivial, but it would represent a critical step towards the development of novel drugs for the prevention, treatment and cure of metabolic alterations, such as impaired glucose homeostasis. Given the contradictions in the literature, it is necessary to revise our current hypotheses, in order to find new therapeutic targets for the treatment of T2DM.

Current treatments of T2DM primarily focus on two actions: to improve insulin secretion by secretagogues; and to improve peripheral insulin sensitivity. In fact, current treatments usually combine both types, secretagogues as sulfonylureas (SFUs) or glinides, together with drugs that increase insulin effects as pioglitazone or metformin<sup>191,192</sup>. On the other hand, incretins are also commonly used to stimulate insulin secretion by pancreatic  $\beta$ -cells and to reduce blood glucose levels, such as dipeptidyl peptidase-4 (DPP-4) inhibitors or glucagon-like peptide-1 (GLP-1) agonist<sup>193</sup>.

### Deciphering the role of IDE as a new therapeutic target for the treatment of T2DM

Recently, it has been proposed that pharmacological approaches towards regulation of hepatic insulin homeostasis may help diabetic patients to achieve better metabolic control of whole-body glucose homeostasis<sup>173</sup>. But these approaches suffer from a lack of knowledge about the regulation of hepatic insulin clearance. Several studies describe IDE as the major enzyme involved in the insulin degradation process *in vitro*<sup>165</sup>. So far, emerging knowledge using the total-IDE-KO mouse has spurred the notion that inhibition of IDE activity leads to hyperinsulinemia<sup>170</sup>. However, this mouse model developed insulin resistance and glucose intolerance, which was explained by the authors as a secondary phenotype due to hyperinsulinemia<sup>170</sup>. These observations have prompted the development of new compounds with inhibitory activity on IDE, but with controversial results regarding the capacity of regulation of whole-body glucose homeostasis<sup>173</sup>. Therefore, the role of IDE in the regulation of hepatic plasma insulin clearance, and the effectiveness of pharmacological approaches to inhibit IDE activity remains unclear.

To shed light to these issues, we have developed a novel mouse model featuring liver-specific knockout of IDE (L-IDE-KO). We demonstrate in this work that ablation of hepatic *Idc* causes hyperglycemia, glucose intolerance and insulin resistance, independently of plasma insulin levels, food intake and body weight in male and female mice of 1 and 3 months of age. In L-IDE-KO female

mice, this phenotype is developed at early ages, but in L-IDE-KO male mice, the phenotype gets worse with aging. Insulin resistance, in both female and male L-IDE-KO mice, was assessed by different experimental approaches such as IPITT and HOMA index.

In this way, our results partially coincide with those obtained during the metabolic characterization of total-IDE-KO mice, where Farris *et al.*<sup>157</sup> and Abdul-Hay *et al.*<sup>170</sup> found that IDE total knock-out mice had increased fasting circulating insulin levels, were glucose intolerant and showed insulin resistance; however, Steneberg *et al.*<sup>171</sup> found that total-IDE-KO mice had normal fasting circulating insulin concentrations and did not find insulin resistance, despite being hyperglycemic and glucose intolerant.

In our study, to elucidate IDE's role in hepatic insulin clearance, plasma insulin levels were measured after intra-orbital insulin dose-administration, with the purpose of assessing the liver's ability to carry out insulin clearance processes in the presence or absence of IDE. Our data showed no differences in hepatic insulin clearance ratio between WT and L-IDE-KO mice. In addition, we must take into account that clearance of circulating insulin occurs primarily in liver and in less amount in the kidney. In this way, in order to reject the hypothesis about a possible insulin clearance compensation by the kidney as a response of hepatic IDE absence, kidney IDE amount was analyzed in WT and L-IDE-KO mice. The observed results not only showed that there is no IDE overexpression as compensatory mechanism in the kidney, but actually showed a decrease of kidney IDE levels. Therefore, these findings indicate that IDE is not the principal or rate-limiting factor involved in insulin clearance processes *in vivo*, supporting the theory raised by Durham *et al.*<sup>175</sup>, but they also help to clarify the mechanisms underlying hepatic insulin clearance. In addition, in view of our results, we can hypothesize that the phenotypes exhibited by total-IDE-KO mice characterized by Farris *et al.*<sup>157</sup> and Abdul-Hay *et al.*<sup>170</sup>, which include hyperinsulinemia, glucose intolerance and insulin resistance, are a consequence of the insulin resistance generated mainly in peripheral tissues, and not because of a deficiency in insulin clearance associated with the lack of IDE. Furthermore, one

needs to take into account that their mice are total KO with IDE lost in all cell types, which complicates the interpretation of the observed phenotype.

By utilizing Cre-mediated, tissue-specific ablation of *Ide*, we have developed an ideal mouse model to help elucidate the involvement of IDE in hepatic insulin clearance. By excluding IDE as a significant mediator of this process, we can postulate that other proteins might be more critical for insulin clearance, such as carcinoembryonic antigen-related cell adhesion molecule 1 (CEACAM1), a substrate of the IR in liver which has been described as the main modulator of hepatic insulin clearance by Poy *et al.*<sup>98</sup>.

In summary, although some studies using the total-IDE-KO mouse model support the notion that hyperinsulinemia is induced by a deficiency in hepatic plasma insulin clearance associated with the deficiency of IDE; our L-IDE-KO mouse model does not support the notion that IDE has a major role in hepatic plasma insulin clearance.

#### Hepatic depletion of IDE impairs intracellular insulin signaling

The hyperglycemia, glucose intolerance and insulin resistance displayed by L-IDE-KO mice were associated with reduced levels of membrane-associated IR $\beta$ . Abdul-Hay *et al.*<sup>170</sup> showed similar results, albeit in the context of hyperinsulinemia which was not present in our mouse model. In addition, our study associates the lack of hepatic IDE, not only with a decrease of IR, but also with a reduction of insulin receptor phosphorylation levels in the presence of insulin. This is probably due to a failure in insulin receptor recycling process once it is endocytosed, as a result of this failure it will be an inability to dissociate insulin-IR complexes, remaining the insulin-IR complex into endosomes in the cytosol. As consequence, hepatic insulin-signaling pathway is blocked in absence of hepatic IDE.

Given that insulin regulates a plethora of metabolic processes in the liver, such as protein and lipid synthesis, cellular proliferation and differentiation, and glucose metabolism, we were interested to analyze the intracellular insulin-

signaling pathway in the L-IDE-KO mice. Specifically, we analyzed phosphorylation levels of AKT1, involved in protein synthesis, cell survival, and inhibition of apoptosis<sup>57,194,195</sup>; and AKT2, which regulates metabolic processes exclusively<sup>57,58,194,195</sup>. In addition, we must take into account that AKT is considered a critical node of the insulin-signaling pathway<sup>47</sup> and regulates the activity of other kinases downstream, such as: GSK3, involved in glycogen production<sup>47,59</sup>; SREBP-1c, a lipogenesis and cholesterol homeostasis regulator<sup>60,61</sup>; and FoxO1, a gluconeogenesis regulator<sup>62,95</sup>. Answering this concern, we have found that reduced insulin receptor phosphorylation levels were associated with impaired insulin signaling at the level of AKT1 and AKT2.

Consistent with a reduction in the activity of AKT2, we observed that the mRNA levels of genes involved in the regulation of gluconeogenesis, such as *Pck1*<sup>99,134,135</sup> and *G6pc*<sup>137,138</sup>, were significantly elevated in the L-IDE-KO mice under fasting and non-fasting conditions. We hypothesize that the reduced ability of AKT2 to phosphorylate FoxO1 leads to the translocation from the cytoplasm to the nucleus of the transcription factor<sup>95,97,99</sup>. In the nucleus, FoxO1 promotes the transcription of *Pck1* and *G6pc*, unleashing hepatic gluconeogenesis. Interestingly, the IPPTT did not support this hypothesis, since plasma glucose levels remained unaltered during the test. These results may be explained in two ways: First, pyruvate is not the best gluconeogenic substrate in our conditions, and the test should be repeated using other gluconeogenic substrates such as glycerol, lactate, etc. Second, FoxO1 not only controls the expression of gluconeogenic genes, but also regulates glycogenolysis. Thus, the main impact of insulin resistance on FoxO1 may impact the regulation of glycogenolysis.

Another downstream target of AKT2 is GSK3, which regulates glycogen synthesis. In response to insulin, AKT2 phosphorylates and inactivates GSK3, leading to activation of GS and glycogen synthesis. In the absence of insulin, AKT2 no longer phosphorylates GSK3, which in turn inactivates GS by phosphorylation, leading to inhibition of glycogen synthesis<sup>47,59,99</sup>. Surprisingly, we found that phosphorylation levels of GSK3 were significantly augmented in both, fasting and non-fasting conditions, in the L-IDE-KO mice. This result was

completely unexpected. We hypothesize that, through an unknown kinase, GSK3 is phosphorylated in an attempt to compensate for the loss-of-function of AKT2 and maintain the GS capacity upon insulin stimulation. This compensatory mechanism may be responsible for the weak phenotype of blood glucose levels in the L-IDE-KO mice. In addition, this compensatory mechanism may also explain that hepatic glycogen levels are similar between L-IDE-KO and control littermates.

On the other hand, regulation of hepatic glycogen stores is also mediated by the expression or activity of enzymes involved in the glycogenolysis process, such as the glycogen phosphorylase<sup>119,127</sup>. We have not assessed the activity and protein levels of this enzyme in this work, but certainly, we ought to investigate the impact of hepatic *Ide* ablation on glycogenolysis to explain the metabolic phenotype of L-IDE-KO mice.

Likewise, we did not investigate the impact of hepatic IDE ablation on other cell processes, such as protein synthesis and apoptosis, which could be studied in the future to further clarify the role of IDE in these processes.

#### Regulation of IDE levels by insulin in hepatocytes

Other interesting findings were discovered after liver and skeletal muscle analysis of WT mice. For example, the finding that hepatic IDE levels diminished under insulin stimulus, while IDE levels in skeletal muscle remained unaltered. In fact, Pivovarova *et al*<sup>156</sup> observed increased IDE activity under normal glucose concentrations when human hepatoma (HepG2) cells were treated with insulin; however, under high glucose concentrations, insulin did not induce changes in IDE activity. In this way, these findings suggest that hyperglycemia established in T2DM induces a disturbance in IDE activity<sup>156</sup>.

These data open another research direction, which suggests that IDE function is regulated differently depending on the tissue; in addition, IDE probably has other functions which have not yet been elucidated.

### Impact of hepatic depletion of IDE on lipid metabolism

The liver is a main organ involved in the regulation of glucose and lipid metabolism through the action of insulin and glucagon. In the fasting state, the predominant hormone is glucagon, which promotes hepatic glycogenolysis and gluconeogenesis. In the fed state, insulin takes control of glucose metabolism and inhibits glycogenolysis and gluconeogenesis processes. However, insulin also regulates hepatic lipid metabolism promoting lipogenesis and fat accumulation. Insulin stimulates *de novo* lipogenesis through the stimulation and combined action of three transcription factors: LXR, SREBP-1c and carbohydrate-responsive element-binding protein (ChREBP). These transcription factors promote the expression of lipogenic genes and fatty acid accumulation in the liver. The process involves three steps: 1) *de novo* lipogenesis, 2) fatty acid esterification, and 3) very-low-density lipoprotein (VLDL) secretion<sup>196</sup>. Because insulin is necessary for hepatic lipogenesis, we might hypothesize that hepatic insulin resistance would decrease hepatic triglyceride synthesis and secretion, leading to reduced plasma triglyceride levels. However, insulin resistance in mice and humans is associated with hypertriglyceridemia. How can these two observations be reconciled? To resolve this paradox, it has been proposed that there may be pathway-selective insulin resistance<sup>197,198</sup>. That is, there might be distinct insulin-sensitive signaling pathways that independently modulate glucose and lipid metabolism. The main framework of this concept of selective hepatic insulin resistance is grounded in the notion that with selective insulin resistance, insulin fails to suppress hepatic glucose output (glycogenolysis and gluconeogenesis), and yet still augments hepatic lipogenesis. Overall, this model proposes that insulin-mediated regulation of glucose metabolism is impaired, whereas insulin-mediated regulation of lipid metabolism remains intact.

Because our L-IDE-KO mouse model does not exhibit hypertriglyceridemia, but hepatic glucose metabolism is altered, we propose that hepatic ablation of *Ide* causes selective hepatic insulin resistance (**Figure 77**).

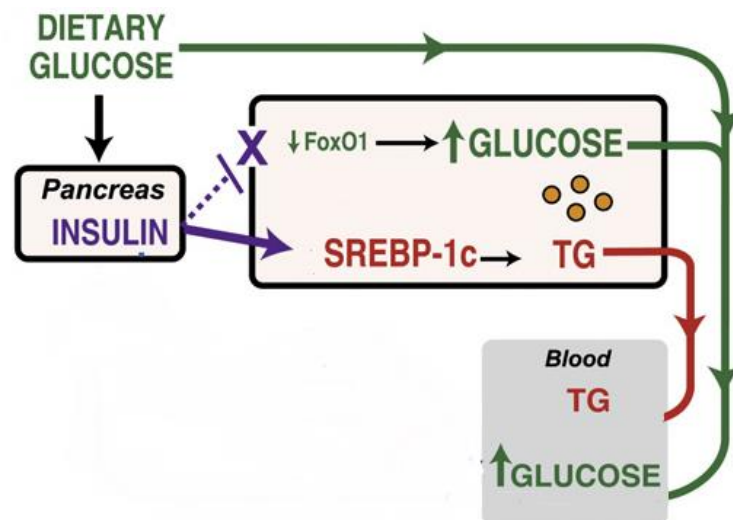


**Figure 77:** Selective insulin resistance in the liver of L-IDE-KO mice. Adapted from Brown MS. and Goldstein JL.<sup>197</sup>.

The liver has the capacity to convert glucose to lipids through *de novo* lipogenesis, but this metabolic feature in physiological terms is a relatively minor metabolic pathway. However, under conditions of carbohydrate overfeeding this pathway becomes relevant. It would be worthy to investigate the impact of hepatic ablation of *Ide* in mice fed a carbohydrate rich diet. In this line of thinking, glycogen synthesis is the metabolic pathway responsible for the major fate of glucose in the liver. Spillover of glucose due to impaired glycogen synthesis is diverted to glucose oxidation and lipid synthesis. In our mouse model, the pathway of glycogen synthesis seems not to be affected by deletion of *Ide*, which may support the hypothesis that glucose partitioning to *de novo* lipogenesis is not affected.

We propose that hepatic *Ide* ablation causes selective hepatic insulin resistance, i.e. triglycerides synthesis was not affected, cholesterol synthesis seems to be altered. In this way, we hypothesize that the regulation of the main transcription factors involved in cholesterol synthesis, SREBP-1a and SREBP-2<sup>199</sup>, may be downregulated in parallel with hepatic insulin resistance. In this manner, the lower circulating cholesterol levels exhibited by L-IDE-KO mice could be a result of another selective hepatic insulin resistance which alters the expression of SREBP-1a and SREBP-2 transcription factors<sup>199</sup> (**Figure 78**).

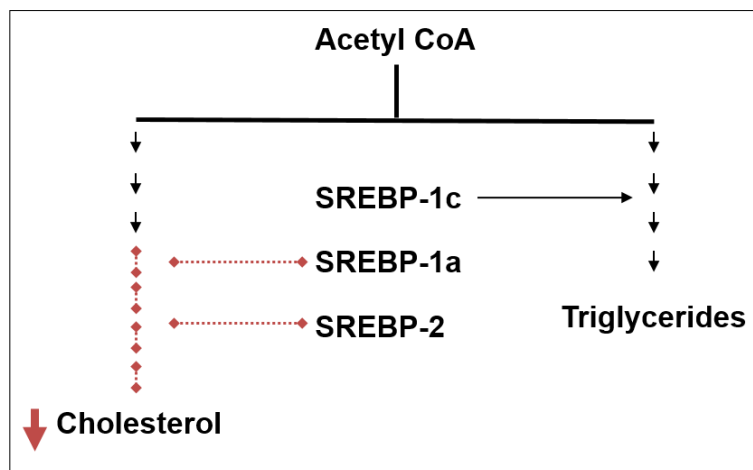


**Figure 78:** Liver transcriptional control of cholesterol and triglycerides synthesis.

### Impact of hepatic insulin resistance on peripheral insulin sensitivity

Hepatic insulin resistance in the L-IDE-KO mouse was not associated with skeletal muscle insulin resistance. Insulin was able to stimulate the insulin-signaling pathway in the muscle cells of L-IDE-KO mice. So far, our knowledge about the etiology of muscle insulin resistance is focused on the ectopic accumulation of fat in the skeletal muscle<sup>68</sup>. As reviewed by Samuel and Shulman<sup>68</sup>, intracellular accumulation of diacylglycerol mediates activation of protein kinase C- $\theta$  (PKC $\theta$ ) leading to phosphorylation of IRS1/2 in serine residues. This molecular mechanism causes impaired insulin signaling and diminished translocation of vesicle-containing GLUT4 to plasma membrane. Plasma FFA and triglyceride levels are not elevated in our L-IDE-KO mice; this is consistent with insulin sensitivity of the skeletal muscle. Therefore, the increase in plasma glucose levels in the L-IDE-KO mice most likely is due to impaired hepatic glucose metabolism, rather than altered glucose uptake in skeletal muscle.

Likewise, we have observed that insulin-stimulated reductions in plasma FFA levels are significantly larger in the L-IDE-KO mice compared to control mice. These data support the notion that lipolysis is more effectively suppressable in the adipose tissue of the L-IDE-KO mice, which may be due to enhanced insulin

sensitivity in this tissue. Further research is warranted to investigate the impact of hepatic ablation of *Ide* on adipose tissue in L-IDE-KO mice.

#### Impact of hepatic ablation of *Ide* on other targets

IDE has been described as a 110-kDa metalloprotease. The main catalytic function attributed to IDE is the degradation of insulin, although it also degrades a number of other substrates, including glucagon, amylin and A $\beta$ <sup>96,159,160</sup>.

It should be noted that IDE has been described as one of the main enzymes involved in insulin clearance due to its affinity for insulin<sup>173,200</sup>. However, Durham *et al.*<sup>175</sup> proposed that IDE is not the main enzyme involved in plasma insulin clearance *in vivo*, but they emphasized its fundamental role in amylin clearance.

We showed that hepatic depletion of *Ide* is associated with augmented plasma glucagon levels. This phenotype was more pronounced at young ages. Interestingly, dysregulated glucagon clearance is not accompanied by plasma insulin levels alterations at early ages. We must take into account that the plasma glucagon clearance is not fully understood. Dobbins *et al.*<sup>201</sup> indicate that glucagon clearance in dogs occurs in the liver and kidneys, preferentially in the liver<sup>201</sup>. Other studies propose that glucagon degradation occurs in the plasma membrane of hepatocytes through receptors involving both saturable and non-saturable mechanisms<sup>120</sup>. However, studies performed by Deacon *et al.*<sup>202</sup>, Zhou *et al.*<sup>203</sup> and Lefebvre *et al.*<sup>204</sup> in pigs and dogs indicate that kidneys are the most important tissue for glucagon elimination, by a molecular mechanism that involves the dipeptidyl peptidase-4 (DPP-4) enzyme located in the renal tubular brush border. In fact, the mechanism of glucagon clearance process in mice is unknown. Therefore, our L-IDE-KO mouse model represents a valuable tool for investigating the molecular mechanisms of plasma glucagon clearance.

On the other hand, IDE is one of the principal known amylin- and A $\beta$ -degrading enzymes<sup>159,160</sup>. First of all, we must keep in mind that amylin and A $\beta$  share several features, such as similar  $\beta$ -sheet secondary structures<sup>205</sup>, bind to the same amylin receptor<sup>206</sup> and can be degraded by IDE<sup>151,160,178</sup>. In spite of this,

rodent amylin structure is quite different than others, including human amylin, because rodent amylin displays proline at residues 20-29 and does not generate amyloid fibrils; while, amylin from other species, such as human amylin, create  $\beta$ -pleated sheet formation around residues 20-29 of the primary sequence generating amyloid fibrils spontaneously<sup>207</sup>. Amylin is co-secreted with insulin by pancreatic  $\beta$ -cells in a ratio of approximately 1:100, and contributes to glycemic control<sup>208</sup>. In addition, increased circulating amylin levels are associated with insulin resistance, in which insulin secretion and consequently, amylin secretion is augmented. This metabolic alteration induces pancreatic  $\beta$ -cells dysfunction, characterized by the accumulation of amyloid deposits<sup>209,210</sup>. In this context, given that amylin and insulin are co-secreted, our findings in L-IDE-KO mice—which showed hyperglycemia, glucose intolerance and insulin resistance, but unchanged circulating plasma amylin levels—suggest that insulin resistance was primarily caused by impaired hepatic insulin signaling, and was not accompanied by augmented insulin secretion.

Summarizing, our analysis and metabolic characterization of L-IDE-KO mice resolve conflicting ideas about the role of hepatic IDE in glucose homeostasis and insulin action *in vivo*. The absence of hepatic IDE causes insulin resistance, glucose intolerance, and hyperglycemia, through molecular mechanisms which involve impaired hepatic insulin signaling, leading to upregulation of gluconeogenic genes. In addition, our study supports the notion that IDE has not a principal or rate-limiting regulator of plasma insulin levels *in vivo*, but may be more relevant for the hepatic clearance of plasma glucagon. From a therapeutic perspective, our results suggest that pharmacological inhibition of IDE would be contraindicated as a therapeutic approach to diabetes treatment.



## **Conclusions**



## **7 CONCLUSIONS**

1. We demonstrate that IDE is not the principal enzyme involved in hepatic plasma insulin clearance in mice. However, our study reveals a potential role of IDE in hepatic plasma clearance of glucagon.
2. The absence of hepatic IDE disrupts whole-body glucose homeostasis while triggering insulin resistance in mice. These results suggest that IDE is a new agent in the etiology of hepatic insulin resistance.
3. We have identified a new molecular mechanism by which IDE causes hepatic insulin resistance independently of the proteolytic activity of IDE. This mechanism involves diminished plasma membrane insulin receptor levels.
4. Our work challenges the notion that pharmacological inhibition of IDE represents a new therapeutic approach for the treatment of T2DM.



## **References**



## **8 REFERENCES**

1. IDF diabetes atlas - Home. Available at: <http://www.diabetesatlas.org/>.
2. Rathmann, W. & Giani, G. Global prevalence of diabetes: estimates for the year 2000 and projections for 2030. *Diabetes Care* **27**, 2568–2569; author reply 2569 (2004).
3. User, S. IDF diabetes atlas - Across the globe. Available at: <http://www.diabetesatlas.org/across-the-globe.html>.
4. Soriguer, F. *et al.* Prevalence of diabetes mellitus and impaired glucose regulation in Spain: the Di@bet.es Study. *Diabetologia* **55**, 88–93 (2012).
5. Mathers, C. D. & Loncar, D. Projections of global mortality and burden of disease from 2002 to 2030. *PLoS Med.* **3**, e442 (2006).
6. WHO | *Global report on diabetes*. WHO Available at: <http://www.who.int/diabetes/global-report/en/>.
7. Lopez-Bastida, J., Boronat, M., Moreno, J. O. & Schurer, W. Costs, outcomes and challenges for diabetes care in Spain. *Glob. Health* **9**, 17 (2013).
8. Alberti, K. G. & Zimmet, P. Z. Definition, diagnosis and classification of diabetes mellitus and its complications. Part 1: diagnosis and classification of diabetes mellitus provisional report of a WHO consultation. *Diabet. Med. J. Br. Diabet. Assoc.* **15**, 539–553 (1998).
9. Seino, Y. *et al.* Report of the committee on the classification and diagnostic criteria of diabetes mellitus. *J. Diabetes Investig.* **1**, 212–228 (2010).

10. Genuth, S. *et al.* Follow-up report on the diagnosis of diabetes mellitus. *Diabetes Care* **26**, 3160–3167 (2003).
11. Bach, J. F. Insulin-dependent diabetes mellitus as an autoimmune disease. *Endocr. Rev.* **15**, 516–542 (1994).
12. Eisenbarth, G. S. Type I diabetes mellitus. A chronic autoimmune disease. *N. Engl. J. Med.* **314**, 1360–1368 (1986).
13. Imagawa, A., Hanafusa, T., Miyagawa, J. & Matsuzawa, Y. A novel subtype of type 1 diabetes mellitus characterized by a rapid onset and an absence of diabetes-related antibodies. Osaka IDDM Study Group. *N. Engl. J. Med.* **342**, 301–307 (2000).
14. Kahn, S. E. The pathophysiologic defects of type 2 diabetes. Abnormal insulin action and impaired insulin secretion. *Postgrad. Med.* **107**, 11–15 (2000).
15. Unoki, H. *et al.* SNPs in KCNQ1 are associated with susceptibility to type 2 diabetes in East Asian and European populations. *Nat. Genet.* **40**, 1098–1102 (2008).
16. Yasuda, K. *et al.* Variants in KCNQ1 are associated with susceptibility to type 2 diabetes mellitus. *Nat. Genet.* **40**, 1092–1097 (2008).
17. Zimmet, P., Alberti, K. G. & Shaw, J. Global and societal implications of the diabetes epidemic. *Nature* **414**, 782–787 (2001).
18. Body mass index - BMI. (2017). Available at: <http://www.euro.who.int/en/health-topics/disease-prevention/nutrition/a-healthy-lifestyle/body-mass-index-bmi>.

19. Clinical Guidelines on the Identification, Evaluation, and Treatment of Overweight and Obesity in Adults--The Evidence Report. National Institutes of Health. *Obes. Res.* **6 Suppl 2**, 51S–209S (1998).
20. WHO | Global status report on noncommunicable diseases 2014. *WHO* Available at: <http://www.who.int/nmh/publications/ncd-status-report-2014/en/>.
21. WHO | Global Health Observatory | Map Gallery. Available at: <http://gamapserver.who.int/mapLibrary/app/searchResults.aspx>.
22. Waxman, A. & World Health Assembly. WHO global strategy on diet, physical activity and health. *Food Nutr. Bull.* **25**, 292–302 (2004).
23. Meigs, J. B. *et al.* Body mass index, metabolic syndrome, and risk of type 2 diabetes or cardiovascular disease. *J. Clin. Endocrinol. Metab.* **91**, 2906–2912 (2006).
24. Saltiel, A. R. & Kahn, C. R. Insulin signalling and the regulation of glucose and lipid metabolism. *Nature* **414**, 799–806 (2001).
25. Gebreab, S. Y. *et al.* Neighborhood social and physical environments and type 2 diabetes mellitus in African Americans: The Jackson Heart Study. *Health Place* **43**, 128–137 (2016).
26. Jackson, W. P. Diabetes and related variables among the five main racial groups in South Africa: comparisons from population studies. *Postgrad. Med. J.* **48**, 391–398 (1972).
27. Wilson, P. W., McGee, D. L. & Kannel, W. B. Obesity, very low density lipoproteins, and glucose intolerance over fourteen years: The Framingham Study. *Am. J. Epidemiol.* **114**, 697–704 (1981).

28. Ohlson, L. O. *et al.* Diabetes mellitus in Swedish middle-aged men. The study of men born in 1913 and 1923. *Diabetologia* **30**, 386–393 (1987).
29. Modan, M. *et al.* Effect of past and concurrent body mass index on prevalence of glucose intolerance and type 2 (non-insulin-dependent) diabetes and on insulin response. The Israel study of glucose intolerance, obesity and hypertension. *Diabetologia* **29**, 82–89 (1986).
30. Swinburn, B. A. *et al.* The global obesity pandemic: shaped by global drivers and local environments. *Lancet Lond. Engl.* **378**, 804–814 (2011).
31. Tackling obesity in England. *Health Educ. Res.* **16**, 399–400 (2001).
32. Henquin, J. C. Triggering and amplifying pathways of regulation of insulin secretion by glucose. *Diabetes* **49**, 1751–1760 (2000).
33. Steiner, D. F. & Oyer, P. E. The biosynthesis of insulin and a probable precursor of insulin by a human islet cell adenoma. *Proc. Natl. Acad. Sci. U. S. A.* **57**, 473–480 (1967).
34. DeFronzo, R. A. Lilly lecture 1987. The triumvirate: beta-cell, muscle, liver. A collusion responsible for NIDDM. *Diabetes* **37**, 667–687 (1988).
35. Kumar, S. & O’Rahilly, S. *Insulin Resistance: Insulin Action and its Disturbances in Disease*. (John Wiley & Sons, 2005).
36. Lewis, G. F., Zinman, B., Groenewoud, Y., Vranic, M. & Giacca, A. Hepatic glucose production is regulated both by direct hepatic and extrahepatic effects of insulin in humans. *Diabetes* **45**, 454–462 (1996).

37. Rebrin, K., Steil, G. M., Getty, L. & Bergman, R. N. Free fatty acid as a link in the regulation of hepatic glucose output by peripheral insulin. *Diabetes* **44**, 1038–1045 (1995).
38. DeFronzo, R. A. Banting Lecture. From the triumvirate to the ominous octet: a new paradigm for the treatment of type 2 diabetes mellitus. *Diabetes* **58**, 773–795 (2009).
39. Plum, L., Belgardt, B. F. & Brüning, J. C. Central insulin action in energy and glucose homeostasis. *J. Clin. Invest.* **116**, 1761–1766 (2006).
40. Schwartz, M. W., Woods, S. C., Porte, D., Seeley, R. J. & Baskin, D. G. Central nervous system control of food intake. *Nature* **404**, 661–671 (2000).
41. Matsuda, M. *et al.* Altered hypothalamic function in response to glucose ingestion in obese humans. *Diabetes* **48**, 1801–1806 (1999).
42. Clark, M. G. *et al.* Blood flow and muscle metabolism: a focus on insulin action. *Am. J. Physiol. Endocrinol. Metab.* **284**, E241-258 (2003).
43. Newsholme, E. A. & Dimitriadis, G. Integration of biochemical and physiologic effects of insulin on glucose metabolism. *Exp. Clin. Endocrinol. Diabetes Off. J. Ger. Soc. Endocrinol. Ger. Diabetes Assoc.* **109 Suppl 2**, S122-134 (2001).
44. Boucher, J., Kleinridders, A. & Kahn, C. R. Insulin receptor signaling in normal and insulin-resistant states. *Cold Spring Harb. Perspect. Biol.* **6**, (2014).
45. Lee, J. & Pilch, P. F. The insulin receptor: structure, function, and signaling. *Am. J. Physiol.* **266**, C319-334 (1994).

46. Lee, J., Pilch, P. F., Shoelson, S. E. & Scarlata, S. F. Conformational changes of the insulin receptor upon insulin binding and activation as monitored by fluorescence spectroscopy. *Biochemistry (Mosc.)* **36**, 2701–2708 (1997).
47. Taniguchi, C. M., Emanuelli, B. & Kahn, C. R. Critical nodes in signalling pathways: insights into insulin action. *Nat. Rev. Mol. Cell Biol.* **7**, 85–96 (2006).
48. Previs, S. F., Withers, D. J., Ren, J. M., White, M. F. & Shulman, G. I. Contrasting effects of IRS-1 versus IRS-2 gene disruption on carbohydrate and lipid metabolism in vivo. *J. Biol. Chem.* **275**, 38990–38994 (2000).
49. Maheux, P., Chen, Y. D., Polonsky, K. S. & Reaven, G. M. Evidence that insulin can directly inhibit hepatic glucose production. *Diabetologia* **40**, 1300–1306 (1997).
50. Escobedo, J. A. *et al.* cDNA cloning of a novel 85 kd protein that has SH2 domains and regulates binding of PI3-kinase to the PDGF beta-receptor. *Cell* **65**, 75–82 (1991).
51. Hiles, I. D. *et al.* Phosphatidylinositol 3-kinase: structure and expression of the 110 kd catalytic subunit. *Cell* **70**, 419–429 (1992).
52. Carpenter, C. L. & Cantley, L. C. Phosphoinositide kinases. *Curr. Opin. Cell Biol.* **8**, 153–158 (1996).
53. Franke, T. F., Kaplan, D. R., Cantley, L. C. & Toker, A. Direct regulation of the Akt proto-oncogene product by phosphatidylinositol-3,4-bisphosphate. *Science* **275**, 665–668 (1997).

54. Vanhaesebroeck, B. & Alessi, D. R. The PI3K-PDK1 connection: more than just a road to PKB. *Biochem. J.* **346 Pt 3**, 561–576 (2000).
55. Sarbassov, D. D., Guertin, D. A., Ali, S. M. & Sabatini, D. M. Phosphorylation and regulation of Akt/PKB by the rictor-mTOR complex. *Science* **307**, 1098–1101 (2005).
56. Cybulski, N. & Hall, M. N. TOR complex 2: a signaling pathway of its own. *Trends Biochem. Sci.* **34**, 620–627 (2009).
57. Cho, H., Thorvaldsen, J. L., Chu, Q., Feng, F. & Birnbaum, M. J. Akt1/PKB $\alpha$  is required for normal growth but dispensable for maintenance of glucose homeostasis in mice. *J. Biol. Chem.* **276**, 38349–38352 (2001).
58. Cho, H. *et al.* Insulin resistance and a diabetes mellitus-like syndrome in mice lacking the protein kinase Akt2 (PKB  $\beta$ ). *Science* **292**, 1728–1731 (2001).
59. Bollen, M., Keppens, S. & Stalmans, W. Specific features of glycogen metabolism in the liver. *Biochem. J.* **336 (Pt 1)**, 19–31 (1998).
60. Horton, J. D., Goldstein, J. L. & Brown, M. S. SREBPs: activators of the complete program of cholesterol and fatty acid synthesis in the liver. *J. Clin. Invest.* **109**, 1125–1131 (2002).
61. Yokoyama, C. *et al.* SREBP-1, a basic-helix-loop-helix-leucine zipper protein that controls transcription of the low density lipoprotein receptor gene. *Cell* **75**, 187–197 (1993).
62. Manning, B. D. & Cantley, L. C. AKT/PKB signaling: navigating downstream. *Cell* **129**, 1261–1274 (2007).

63. Titchenell, P. M., Lazar, M. A. & Birnbaum, M. J. Unraveling the Regulation of Hepatic Metabolism by Insulin. *Trends Endocrinol. Metab. TEM* **28**, 497–505 (2017).
64. Kahn, B. B. & Flier, J. S. Obesity and insulin resistance. *J. Clin. Invest.* **106**, 473–481 (2000).
65. Reaven, G. M. Banting lecture 1988. Role of insulin resistance in human disease. *Diabetes* **37**, 1595–1607 (1988).
66. Kahn, C. R. Insulin resistance, insulin insensitivity, and insulin unresponsiveness: a necessary distinction. *Metabolism.* **27**, 1893–1902 (1978).
67. Abdul-Ghani, M. A. & DeFronzo, R. A. Pathogenesis of insulin resistance in skeletal muscle. *J. Biomed. Biotechnol.* **2010**, 476279 (2010).
68. Samuel, V. T. & Shulman, G. I. The pathogenesis of insulin resistance: integrating signaling pathways and substrate flux. *J. Clin. Invest.* **126**, 12–22 (2016).
69. Frayn, K. N. Adipose tissue and the insulin resistance syndrome. *Proc. Nutr. Soc.* **60**, 375–380 (2001).
70. Griffin, M. E. *et al.* Free fatty acid-induced insulin resistance is associated with activation of protein kinase C theta and alterations in the insulin signaling cascade. *Diabetes* **48**, 1270–1274 (1999).
71. Roden, M. *et al.* Mechanism of free fatty acid-induced insulin resistance in humans. *J. Clin. Invest.* **97**, 2859–2865 (1996).

72. Reaven, G. M., Hollenbeck, C., Jeng, C. Y., Wu, M. S. & Chen, Y. D. Measurement of plasma glucose, free fatty acid, lactate, and insulin for 24 h in patients with NIDDM. *Diabetes* **37**, 1020–1024 (1988).
73. Boden, G., Lebed, B., Schatz, M., Homko, C. & Lemieux, S. Effects of acute changes of plasma free fatty acids on intramyocellular fat content and insulin resistance in healthy subjects. *Diabetes* **50**, 1612–1617 (2001).
74. Krssak, M. *et al.* Intramyocellular lipid concentrations are correlated with insulin sensitivity in humans: a <sup>1</sup>H NMR spectroscopy study. *Diabetologia* **42**, 113–116 (1999).
75. Perseghin, G. *et al.* Intramyocellular triglyceride content is a determinant of in vivo insulin resistance in humans: a <sup>1</sup>H-<sup>13</sup>C nuclear magnetic resonance spectroscopy assessment in offspring of type 2 diabetic parents. *Diabetes* **48**, 1600–1606 (1999).
76. Manco, M., Calvani, M. & Mingrone, G. Effects of dietary fatty acids on insulin sensitivity and secretion. *Diabetes Obes. Metab.* **6**, 402–413 (2004).
77. Yu, C. *et al.* Mechanism by which fatty acids inhibit insulin activation of insulin receptor substrate-1 (IRS-1)-associated phosphatidylinositol 3-kinase activity in muscle. *J. Biol. Chem.* **277**, 50230–50236 (2002).
78. Shoelson, S. E., Lee, J. & Goldfine, A. B. Inflammation and insulin resistance. *J. Clin. Invest.* **116**, 1793–1801 (2006).
79. Hotamisligil, G. S. Inflammation and metabolic disorders. *Nature* **444**, 860–867 (2006).

80. Hotamisligil, G. S., Shargill, N. S. & Spiegelman, B. M. Adipose expression of tumor necrosis factor- $\alpha$ : direct role in obesity-linked insulin resistance. *Science* **259**, 87–91 (1993).
81. Uysal, K. T., Wiesbrock, S. M., Marino, M. W. & Hotamisligil, G. S. Protection from obesity-induced insulin resistance in mice lacking TNF- $\alpha$  function. *Nature* **389**, 610–614 (1997).
82. Hotamisligil, G. S. *et al.* IRS-1-mediated inhibition of insulin receptor tyrosine kinase activity in TNF- $\alpha$ - and obesity-induced insulin resistance. *Science* **271**, 665–668 (1996).
83. Rotter, V., Nagaev, I. & Smith, U. Interleukin-6 (IL-6) induces insulin resistance in 3T3-L1 adipocytes and is, like IL-8 and tumor necrosis factor- $\alpha$ , overexpressed in human fat cells from insulin-resistant subjects. *J. Biol. Chem.* **278**, 45777–45784 (2003).
84. Sartipy, P. & Loskutoff, D. J. Monocyte chemoattractant protein 1 in obesity and insulin resistance. *Proc. Natl. Acad. Sci. U. S. A.* **100**, 7265–7270 (2003).
85. Schinner, S., Scherbaum, W. A., Bornstein, S. R. & Barthel, A. Molecular mechanisms of insulin resistance. *Diabet. Med. J. Br. Diabet. Assoc.* **22**, 674–682 (2005).
86. Yan, J. *Epigenetic influences on type 2 diabetes and obesity*. (Inst för molekylär medicin och kirurgi / Dept of Molecular Medicine and Surgery, 2011).

87. Weyer, C., Bogardus, C. & Pratley, R. E. Metabolic characteristics of individuals with impaired fasting glucose and/or impaired glucose tolerance. *Diabetes* **48**, 2197–2203 (1999).
88. Perriello, G. *et al.* Evidence of increased systemic glucose production and gluconeogenesis in an early stage of NIDDM. *Diabetes* **46**, 1010–1016 (1997).
89. Krauss, R. M. Lipids and lipoproteins in patients with type 2 diabetes. *Diabetes Care* **27**, 1496–1504 (2004).
90. Groop, L. C. *et al.* Glucose and free fatty acid metabolism in non-insulin-dependent diabetes mellitus. Evidence for multiple sites of insulin resistance. *J. Clin. Invest.* **84**, 205–213 (1989).
91. Sommerfeld, A., Krones-Herzig, A. & Herzig, S. Transcriptional co-factors and hepatic energy metabolism. *Mol. Cell. Endocrinol.* **332**, 21–31 (2011).
92. Dey, A. & Chandrasekaran, K. Hyperglycemia induced changes in liver: in vivo and in vitro studies. *Curr. Diabetes Rev.* **5**, 67–78 (2009).
93. Ramnanan, C. J., Edgerton, D. S., Kraft, G. & Cherrington, A. D. Physiologic action of glucagon on liver glucose metabolism. *Diabetes Obes. Metab.* **13 Suppl 1**, 118–125 (2011).
94. Edgerton, D. S. *et al.* Effects of insulin on the metabolic control of hepatic gluconeogenesis in vivo. *Diabetes* **58**, 2766–2775 (2009).
95. Gross, D. N., van den Heuvel, A. P. J. & Birnbaum, M. J. The role of FoxO in the regulation of metabolism. *Oncogene* **27**, 2320–2336 (2008).
96. Duckworth, W. C., Bennett, R. G. & Hamel, F. G. Insulin degradation: progress and potential. *Endocr. Rev.* **19**, 608–624 (1998).

97. Kido, Y., Nakae, J. & Accili, D. Clinical review 125: The insulin receptor and its cellular targets. *J. Clin. Endocrinol. Metab.* **86**, 972–979 (2001).
98. Poy, M. N. *et al.* CEACAM1 regulates insulin clearance in liver. *Nat. Genet.* **30**, 270–276 (2002).
99. Ramnanan, C. J. *et al.* Molecular characterization of insulin-mediated suppression of hepatic glucose production in vivo. *Diabetes* **59**, 1302–1311 (2010).
100. Zhang, W. *et al.* FoxO1 regulates multiple metabolic pathways in the liver: effects on gluconeogenic, glycolytic, and lipogenic gene expression. *J. Biol. Chem.* **281**, 10105–10117 (2006).
101. Thorens, B. GLUT2, glucose sensing and glucose homeostasis. *Diabetologia* **58**, 221–232 (2015).
102. Olson, A. L. & Pessin, J. E. Structure, function, and regulation of the mammalian facilitative glucose transporter gene family. *Annu. Rev. Nutr.* **16**, 235–256 (1996).
103. Frayn, K. N. *Metabolic regulation: a human perspective.* (John Wiley & Sons, 2009).
104. Leturque, A., Brot-Laroche, E. & Le Gall, M. GLUT2 mutations, translocation, and receptor function in diet sugar managing. *Am. J. Physiol. Endocrinol. Metab.* **296**, E985–992 (2009).
105. Mueckler, M. & Thorens, B. The SLC2 (GLUT) family of membrane transporters. *Mol. Aspects Med.* **34**, 121–138 (2013).

106. Aschenbach, J. R., Steglich, K., Gäbel, G. & Honscha, K. U. Expression of mRNA for glucose transport proteins in jejunum, liver, kidney and skeletal muscle of pigs. *J. Physiol. Biochem.* **65**, 251–266 (2009).
107. Wilson, J. E. Isozymes of mammalian hexokinase: structure, subcellular localization and metabolic function. *J. Exp. Biol.* **206**, 2049–2057 (2003).
108. Cárdenas, M. L., Cornish-Bowden, A. & Ureta, T. Evolution and regulatory role of the hexokinases. *Biochim. Biophys. Acta* **1401**, 242–264 (1998).
109. Lenzen, S. A fresh view of glycolysis and glucokinase regulation: history and current status. *J. Biol. Chem.* **289**, 12189–12194 (2014).
110. De Meirleir, L. Defects of pyruvate metabolism and the Krebs cycle. *J. Child Neurol.* **17 Suppl 3**, 3S26-33; discussion 3S33-34 (2002).
111. Hirota, K. *et al.* A combination of HNF-4 and Foxo1 is required for reciprocal transcriptional regulation of glucokinase and glucose-6-phosphatase genes in response to fasting and feeding. *J. Biol. Chem.* **283**, 32432–32441 (2008).
112. Ganjam, G. K., Dimova, E. Y., Unterman, T. G. & Kietzmann, T. FoxO1 and HNF-4 are involved in regulation of hepatic glucokinase gene expression by resveratrol. *J. Biol. Chem.* **284**, 30783–30797 (2009).
113. Kim, T.-H. *et al.* Interrelationship between liver X receptor alpha, sterol regulatory element-binding protein-1c, peroxisome proliferator-activated receptor gamma, and small heterodimer partner in the transcriptional regulation of glucokinase gene expression in liver. *J. Biol. Chem.* **284**, 15071–15083 (2009).

114. Roth, U., Curth, K., Unterman, T. G. & Kietzmann, T. The transcription factors HIF-1 and HNF-4 and the coactivator p300 are involved in insulin-regulated glucokinase gene expression via the phosphatidylinositol 3-kinase/protein kinase B pathway. *J. Biol. Chem.* **279**, 2623–2631 (2004).
115. Roth, U., Jungermann, K. & Kietzmann, T. Modulation of glucokinase expression by hypoxia-inducible factor 1 and upstream stimulatory factor 2 in primary rat hepatocytes. *Biol. Chem.* **385**, 239–247 (2004).
116. Kim, M. Y. *et al.* Adenovirus-mediated overexpression of Tcfe3 ameliorates hyperglycaemia in a mouse model of diabetes by upregulating glucokinase in the liver. *Diabetologia* **56**, 635–643 (2013).
117. Bechmann, L. P. *et al.* Glucokinase links Krüppel-like factor 6 to the regulation of hepatic insulin sensitivity in nonalcoholic fatty liver disease. *Hepatol. Baltim. Md* **55**, 1083–1093 (2012).
118. Oosterveer, M. H. & Schoonjans, K. Hepatic glucose sensing and integrative pathways in the liver. *Cell. Mol. Life Sci. CMLS* **71**, 1453–1467 (2014).
119. Han, H.-S., Kang, G., Kim, J. S., Choi, B. H. & Koo, S.-H. Regulation of glucose metabolism from a liver-centric perspective. *Exp. Mol. Med.* **48**, e218 (2016).
120. Authier, F. & Desbuquois, B. Glucagon receptors. *Cell. Mol. Life Sci. CMLS* **65**, 1880–1899 (2008).
121. Ekberg, K. *et al.* Contributions by kidney and liver to glucose production in the postabsorptive state and after 60 h of fasting. *Diabetes* **48**, 292–298 (1999).

122. Shearer, J. & Graham, T. E. Novel aspects of skeletal muscle glycogen and its regulation during rest and exercise. *Exerc. Sport Sci. Rev.* **32**, 120–126 (2004).
123. Greenberg, C. C., Jurczak, M. J., Danos, A. M. & Brady, M. J. Glycogen branches out: new perspectives on the role of glycogen metabolism in the integration of metabolic pathways. *Am. J. Physiol. Endocrinol. Metab.* **291**, E1-8 (2006).
124. Roach, P. J., Depaoli-Roach, A. A., Hurley, T. D. & Tagliabracci, V. S. Glycogen and its metabolism: some new developments and old themes. *Biochem. J.* **441**, 763–787 (2012).
125. Sherwood, L. *Human Physiology: From Cells to Systems*. (Cengage Learning, 2015).
126. Jelinek, L. J. *et al.* Expression cloning and signaling properties of the rat glucagon receptor. *Science* **259**, 1614–1616 (1993).
127. Agius, L. Role of glycogen phosphorylase in liver glycogen metabolism. *Mol. Aspects Med.* **46**, 34–45 (2015).
128. Jiang, G. & Zhang, B. B. Glucagon and regulation of glucose metabolism. *Am. J. Physiol. Endocrinol. Metab.* **284**, E671-678 (2003).
129. Ali, S. & Drucker, D. J. Benefits and limitations of reducing glucagon action for the treatment of type 2 diabetes. *Am. J. Physiol. Endocrinol. Metab.* **296**, E415-421 (2009).
130. Tirone, T. A. & Brunicardi, F. C. Overview of glucose regulation. *World J. Surg.* **25**, 461–467 (2001).

131. Pilkis, S. J. & Claus, T. H. Hepatic gluconeogenesis/glycolysis: regulation and structure/function relationships of substrate cycle enzymes. *Annu. Rev. Nutr.* **11**, 465–515 (1991).
132. Brosnan, J. T. Pathways of carbon flux in gluconeogenesis. *Fed. Proc.* **41**, 91–95 (1982).
133. Nuttall, F. Q., Ngo, A. & Gannon, M. C. Regulation of hepatic glucose production and the role of gluconeogenesis in humans: is the rate of gluconeogenesis constant? *Diabetes Metab. Res. Rev.* **24**, 438–458 (2008).
134. Hanson, R. W. & Garber, A. J. Phosphoenolpyruvate carboxykinase. I. Its role in gluconeogenesis. *Am. J. Clin. Nutr.* **25**, 1010–1021 (1972).
135. Hanson, R. W. & Reshef, L. Regulation of phosphoenolpyruvate carboxykinase (GTP) gene expression. *Annu. Rev. Biochem.* **66**, 581–611 (1997).
136. Hers, H. G. & Hue, L. Gluconeogenesis and related aspects of glycolysis. *Annu. Rev. Biochem.* **52**, 617–653 (1983).
137. Nordlie, R. C., Foster, J. D. & Lange, A. J. Regulation of glucose production by the liver. *Annu. Rev. Nutr.* **19**, 379–406 (1999).
138. van Schaftingen, E. & Gerin, I. The glucose-6-phosphatase system. *Biochem. J.* **362**, 513–532 (2002).
139. Cano, N. Bench-to-bedside review: glucose production from the kidney. *Crit. Care Lond. Engl.* **6**, 317–321 (2002).
140. Mitrakou, A. Kidney: its impact on glucose homeostasis and hormonal regulation. *Diabetes Res. Clin. Pract.* **93 Suppl 1**, S66-72 (2011).

141. Gerich, J. E., Meyer, C., Woerle, H. J. & Stumvoll, M. Renal gluconeogenesis: its importance in human glucose homeostasis. *Diabetes Care* **24**, 382–391 (2001).
142. Nakae, J., Park, B. C. & Accili, D. Insulin stimulates phosphorylation of the forkhead transcription factor FKHR on serine 253 through a Wortmannin-sensitive pathway. *J. Biol. Chem.* **274**, 15982–15985 (1999).
143. Haeusler, R. A., Kaestner, K. H. & Accili, D. FoxOs function synergistically to promote glucose production. *J. Biol. Chem.* **285**, 35245–35248 (2010).
144. Matsumoto, M., Poci, A., Rossetti, L., Depinho, R. A. & Accili, D. Impaired regulation of hepatic glucose production in mice lacking the forkhead transcription factor Foxo1 in liver. *Cell Metab.* **6**, 208–216 (2007).
145. Oh, K.-J., Han, H.-S., Kim, M.-J. & Koo, S.-H. CREB and FoxO1: two transcription factors for the regulation of hepatic gluconeogenesis. *BMB Rep.* **46**, 567–574 (2013).
146. Ozcan, L. *et al.* Calcium signaling through CaMKII regulates hepatic glucose production in fasting and obesity. *Cell Metab.* **15**, 739–751 (2012).
147. Arias, J. *et al.* Activation of cAMP and mitogen responsive genes relies on a common nuclear factor. *Nature* **370**, 226–229 (1994).
148. Nakae, J., Kitamura, T., Silver, D. L. & Accili, D. The forkhead transcription factor Foxo1 (Fkhr) confers insulin sensitivity onto glucose-6-phosphatase expression. *J. Clin. Invest.* **108**, 1359–1367 (2001).

149. Rena, G., Guo, S., Cichy, S. C., Unterman, T. G. & Cohen, P. Phosphorylation of the transcription factor forkhead family member FKHR by protein kinase B. *J. Biol. Chem.* **274**, 17179–17183 (1999).
150. Brunet, A. *et al.* Akt promotes cell survival by phosphorylating and inhibiting a Forkhead transcription factor. *Cell* **96**, 857–868 (1999).
151. Shen, Y., Joachimiak, A., Rosner, M. R. & Tang, W.-J. Structures of human insulin-degrading enzyme reveal a new substrate recognition mechanism. *Nature* **443**, 870–874 (2006).
152. Tang, W.-J. Targeting Insulin-Degrading Enzyme to Treat Type 2 Diabetes Mellitus. *Trends Endocrinol. Metab. TEM* **27**, 24–34 (2016).
153. Farris, W., Leissring, M. A., Hemming, M. L., Chang, A. Y. & Selkoe, D. J. Alternative splicing of human insulin-degrading enzyme yields a novel isoform with a decreased ability to degrade insulin and amyloid beta-protein. *Biochemistry (Mosc.)* **44**, 6513–6525 (2005).
154. Leissring, M. A. *et al.* Alternative translation initiation generates a novel isoform of insulin-degrading enzyme targeted to mitochondria. *Biochem. J.* **383**, 439–446 (2004).
155. Rubenstein, A. H., Pottenger, L. A., Mako, M., Getz, G. S. & Steiner, D. F. The metabolism of proinsulin and insulin by the liver. *J. Clin. Invest.* **51**, 912–921 (1972).
156. Pivovarova, O., Gögebakan, O., Pfeiffer, A. F. H. & Rudovich, N. Glucose inhibits the insulin-induced activation of the insulin-degrading enzyme in HepG2 cells. *Diabetologia* **52**, 1656–1664 (2009).

157. Farris, W. *et al.* Insulin-degrading enzyme regulates the levels of insulin, amyloid beta-protein, and the beta-amyloid precursor protein intracellular domain in vivo. *Proc. Natl. Acad. Sci. U. S. A.* **100**, 4162–4167 (2003).
158. Farris, W. *et al.* Partial loss-of-function mutations in insulin-degrading enzyme that induce diabetes also impair degradation of amyloid beta-protein. *Am. J. Pathol.* **164**, 1425–1434 (2004).
159. Bennett, R. G., Duckworth, W. C. & Hamel, F. G. Degradation of amylin by insulin-degrading enzyme. *J. Biol. Chem.* **275**, 36621–36625 (2000).
160. Qiu, W. Q. *et al.* Insulin-degrading enzyme regulates extracellular levels of amyloid beta-protein by degradation. *J. Biol. Chem.* **273**, 32730–32738 (1998).
161. Manolopoulou, M., Guo, Q., Malito, E., Schilling, A. B. & Tang, W.-J. Molecular basis of catalytic chamber-assisted unfolding and cleavage of human insulin by human insulin-degrading enzyme. *J. Biol. Chem.* **284**, 14177–14188 (2009).
162. McCord, L. A. *et al.* Conformational states and recognition of amyloidogenic peptides of human insulin-degrading enzyme. *Proc. Natl. Acad. Sci. U. S. A.* **110**, 13827–13832 (2013).
163. Guo, Q., Manolopoulou, M., Bian, Y., Schilling, A. B. & Tang, W.-J. Molecular basis for the recognition and cleavages of IGF-II, TGF-alpha, and amylin by human insulin-degrading enzyme. *J. Mol. Biol.* **395**, 430–443 (2010).

164. Bennett, R. G., Fawcett, J., Kruer, M. C., Duckworth, W. C. & Hamel, F. G. Insulin inhibition of the proteasome is dependent on degradation of insulin by insulin-degrading enzyme. *J. Endocrinol.* **177**, 399–405 (2003).
165. Hamel, F. G., Bennett, R. G. & Duckworth, W. C. Regulation of multicatalytic enzyme activity by insulin and the insulin-degrading enzyme. *Endocrinology* **139**, 4061–4066 (1998).
166. Bennett, R. G., Hamel, F. G. & Duckworth, W. C. Identification and isolation of a cytosolic proteolytic complex containing insulin degrading enzyme and the multicatalytic proteinase. *Biochem. Biophys. Res. Commun.* **202**, 1047–1053 (1994).
167. Fawcett, J. & Duckworth, W. C. Hyperglycaemia and hyperinsulinaemia: is insulin-degrading enzyme the missing link? *Diabetologia* **52**, 1457–1460 (2009).
168. Hyun, J. & Hashimoto, C. Physiological effects of manipulating the level of insulin-degrading enzyme in insulin-producing cells of *Drosophila*. *Fly (Austin)* **5**, 53–57 (2011).
169. Fakhrai-Rad, H. *et al.* Insulin-degrading enzyme identified as a candidate diabetes susceptibility gene in GK rats. *Hum. Mol. Genet.* **9**, 2149–2158 (2000).
170. Abdul-Hay, S. O. *et al.* Deletion of insulin-degrading enzyme elicits antipodal, age-dependent effects on glucose and insulin tolerance. *PLoS One* **6**, e20818 (2011).

171. Steneberg, P. *et al.* The type 2 diabetes-associated gene *ide* is required for insulin secretion and suppression of  $\alpha$ -synuclein levels in  $\beta$ -cells. *Diabetes* **62**, 2004–2014 (2013).
172. Leissring, M. A. *et al.* Designed inhibitors of insulin-degrading enzyme regulate the catabolism and activity of insulin. *PLoS One* **5**, e10504 (2010).
173. Maianti, J. P. *et al.* Anti-diabetic activity of insulin-degrading enzyme inhibitors mediated by multiple hormones. *Nature* **511**, 94–98 (2014).
174. Çakir, B. *et al.* Structure based discovery of small molecules to regulate the activity of human insulin degrading enzyme. *PLoS One* **7**, e31787 (2012).
175. Durham, T. B. *et al.* Dual Exosite-binding Inhibitors of Insulin-degrading Enzyme Challenge Its Role as the Primary Mediator of Insulin Clearance in Vivo. *J. Biol. Chem.* **290**, 20044–20059 (2015).
176. Pivovarova, O. *et al.* Hepatic insulin clearance is closely related to metabolic syndrome components. *Diabetes Care* **36**, 3779–3785 (2013).
177. Epting, C. L. *et al.* Stem cell antigen-1 localizes to lipid microdomains and associates with insulin degrading enzyme in skeletal myoblasts. *J. Cell. Physiol.* **217**, 250–260 (2008).
178. Bennett, R. G., Hamel, F. G. & Duckworth, W. C. An insulin-degrading enzyme inhibitor decreases amylin degradation, increases amylin-induced cytotoxicity, and increases amyloid formation in insulinoma cell cultures. *Diabetes* **52**, 2315–2320 (2003).
179. Hogan, M. F. *et al.* Inhibition of Insulin-Degrading Enzyme Does Not Increase Islet Amyloid Deposition in Vitro. *Endocrinology* **157**, 3462–3468 (2016).

180. Godoy-Matos, A. F. The role of glucagon on type 2 diabetes at a glance. *Diabetol. Metab. Syndr.* **6**, 91 (2014).
181. Hamel, F. G., Fawcett, J., Tsui, B. T., Bennett, R. G. & Duckworth, W. C. Effect of nelfinavir on insulin metabolism, proteasome activity and protein degradation in HepG2 cells. *Diabetes Obes. Metab.* **8**, 661–668 (2006).
182. Pivovarova, O., Höhn, A., Grune, T., Pfeiffer, A. F. H. & Rudovich, N. Insulin-degrading enzyme: new therapeutic target for diabetes and Alzheimer's disease? *Ann. Med.* **48**, 614–624 (2016).
183. Salgado, A. L. F. de A. *et al.* Insulin resistance index (HOMA-IR) in the differentiation of patients with non-alcoholic fatty liver disease and healthy individuals. *Arq. Gastroenterol.* **47**, 165–169 (2010).
184. Matthews, D. R. *et al.* Homeostasis model assessment: insulin resistance and beta-cell function from fasting plasma glucose and insulin concentrations in man. *Diabetologia* **28**, 412–419 (1985).
185. Srodulski, S. *et al.* Neuroinflammation and neurologic deficits in diabetes linked to brain accumulation of amylin. *Mol. Neurodegener.* **9**, 30 (2014).
186. Jiménez-Palomares, M. *et al.* Increased A $\beta$  production prompts the onset of glucose intolerance and insulin resistance. *Am. J. Physiol. Endocrinol. Metab.* **302**, E1373-1380 (2012).
187. Chen, L., Chen, R., Wang, H. & Liang, F. Mechanisms Linking Inflammation to Insulin Resistance. *Int. J. Endocrinol.* **2015**, 508409 (2015).

188. Succurro, E. *et al.* Insulin secretion in metabolically obese, but normal weight, and in metabolically healthy but obese individuals. *Obes. Silver Spring Md* **16**, 1881–1886 (2008).
189. Lee, K. Metabolically obese but normal weight (MONW) and metabolically healthy but obese (MHO) phenotypes in Koreans: characteristics and health behaviors. *Asia Pac. J. Clin. Nutr.* **18**, 280–284 (2009).
190. Denis, G. V. & Obin, M. S. 'Metabolically healthy obesity': origins and implications. *Mol. Aspects Med.* **34**, 59–70 (2013).
191. Hanefeld, M. *et al.* One-year glycemetic control with a sulfonylurea plus pioglitazone versus a sulfonylurea plus metformin in patients with type 2 diabetes. *Diabetes Care* **27**, 141–147 (2004).
192. Hanefeld, M. Pioglitazone and sulfonylureas: effectively treating type 2 diabetes. *Int. J. Clin. Pract. Suppl.* 20–27 (2007). doi:10.1111/j.1742-1241.2007.01361.x
193. Brunton, S. GLP-1 receptor agonists vs. DPP-4 inhibitors for type 2 diabetes: is one approach more successful or preferable than the other? *Int. J. Clin. Pract.* **68**, 557–567 (2014).
194. Heron-Milhavet, L., Khouya, N., Fernandez, A. & Lamb, N. J. Akt1 and Akt2: differentiating the aktion. *Histol. Histopathol.* **26**, 651–662 (2011).
195. Héron-Milhavet, L. *et al.* Only Akt1 is required for proliferation, while Akt2 promotes cell cycle exit through p21 binding. *Mol. Cell. Biol.* **26**, 8267–8280 (2006).

196. Strable, M. S. & Ntambi, J. M. Genetic control of de novo lipogenesis: role in diet-induced obesity. *Crit. Rev. Biochem. Mol. Biol.* **45**, 199–214 (2010).
197. Brown, M. S. & Goldstein, J. L. Selective versus total insulin resistance: a pathogenic paradox. *Cell Metab.* **7**, 95–96 (2008).
198. Titchenell, P. M. *et al.* Direct Hepatocyte Insulin Signaling Is Required for Lipogenesis but Is Dispensable for the Suppression of Glucose Production. *Cell Metab.* **23**, 1154–1166 (2016).
199. Fon Tacer, K., Kuzman, D., Seliskar, M., Pompon, D. & Rozman, D. TNF- $\alpha$  interferes with lipid homeostasis and activates acute and proatherogenic processes. *Physiol. Genomics* **31**, 216–227 (2007).
200. Chesneau, V. & Rosner, M. R. Functional human insulin-degrading enzyme can be expressed in bacteria. *Protein Expr. Purif.* **19**, 91–98 (2000).
201. Dobbins, R. L. *et al.* Compartmental modeling of glucagon kinetics in the conscious dog. *Metabolism.* **44**, 452–459 (1995).
202. Deacon, C. F. *et al.* Differential regional metabolism of glucagon in anesthetized pigs. *Am. J. Physiol. Endocrinol. Metab.* **285**, E552-560 (2003).
203. Zhou, A., Pacini, G., Ahrén, B. & D'Argenio, D. Z. Glucagon clearance is regulated by nutritional state: evidence from experimental studies in mice. *Diabetologia* **57**, 801–808 (2014).
204. Lefebvre, P. J., Luyckx, A. S. & Nizet, H. Renal handling of endogenous glucagon in the dog: comparison with insulin. *Metabolism.* **23**, 753–761 (1974).

205. Lim, H.-K. *et al.* Altered verbal working memory process in patients with Alzheimer's disease: an fMRI investigation. *Neuropsychobiology* **57**, 181–187 (2008).
206. Fu, W. *et al.* Amyloid  $\beta$  (A $\beta$ ) peptide directly activates amylin-3 receptor subtype by triggering multiple intracellular signaling pathways. *J. Biol. Chem.* **287**, 18820–18830 (2012).
207. Westermark, P., Engström, U., Johnson, K. H., Westermark, G. T. & Betsholtz, C. Islet amyloid polypeptide: pinpointing amino acid residues linked to amyloid fibril formation. *Proc. Natl. Acad. Sci. U. S. A.* **87**, 5036–5040 (1990).
208. Scherbaum, W. A. The role of amylin in the physiology of glycemic control. *Exp. Clin. Endocrinol. Diabetes Off. J. Ger. Soc. Endocrinol. Ger. Diabetes Assoc.* **106**, 97–102 (1998).
209. Kahn, S. E., Andrikopoulos, S. & Verchere, C. B. Islet amyloid: a long-recognized but underappreciated pathological feature of type 2 diabetes. *Diabetes* **48**, 241–253 (1999).
210. Johnson, K. H., O'Brien, T. D., Betsholtz, C. & Westermark, P. Islet amyloid, islet-amyloid polypeptide, and diabetes mellitus. *N. Engl. J. Med.* **321**, 513–518 (1989).